Mitochondrial unfolded protein response, its molecular mechanism and physiological impact

THÈSE N° 7352 (2016)

PRÉSENTÉE LE 11 NOVEMBRE 2016
À LA FACULTÉ DES SCIENCES DE LA VIE
CHAIRE NESTLÉ EN MÉTABOLISME ÉNERGÉTIQUE
PROGRAMME DOCTORAL EN BIOTECHNOLOGIE ET GÉNIE BIOLOGIQUE

ÉCOLE POLYTECHNIQUE FÉDÉRALE DE LAUSANNE

POUR L'OBTENTION DU GRADE DE DOCTEUR ÈS SCIENCES

PAR

Virginija JOVAISAITE

acceptée sur proposition du jury:

Prof. A. Radenovic, présidente du jury
Prof. J. Auwerx, directeur de thèse
Prof. E. Nollen, rapporteuse
Prof. A. Trifunovic, rapporteuse
Prof. P. Gönczy, rapporteur

ÉCOLE POLYTECHNIQUE
FÉDÉRALE DE LAUSANNE

Suisse
2016

Summary

Mitochondria are the main producers of ATP, the energy currency of the cell, and they perform a wide array of other fundamental functions. These organelles are essential not only for cellular metabolism, but also for organismal physiology and lifespan. A recently discovered mitochondrial unfolded protein response (UPR^{mt}) maintains the mitochondrial proteostasis by managing protein quality control (PQC) network during proteotoxic stress. Recent findings show that activation of this repair pathway improves mitochondrial function and is associated with increased longevity.

My thesis aims to expand the knowledge about the UPR^{mt} by exploring its molecular mechanism and impact on mitochondrial stress induced longevity. We performed three studies:

Identification of two epigenetic UPR^{mt} regulators (chapter 2). In collaboration with Prof. Dillin's laboratory (UCB, USA), we identified the conserved histone demethylases *jmjd-1.2*/PHF8 and *jmjd-3.1*/JMJD3 as positive regulators of UPR^{mt} and longevity in response to mitochondrial electron transport chain (ETC) dysfunction across species. A systems genetics analysis of data from the BXD mouse genetic reference population (GRP) further indicates conserved roles of the mammalian orthologs of these demethylases in longevity and UPR^{mt} signaling. These findings illustrate an evolutionary conserved epigenetic mechanism that determines the rate of aging, downstream of mitochondrial perturbations.

Relation between UPR^{mt} and TCA cycle (chapter 3). We investigated the effects of genetic perturbations of the TCA cycle on the UPR^{mt} and lifespan. We found that downregulation of several TCA cycle enzymes induces UPR^{mt}, but they have divergent effects on lifespan. Restricting the knockdown of these genes to early larval development stages had positive effects on longevity, which was dependent on UPR^{mt}. We analysed the transcriptomes of *C. elegans* with knockdown of these TCA cycle genes and compared them with those obtained after the knockdown of other mitochondrial genes, which are known to induce the UPR^{mt}. We identified a core set of transcripts, which change in

common and which likely represent a signature of mitochondrial dysfunction associated with UPR^{mt} induction.

Bioinformatic analysis of UPR^{mt} (chapter 4). In two collaborative studies, we investigated the UPR^{mt} using newly collected data from the BXD mouse GRP. In the first study, we quantified the transcriptome and proteome from 40 strains of the BXD mouse GRP on two different diets. Integrated molecular profiles were used to characterize the UPR^{mt}, which shows strikingly variant responses at the transcript and protein level that are conserved between *C.elegans*, mice and humans. In the second study, whole genomes of BXD GRP strains were sequenced to detect sequence variants, which were then used to find novel associations within a high coverage phenome of various traits. One of the novel associations included a missense mutation in fumarate hydratase that controls variation in the UPR^{mt} in both mouse and *C. elegans*.

In summary, our work characterized novel epigenetic regulators of UPR^{mt} and associated mitochondrial stress induced longevity, described the connection between the UPR^{mt} and the TCA cycle, and illustrated the conservation of UPR^{mt} in a mouse GRP. These results expand the knowledge about the UPR^{mt} and promote further investigation of its role in longevity and mitochondrial diseases.

Keywords : UPR^{mt}, mitochondria, longevity, gene expression, epigenetics, histone demethylase, metabolism, TCA cycle, BXD, genetic reference population.

Résumé

Les mitochondries sont les principaux producteurs d'ATP, la monnaie énergétique de la cellule, et elles effectuent un large éventail d'autres fonctions fondamentales Ces organelles sont donc essentielles non seulement pour le métabolisme cellulaire, mais aussi pour la physiologie globale de l'organisme et la détermination de la durée de vie. Une réponse mitochondriale récemment découverte, la « mitochondrial unfolded protein response » (UPR^{mt}) (littéralement, la réponse mitochondriale des protéines dénaturées) maintient la protéostase mitochondriale grâce à un contrôle-qualité de protéines (« protein quality control »=PQC) en réponse à un stress protéotoxique. Des découvertes récentes montrent que l'activation de cette voie de réparation améliore la fonction mitochondriale et est associée à une longévité accrue.

Ma thèse vise à élargir les connaissances sur le UPR^{mt} en explorant son mécanisme moléculaire et son impact sur la longévité augmentée par le stress mitochondrial. Nous avons effectué trois études:

Identification de deux régulateurs épigénétiques du UPR^{mt} (chapitre 2). En collaboration avec le laboratoire du Prof. Dillin (UCB, États-Unis), nous avons identifié des déméthylases des histones *jmjd-1.2*/PHF8 et *jmjd-3.1*/JMJD3 comme régulateurs positifs de UPR^{mt} et de la longévité, de manière onservée à travers les espèces, en réponse à un dysfonctionnement de la chaîne de transport des électrons. Par ailleurs, une analyse génétique des bases de données de la population-référence génétique des souris BXD (GRP) indique la conservation du rôle des orthologues mammifères de ces déméthylases dans la longévité et la signalisation de UPR^{mt}. Ces résultats illustrent un mécanisme épigénétique conservé dans l'évolution qui détermine la vitesse de vieillissement, en aval des perturbations mitochondriales.

Relation entre le UPR^{mt} et cycle de Krebs (chapitre 3). Nous avons étudié les effets des perturbations génétiques du cycle de Krebs sur le UPR^{mt} et la durée de vie. Nous avons constaté que la régulation négative de plusieurs enzymes du cycle de Krebs induit le UPR^{mt}, mais ces perturbations ont des effets divergents sur la durée de vie. Le knock-

down de ces gènes limité aux premiers stades de développement larvaire a montré des effets positifs sur la longévité, de manière dépendante du UPR^{mt}. Nous avons analysé les transcriptomes de *C. elegans* en réponse au knockdown des gènes du cycle de Krebs et les avons comparés avec ceux obtenus après knockdown d'autres gènes mitochondriaux connus pour induire le UPR^{mt}. Nous avons pu identifier un ensemble d'ARN messagers, qui changent en commun et qui représentent probablement une signature de la dysfonction mitochondriale associée à l'induction UPR^{mt}.

L'analyse bioinformatique de UPR^{mt} (chapitre 4). Dans deux études collaborative, nous avons étudié le UPR^{mt} en utilisant les nouvelles données recueillies à partir du population-référence génétique des souris BXD. Dans la première étude, nous avons quantifié le transcriptome et le protéome de 40 lignées BXD sujettes à deux régimes différents. L'intégration des profils moléculaires a été utilisée pour caractériser le UPR^{mt} et a montré des réponses considérablement variables au niveau transcriptionnel et protéique, qui sont conservés entre *C. elegans*, la souris et l'humain. Dans la seconde étude, les génomes des lignées BXD ont été entièrement séquencées afin de détecter des variantes de séquence, qui ont ensuite été utilisées pour trouver de nouvelles associations parmi un phénome couvrant de nombreux traits phénotypiques. L'une des nouvelles associations comportait une mutation "missense" dans le gène de la fumarate hydratase, qui contrôle la variation du UPR^{mt} dans la souris et *C. elegans*.

En résumé, notre travail a caractérisé de nouveaux régulateurs épigénétiques du UPR^{mt} et de la longévité causée par le stress mitochondrial, a décrit la connexion entre le UPR^{mt} et le cycle de Krebs, et a illustré la conservation du UPR^{mt} dans la population-référence génétique BXD. Ces résultats élargissent les connaissances sur le UPR^{mt} et encouragent une recherche plus approfondie sur son rôle dans la longévité et les maladies mitochondriales.

Mots-clés : UPR^{mt}, mitochondries, longévité, expression des gènes, épigénétique, histone déméthylase, métabolisme, cycle de Krebs, BXD, population génétique de référence.

Acknowledgements

The four years of my PhD have come to an end and I want to thank the people who helped me along the way.

First of all, I thank my advisor Prof. Johan Auwerx for giving me the opportunity to work in his laboratory in a scientifically exciting atmosphere. Thanks for guiding me and giving me opportunities to learn and participate in various projects. I also thank Prof. Kristina Schoonjans for encouragement and support.

Thanks to Prof. Andrew Dillin for sharing knowledge and resources in our collaboration on the exciting histone demethylase project.

Thanks to Prof. Robert W. Williams for collaboration on the BXD and TCA projects.

Thanks to Prof. Ruedi Aebersol for collaboration on BXD bioinformatics project.

Thanks to Dr. Carsten Merkwirth for a close collaboration on Jmjd project. Even through a big distance, we finished it, thanks to your work, collaborative spirit and motivation. I hope we will meet in real life as well one day. Also thanks to Dr. Kristan Steffen for help with RNA-seq analysis.

Thanks to Dr. Olli Matilainen for help with *C. elegans* experiments, and all the scientific and not only discussions and advices. Thanks to Dr. Pedro M. Quiros for help on Jmjd project and bioinformatics analyses, and for always being available with clever suggestions. Thanks to Adrienne Mottis for a nice experience of working together on various projects, for all the discussions, advices and help during the whole PhD. Thanks to Dr. Evan G. Williams for teaching about BXD and bioinformatics. Thanks to Dr. Laurent Mouchiroud for introducing me to *C. elegans* and advices on various scientific questions. Thanks to Dr. Dongryeol Ryu who taught me a lot of things in the beginning of my PhD, always encouraged me and was available with advice or help when needed. Thanks also to Dr. Xu Wang for help with bioinformatics.

I am grateful for all my colleagues for team spirit and nice atmosphere in the lab. In addition to all the people I already mentioned, thanks to Pan, Elena, Karim, Hongbo, Vera,

Contents

List of figures and tables

Chapter 1   Introduction

Adapted from

* Co-first author

This chapter gives general introduction about UPR^{mt} pathway, its interaction with other cellular pathways and implications in longevity. I conceived and wrote the majority of the text and drew the figures.

1.1 Reaction to stress and adaptive response

One of the keystones driving evolution is the capacity to detect, respond and adapt to various stressors in the environment through the development of defensive mechanisms at a cellular level that protect the entire organism and maintain its capacity to grow and reproduce [1]. A large body of evidence has established that stress adaptation and aging are intimately linked [2]. The concept that stress responses and the aging process share common mechanisms arose initially from studies in model organisms, where the identification of molecular pathways that regulate aging – Insulin/Insulin-like growth factor (IGF), sirtuins, target of rapamycin (TOR), AMP activated kinase (AMPK) – highlighted that intrinsic induction of stress defense programs and the resulting adaptation can increase life expectancy [3]. As a case in point, downregulation of Insulin/IGF-1 signaling promotes stress defense and increases the lifespan from worms to mouse [4-6]. Over time, it became clear that applying moderate levels of stress could trigger beneficial and adaptive stress defense pathways, allowing longer life [7]; this is now known as a "hormetic stress response" and drew the interest of the scientific community for its potential application in the pharmacological management of age-related diseases. Illustrative of such a hormetic stress response is the reaction to the low dose energy stress induced by caloric restriction, which prolongs lifespan in a wide array of species from yeast to primates [8].

Maintenance of protein homeostasis, also known as "proteostasis", which refers to all the cellular pathways that govern the production, folding and degradation of proteins, is essential for cellular and organismal functionality and survival. Complex pathways to ensure proteostasis in different subcellular compartments, defined as Unfolded Protein Responses (UPRs), have evolved in the cytosol, endoplasmic reticulum and mitochondria, which are finely coordinated and require a close communication with the nucleus. Dysfunction of proteostasis is associated with protein aggregation and is a feature of several age-related diseases [9]. While the unfolded protein response in the endoplasmic reticulum (UPR^{ER}) and the cytosolic heat shock response (HSR) were extensively studied [10,11], the mitochondrial unfolded protein response (UPR^{mt}) was more recently discovered and shed light on the complex relationships between this organelle and the nucleus [12].

Mitochondria supply cells with ATP, the cellular energy currency, and are essential for many other aspects of cellular homeostasis, thereby influencing not only cellular metabolism, but also organismal health and lifespan [13,14]. Inborn mitochondrial defects result in severe multisystem diseases and mitochondrial dysfunction also underlies several

common metabolic and neurodegenerative diseases [15,16]. Mitochondrial unfolded protein response (UPR^{mt}) is an emerging adaptive stress response pathway, which ensures optimal quality and function of the mitochondrial proteome. UPR^{mt} internally surveys mitochondrial proteostasis and responds to stress signals by activating an intricate mitochondrial protein quality control (PQC) network [12,17,18]. Here we review the recent literature on proteostasis in different subcellular compartments, mechanisms that trigger UPR^{mt} activation, its signaling pathways, crosstalk with other mitochondrial quality control systems and interactions with the wider network of cellular responses.

1.2 Proteostasis in the cytosol and the endoplasmic reticulum

Most cellular proteins are folded directly after translation in the cytosol with the assistance of chaperones, whereas membrane and secreted proteins fold and mature in the endoplasmic reticulum. Specific response mechanisms help to cope with the accumulation of misfolded proteins in these cellular compartments and include the irreducible steps of detection of cellular stress, transduction of the stress signal to the nucleus, triggering of the defense programs and restoration of cellular homeostasis. Upon sustained stress, when response mechanisms fail to restore homeostasis, apoptotic pathways may be activated as a last line of defense to ensure survival of the multicellular organism.

HSR manages denatured proteins in the cytosol [11,19]. The major player is the transcription factor, Heat Shock Factor (HSF1), which is activated during cellular stress and induces the transcription of chaperones and other protective genes. Under normal conditions HSF1 is bound to the cytosolic chaperones HSP90 and HSP70 in a monomeric inactive form. When the load of unfolded proteins increases, these chaperones will dissociate from HSF1 and be recruited to unfolded proteins. HSF1 then trimerizes and translocates to the nucleus, where it is posttranslationaly modified and activates the transcription of heat shock proteins (HSPs).

UPR^{ER} is mediated by three transmembrane sensors: inositol requiring element 1 (IRE1), PKR-like ER kinase (PERK) and activating transcription factor 6 (ATF6), which are retained in an inactive state by the chaperone BiP/GRP78 [10]. During ER stress, released and activated sensors elicit the following main responses to unfolded protein stress. PERK phosphorylates and thereby inhibits the eukaryotic translation initiation factor 2a (eIF2α) to prevent further protein synthesis, ATF6 is proteolytically cleaved and translocates to the nucleus to induce the transcription of ER chaperones, while IRE1 splices the mRNA of *XBP1*, leading to a functional transcription factor which consequently activates genes

involved in misfolded protein export and degradation. Prolonged UPR[ER] induces apoptosis via several pathways downstream of PERK, ATF6 and IRE1, including c-Jun N-terminal kinase (JNK), transcription factor C/EBP homologous protein (CHOP) and B-cell lymphoma 2 (BCL2) family proteins, which activate proapoptotic factors subsequently leading to the final execution of cell death [20].

1.3 Proteostasis in the mitochondria

Mitochondria are evolutionarily derived from proteobacteria that evolved in symbiosis within eukaryotic cells [21]. Mitochondria contain multiple copies of the circular mitochondrial DNA (mtDNA), a vestige of the proteobacterial genome, which encodes 13 protein constituents of the multiprotein complexes of the electron transport chain (ETC). The remainder of the mitochondrial proteome (~1500 proteins) is transcribed from the nuclear DNA (nDNA). After translation in the cytoplasm, these nuclear encoded proteins are imported, folded and assembled within the mitochondria [22,23]. Four out of five ETC complexes contain proteins encoded in both genomes, requiring a robust synchrony between the mitochondrial and nuclear genome to warrant optimal mitochondrial function [24].

Proteostasis in the mitochondria is ensured by an elaborate protein quality control (PQC) network, composed of two main functional groups of proteins, chaperones and proteases [25,26]. Chaperones mtHsp70, Hsp60 and Hsp10 fold and assemble proteins that are imported into the mitochondria and refold damaged mitochondrial proteins. Excess proteins that are unassisted by chaperones are digested by ATP-dependent PQC proteases, specific for each mitochondrial compartment: the ClpXP and Lon proteases in the matrix, the i-AAA (Yme1L1) and m-AAA proteases (Afg3l2 and Spg7), acting in the intermembrane space (IMS) and matrix, respectively. Upon mitochondrial proteotoxic stress, these PQC chaperones and proteases are induced as a result of a retrograde mitochondria-to-nucleus signaling termed UPR[mt]. Using mitochondrial chaperones and proteases as UPR[mt] biomarkers, this PQC pathway has now been established in worms, flies, mammalian cell cultures and mice. Various conditions have been shown to trigger the UPR[mt], most of which interfere with the mitochondrial proteostasis either by disturbing the PQC system or by increasing the load of damaged, unfolded or unassembled proteins (Table 1:1).

RNAi based downregulation of components of the mitochondrial protein handling machinery, such as the import proteins TIM-17 and TIM-23 [27,28], the inner membrane

protein scaffold PHB-2 [29,30], the PQC protease SPG-7 [30,31] or the chaperone mtHsp70 [32] all induce the UPR^{mt} in *C. elegans* or in mammals. Moreover, increasing the workload of PQC machinery by overexpression of aggregation-prone proteins, such as a mutant form of ornithine transcarbamylase (OTC-d and EndoG, also activates UPR^{mt} in mammalian cells [32-34] and flies [35]. On a similar note, the treatment with the reactive oxygen species (ROS) generator paraquat, which increases the amount of damaged proteins, also induces UPR^{mt} in *C. elegans* [30,36]. Additionally, pathogenic bacteria can induce UPR^{mt} by production of toxins, which antagonize mitochondrial proteostasis [37,38].

Table 1:1 UPR^{mt} inducing manipulations

	Genetic	**Pharmacological**
protein damage	aggregation prone OTC-Δ [33,35], EndoG [34] overexpression	ROS generator paraquat [36], toxins, produced by pathogenic bacteria [37,38]
interference with PQC	knockdown of *Hspa9* [32], *hsp-60* [30], *dnj-21* [30], *spg-7* [30],	
interference with mitochondrial import and architecture	RNAi of *tim-17*, *tim-23* (RNAi) [27,28], *phb-2* [29,30]	arsenic (III) [27]
mtDNA depletion	RNAi of mtDNA helicase *pif-1* [30], Deletor mice [39]	ethidium bromide [30,40]
interference with mitochondrial translation	downregulation of various cytosolic and mitochondrial ribosomal proteins [30,41]	bacterial and mitochondrial translation inhibitors doxycycline and chloramphenicol [41]
loss of ETC subunits	*cco-1* RNAi [42], *isp-1* (qm150) [43], *clk-1* (qm30) [43] alleles, RNAi of ND75 [44], *Surf1*$^{-/-}$ mice [45]	ETC inhibitors antimycin [36,37], rotenone [36]
sirtuin activation and mitochondrial biogenesis	*sir-2.1* overexpression [46]	PARP inhibitors MRL45696 [47] and AZD2281 [46], NAD^{+} precursor NR [46], rapamycin [41]

Another way to induce the UPR^{mt} is by manipulating ETC assembly either by the downregulation or inhibition of single (or groups of) ETC components, which are encoded by either mtDNA or nDNA [41]. This results in a mismatch between mtDNA and nDNA encoded ETC subunits, creating orphaned unassembled subunits, which stay associated with chaperones; this phenomenon is termed mitonuclear protein imbalance [41]. Thus downregulation of ETC subunits by *cco-1* (complex IV) RNAi [31,42], in *isp-1* (complex III) or *clk-1* (ubiquinone synthesis) mutant strains [42,48], or by using pharmacological ETC inhibitors, such as antimycin [36,37] and rotenone [36], activates the UPR^{mt}. Additionally, downregulation of mitochondrial ribosomal proteins or treatment with the bacterial (also mitochondrial) translation inhibitors doxycycline or chloramphenicol [41], as well as mtDNA

depletion induced by ethidium bromide [30] result in a mitonuclear protein imbalance and consequently induce UPR[mt].

Similarly, the activation of mitochondrial biogenesis by resveratrol or rapamycin [41] also reduces the levels of mitochondrially encoded ETC subunits, triggering the UPR[mt]. Boosting NAD^{+} levels by the NAD^{+} precursor, nicotinamide riboside (NR), or by inhibiting NAD^{+} consumption, as seen after treatment with PARP inhibitors [46], also enhances biogenesis, but the raise in NAD^{+} levels specifically increases the transcription and translation of mtDNA-encoded ETC subunits [47], creating also a mitonuclear imbalance, which triggers the UPR[mt]. In accordance with these findings related to mitochondrial biogenesis, the UPR[mt] can be activated in worms, only if the perturbation in mitochondrial proteostasis takes place during L3/L4 transition [49], which coincides with a major burst in mitochondrial biogenesis [50], further emphasizing its role in the induction of UPR[mt]. The induction of UPR[mt] during biogenesis is in most cases mediated by actvation of sirtuins, protein deacylases, which are major regulators of metabolism and aging [51], namely Sirt1 in mouse or sir-2.1 in worms [39,46,47,52]. In addition to Sirt1, recently, Sirt7 and its downstream target transcription factor GABPβ1 were shown to control the expression of multiple mitochondrial ribosomal proteins, responsible for mitochondrial translation [53]. Although the potential role of Sirt7 in UPR[mt] induction has not yet been examined, given its major impact on mitochondrial ribosomal proteins [41], Sirt7 might be pivotal for mitochondrial proteostasis, while its deficiency could induce UPR[mt].

1.4 UPR[mt] signaling

The first trigger for the UPR[mt] in *C. elegans* is the excess of damaged and unfolded proteins, which are digested by the CLPP-1 protease into small peptides [54], and then transported outside of the mitochondria by the transporter HAF-1 [55] (Figure 1:1). The role of these peptides is unknown yet, but presumably they contribute to weaken mitochondrial import during stress, which on its turn is important for the nuclear translocation of the main UPR[mt] transcriptional regulator ATFS-1 [28]. ATFS-1 is able to shuttle between mitochondria and nucleus due to presence of a mitochondrial targeting sequence (MTS) and a nuclear localization sequence (NLS). In normal conditions, ATFS-1 is imported and degraded by the Lon protease in the mitochondria, but upon mitochondrial stress ATFS-1 translocates into the nucleus [28]. Together with other transcriptional regulators UBL-5 [56] and DVE-1 [54], which also move into the nucleus in stress conditions, ATFS-1 then induces the transcription of UPR[mt] targets in the worm. Of note, the Ubl5 protein levels also correlate tightly with UPR[mt] effector chaperones and proteases

in several tissues in the BXD mouse genetic reference population (GRP) and in humans, which indicates that presumably it is also involved in the initiation of the mammalian UPR[mt] [31]. Interestingly, ATFS-1 does not have an unambiguous sequence homolog in mammals, making it doubtful whether an ATFS-1 counterpart and its shuttling mechanism are conserved in mammalian UPR[mt]. ATFS-1 induces multiple genes with a pleiotropic outcome. It activates the transcription of mitochondrial chaperones and proteases, as well as that of detoxification enzymes to neutralize the generation of ROS, and of mitochondrial transporters, which presumably correct the import deficit after the resolution of the perturbation [28] (Figure 1:1). ATFS-1 also induces glycolytic genes, which indicates that there is a concomitant transient shift in cellular ATP production from mitochondrial oxidative phosphorylation to cytoplasmic glycolysis during mitochondrial stress [28]. Such a metabolic shift, while maintaining cellular energy supply, avoids overtaxation of mitochondrial energy harvesting in stress situations. How mitochondrial stress in mammals
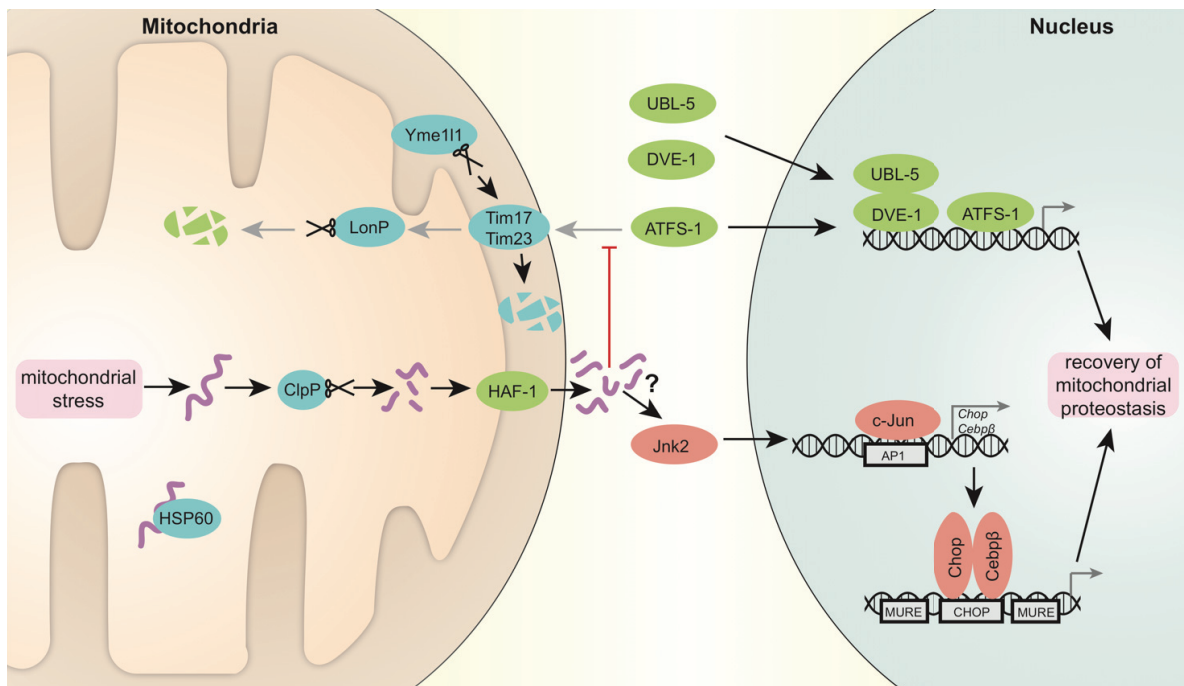
Figure 1:1 Transcriptional regulation of the UPR[mt].

Accumulating unfolded proteins, unassisted by chaperone Hsp60 in stressed mitochondria, are digested by the protease Clpp. The resulting peptides are transported through the double mitochondrial membrane into the cytosol. These peptides presumably stop mitochondrial import, which is also negatively affected by specific degradation of Tim17 component of the translocation pore by protease Yme1l1. As a result, *C. elegans* transcription factor ATFS-1, which in normal conditions is translocated to mitochondria and degraded by protease LonP, moves into the nucleus together with UBL-5 and DVE-1 to activate a reparative transcriptional program. In mammals, Jnk2 triggers c-Jun binding to AP1 sites, leading to the activation of Chop and Cebpβ transcription. Subsequently, Chop and Cebpβ dimers bind to CHOP sites flanked by MUREs and induce UPR[mt] target gene transcription. Proteins characterized in *C. elegans* are marked in green, fly and mammalian system proteins in red and proteins conserved in all the systems are noted in blue (mouse nomenclature is used).

is sensed and triggers UPR^{mt}, and whether it involves the possible generation of peptides similarly as in *C. elegans*, is still unknown. In mammalian cells transfected with OTC-Δ, the UPR^{mt} transcriptional response was shown to involve JNK2 phosphorylation, which triggers c-Jun to bind and activate the CHOP and C/EBPβ promoters [33,57] (Figure 1:1). c-Jun was shown to be also required for UPR^{mt} induction in flies [44] and CHOP induction has been observed upon EndoG overexpression [34] or in complex IV deficient Surf-/-mice [45]. Consequently, UPR^{mt} target gene expression is coordinated by a dimer of the transcription factors CHOP and C/EBPβ, which binds target promoters on a specific CHOP binding site flanked by two UPR^{mt} response elements (MUREs) [58]. MUREs have been identified in the promoters of human mitochondrial PQC chaperones and proteases (HSP60, HSP10 and mtDnaJ, ClpP, YME1L1 and PMPCB), as well as in the enzymes NDUFB2, endonuclease G and thioredoxin 2 [58]. A recent transcriptomics and proteomics analysis revealed that the UPR^{mt} effector proteins Hsp60, Hsp10, mtHsp70, ClpP, Lonp1 and Ubl5 form a tight coexpression network in mice GRPs and human populations, suggestive of their transcriptional control [31]. However, the fact that stronger correlations were observed on protein than on transcript level, indicates also importance of posttranslational mechanisms in UPR^{mt} regulation [31].

1.5 Evidence for conservation of UPR^{mt} pathway in mammals

Although the UPR^{mt} has been intensively investigated in yeast [29], worms [28,30,42,43,54-56], flies [35,44], and mammalian cells [30,33,40,41,46,48], it is not yet defined when and where UPR^{mt} occurs in intact mammals.

We previously demonstrated that mitonuclear protein imbalance, as seen upon reduced expression of *Mrps* and/or inhibition of mitochondrial translation, induces a robust UPR^{mt} in the BXD mouse strains, which translated in a significant lifespan extension [41]. As further proof of concept that similar mechanisms could activate the UPR^{mt} across species, we recently showed that subtle variations in the expression of orthologs of two prototypical UPR^{mt} components—i.e. *cco-1*, a nuclear encoded component of ETC complex IV [42] and the protease *spg-7* [30]—whose loss-of-function trigger worm UPR^{mt}, also induce a UPR^{mt} signature in unchallenged mice from the BXD GRPs [31]. These robust correlations on a population levels are remarkable as they indicate that the UPR^{mt} is a physiological pathway, which is not only activated by robust genetic or pharmacological perturbations, but has a role in subtle homeostatic processes [31], that can impact on lifespan [41]. The tight correlation and regulation of the UPR^{mt} was furthermore also conserved in several different human tissues, supporting the cross-species nature of the UPR^{mt} [31].

In addition to these data coming from holistic genetic approaches, recently also single gene perturbations in mice have been linked with the UPR^{mt}. A UPR^{mt} signature was for instance detected in muscles of mtDNA *Deletor* and *Sco2$^{KO/KI}$* mice, models of inherited mitochondrial myopathies [39,52]. Phenotypic analysis of *Surf1$^{-/-}$* mice, deficient in ETC complex IV, also revealed activation of the UPR^{mt} markers Hsp60, ClpP, Lonp and Chop [45]. Furthermore, the UPR^{mt} can also be induced pharmacologically in mice [47]. Like in worms, treatment with PARP inhibitors triggers a robust UPR^{mt} in mice as a consequence of a mitonuclear protein imbalance caused by the enhanced translation of the 13 mtDNA encoded ETC proteins [47]. These emerging data warrant further investigation of the eventual presence of the UPR^{mt} in other mice models and in human patient biopsies.

1.6 UPR^{mt}-induced protective responses

Under stress, several lines of defense are activated by mitochondria. First, production and import of new mitochondrial proteins is temporarily blocked. Specific kinases, GCN-2 in the worm [43] and PKR in mammals [48], phosphorylate eIF2a, which leads to attenuation of global translation (Figure 1:2). In *C. elegans*, reduction of mitochondrial import is important to initiate the UPR^{mt} transcriptional response [28]. Furthermore, specific reduction in mitochondrial import occurs also in mammalian cells upon UPR^{mt}, as the Yme1l1 protease selectively degrades the translocation pore component Tim17A [27]. The reduction of mitochondrial proteins and function during stress is consistent with the reallocation of ATP production to glycolysis in the cytoplasm [28].

In addition, several parallel protective responses are activated upon the UPR^{mt}. SIR-2.1 in worms and mammalian Sirt3 were shown to regulate the UPR^{mt} in part by deacetylating DAF-16 or its mammalian homolog Foxo3a, respectively, which then activates an antioxidant response [34,46] (Figure 1:2). Another major oxidative stress response pathway, coordinated by Nrf2 (NFE2L2), was activated in complex IV deficient *Surf1$^{-/-}$* mice [45]. Interestingly, the Nrf2 pathway is coordinated by c-Jun [59], which also regulates CHOP and C/EBPβ in the context of mammalian UPR^{mt}, as discussed above. On a similar note, in *C. elegans* treated with antimycin or *spg-7* RNAi to induce the UPR^{mt}, pathogen defense and drug detoxification are enhanced [37,38]. The activation of these protective pathways allows the worm to recognize and avoid pathogens, which target mitochondria, and can increase its resistance to a wider network of stressors. For instance, worms and mammalian cells with an active UPR^{mt} are more resistant to ROS generator paraquat [27,46]. Additionally, worm gain-of-function mutants of ATFS-1 with

21
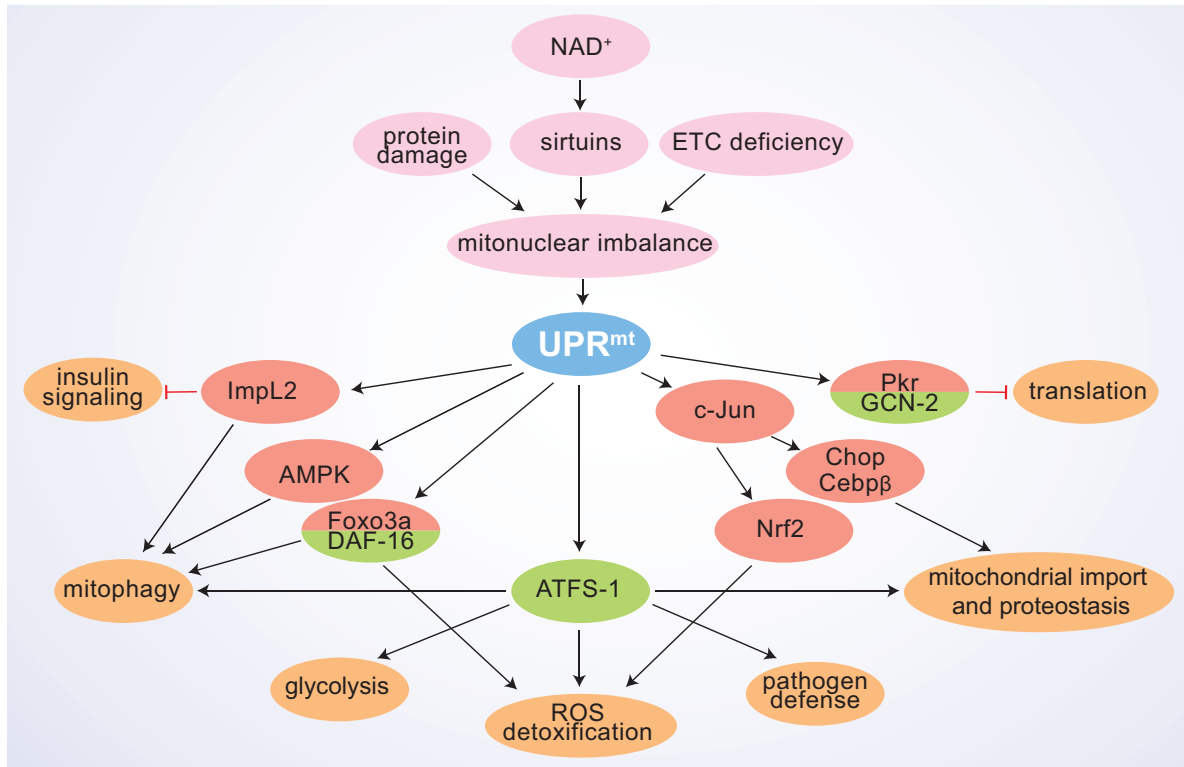
Figure 1:2 The pleiotropic effects of the UPR^{mt}.

A scheme summarizing the principle UPR^{mt} sensor/activator signals and the downstream interacting pathways, with their respective cellular effects. Proteins characterized in the fly and/or mammalian systems are marked in red and those studied in *C. elegans* in green.

constitutively activated UPR^{mt}, are resistant to statin (inhibitors of HMG-CoA reductase) toxicity [60].

Recent findings suggest that mitochondrial remodeling, namely fission and fusion, as well selective removal of terminally defective mitochondria by mitophagy, take place under stress conditions. Both increased fusion [46] and fission [32,35,41] have been detected under UPR^{mt}, which presumably depends on the type and strength of the UPR^{mt} inducer and requires further studies. Increased mitophagy has been observed in mammalian cells and flies overexpressing mutant forms of EndoG [34] or OTC-Δ [32,35,61], as well as upon RNAi inactivation of the ETC component ND75 [44]. In these systems mitophagy is potentially regulated by Foxo3a [34], AMPK [35] and secreted Insulin antagonizing peptide ImpL2, which non-autonomously repressed insulin signaling in distant tissues [44] (Figure 1:2). Whether mitophagy is upregulated in UPR^{mt} inducing conditions in worms, has not been directly investigated, but seems also likely, as autophagy genes are among the ATFS-1 targets [62]. Interestingly, mitophagy and the UPR^{mt} might share the same initial mitochondrial damage detection steps, as in worms, synthesis of ceramide, a sphingolipid which marks domains of mitochondrial dysfunction and induces mitophagy by anchoring

autophagolysosomes to these domains [63], was required for UPR^{mt} activation [37]. Mitophagy is induced by PINK1, that accumulates on the depolarized outer mitochondrial membrane, and then recruits the E3 ubiquitin ligase Parkin, targeting mitochondria to autophagosomes [64]. Mitophagy induction might be altered in UPR^{mt} conditions, as upon OTC-Δ expression in cells, PINK1 and Parkin accumulate on stressed, but not depolarized mitochondria [61]. This might be regulated at the level of PINK1 degradation in basal conditions, in which mitochondrial PQC proteases, namely Lonp1, seem to be also involved [65].

Both mitochondrial dynamics and mitophagy pathways contribute to reconstitution of cellular homeostasis in stress conditions, by redistribution and removal of the irreversibly damaged elements of mitochondrial network. Inability to induce sufficient levels of mitophagy, under strong mitochondrial stress and activation of the UPR^{mt}, induces apoptosis and has negative systemic effects on whole organism physiology [34,35].

1.7 UPR^{mt} systemic effects on aging

Disruption of almost any subunit of the ETC paradoxically extends lifespan in yeast, worms, flies and mice [66-68]. The lifespan extension is associated with typical phenotypes, such as delayed development, small size and reduced fertility. Interference with ETC has hormetic effects on longevity, demonstrated by RNAi dilution experiments: moderate knockdown extends lifespan, while too low and too strong knockdowns either do not have an effect or reduce lifespan, respectively [69]. Moreover, there are specific spatio-temporal restrictions, as selective interference with ETC only in neurons and intestine during larval stages increases worm longevity [42,49]. The UPR^{mt} is almost invariably present [70], follows the same spatio-temporal specifications [42], and is required for lifespan extension in worms with ETC problems [41-43,71]. In flies, disruption of the complex I component ND75 in the muscle by low-levels of RNAi, for a defined time period in the adult stage, activated the UPR^{mt} and increased lifespan [44]. In line with this, the reduced expression of Mrps5, a mitochondrial ribosomal protein, which regulates the translation of mtDNA encoded ETC genes, induces a mitonuclear imbalance resulting in the UPR^{mt}, which correlates with increased lifespan in the BXD mouse GRP [41]. This effect on lifespan in the BXD strains was all the more striking as it was not linked to loss of gene function, but just due to a subtle variation in Mrps5 expression levels. The positive effects of the UPR^{mt} on lifespan are also exemplified in worms [72] and flies [44] with forced overexpression of UPR^{mt} effector chaperones.

23

Despite this rather convincing evidence linking UPR^mt activation and longevity obtained in several independent laboratories and across multiple species (worm, fly, mice), not all UPR^mt inductions may be beneficial [35,73]. This is not too surprising given the hormetic nature of UPR^mt, with a clear dose effect relationship and with well-defined spatio-temporal frames. If the level of mitochondrial stress is too high, the protective effects of UPR^mt may hence be insufficient to counteract the damage, making a beneficial adaptive response become maladaptive.

1.8 Conclusions and perspectives

First described ~20 years ago, the UPR^mt is now emerging as an important regulator of mitochondrial health, interacting with other mitochondrial quality control systems, such as the oxidative stress response, mitochondrial biogenesis and mitophagy. Although some specific UPR^mt regulators and pathways have been described in invertebrates, our knowledge of the exact molecular machinery of the UPR^mt is still evolving and incomplete. Further studies defining the UPR^mt sensors, signal transduction pathways and effectors, particularly in mammals are hence required. Also how the UPR^mt intersects with other cellular signaling pathways, such as those controlled by sirtuins, AMPK or insulin, requires further investigation. The fact that a UPR^mt signal is present in unchallenged mouse and human populations across multiple tissues [31] is an important step towards ascertaining its importance in mammals. It furthermore suggests that this pathway not only has a role in stress defense but also in homeostasis, where the UPR^mt could synchronize mitochondrial and nuclear genomes at the proteome level. We hope that better understanding of the UPR^mt may one day help translate the benefits of the UPR^mt into therapies for rare inherited and common age-related related diseases with mitochondrial dysfunction.

1.9 Hypothesis of the thesis

In my PhD thesis, I focused on three weakly explored aspects about UPR^mt, related to its molecular mechanism, relation to other cellular mechanisms and conservation in mammals.

Epigenetic UPR^mt regulation (chapter 2). UPR^mt is a genetic requirement for increased longevity by ETC dysfunction specifically during *C. elegans* larval development. The temporal requirement for ETC dysfunction to have an effect on UPR^mt and longevity suggests that there exists an epigenetic mechanism, which imprints changes in gene expression during early larval development. To examine this possibility, we performed an RNAi based screen to identify transcriptional regulators of UPR^mt. In collaboration with

another laboratory, we investigated the importance and molecular mechanism of two newly identified epigenetic regulators in ETC dysfunction mediated UPR^{mt} induction and longevity.

Relation between UPR^{mt} and TCA cycle (chapter 3). UPR^{mt} is known as a response to unfolded proteins and various manipulations which trigger proteotoxic stress can be used to induce UPR^{mt}. We hypothesized that UPR^{mt} is related to cellular metabolism and can be also activated by perturbation of TCA cycle. We explored the effects of TCA cycle downregulation on UPR^{mt} and longevity in *C. elegans* and performed gene expression studies to better understand the molecular changes upon UPR^{mt} activation.

Bioinformatic analysis of UPR^{mt} in mammals (chapter 4). UPR^{mt} molecular mechanism and functional significance in mammals is not well explored. Some molecular players are known and UPR^{mt} induction has been observed in various pharmacologically treated or mutant animal models, but many open questions remain. We hypothesized that UPR^{mt} also exists in unstressed animals and novel UPR^{mt} players can be identified using systems genetics. To investigate UPR^{mt} in mammals, we performed bioinformatics analysis using genetic reference population resources. We used gene expression data in multiple tissues and various systems genetics tools, to examine UPR^{mt} conservation in mammals and search for novel associations with other genes.

Chapter 2   Two conserved histone demethylases regulate mitochondrial stress-induced longevity

Adapted from

Merkwirth C.*, <u>Jovaisaite V.*</u>, Durieux J., Matilainen O., Jordan S.D., Quiros P.M., Steffen K.K., Williams E.G., Mouchiroud L., Tronnes S.U., Murillo V., Wolff S.C., Shaw R.J., Auwerx J.[§], Dillin A.[§]. Two Conserved Histone Demethylases Regulate Mitochondrial Stress -Induced Longevity. Cell, 2016

* Co-first author

[§] Co-corresponding author

This chapter characterizes two novel epigenetic UPR[mt] and associated mitochondrial stress induced longevity regulators *jmjd-1.2* and *jmjd-3.1*. Together with C.M, J.A and A.D, I conceived the study and wrote the manuscript. I performed the majority of *C. elegans* based experiments with *jmjd-3.1* and conducted analyses of RNA-seq data and bioinformatics using BXD genetic reference population.

2.1 Summary

Across eukaryotic species, mild mitochondrial stress can have beneficial effects on the lifespan of organisms. Mitochondrial dysfunction activates an unfolded protein response (UPR^{mt}), a stress signaling mechanism designed to ensure mitochondrial homeostasis. Perturbation of mitochondria during larval development in *C. elegans* not only delays aging but also maintains UPR^{mt} signaling, suggesting an epigenetic mechanism that modulates both longevity and mitochondrial proteostasis throughout life. We identify the conserved histone lysine demethylases *jmjd-1.2*/PHF8 and *jmjd-3.1*/JMJD3 as positive regulators of lifespan in response to mitochondrial dysfunction across species. Reduction-of-function of the demethylases potently suppresses longevity and UPR^{mt} induction while gain-of-function is sufficient to extend lifespan in an UPR^{mt}-dependent manner. A systems genetics approach in the BXD mouse reference population further indicates conserved roles of the mammalian orthologs in longevity and UPR^{mt} signaling. These findings illustrate an evolutionary conserved epigenetic mechanism that determines the rate of aging downstream of mitochondrial perturbations.

2.2 Graphical abstract
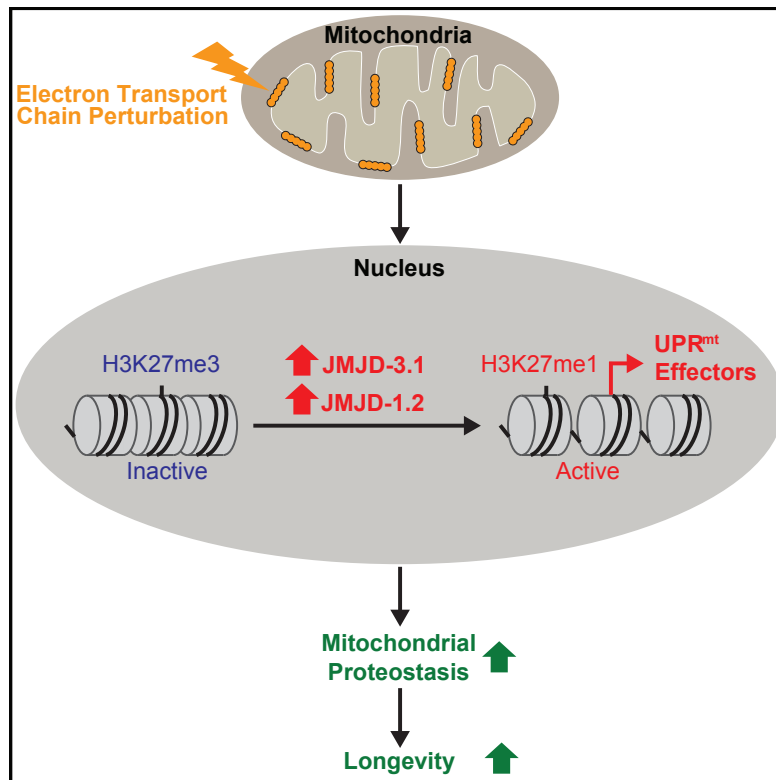
Mitochondrial perturbations early in life can have beneficial effects on the lifespan of organisms. The conserved histone lysine demethylases JMJD-1.2 and JMJD-3.1 promote longevity and coordinate transcriptional outputs in response to mitochondrial dysfunction, thereby revealing an epigenetic mode for the regulation of stress signaling and lifespan dependent on mitochondrial activities.

2.3 Highlights

- H3K27 demethylases *jmjd-1.2* and *jmjd-3.1* are required for ETC-mediated longevity

- *jmjd-1.2* and *jmjd-3.1* are necessary and sufficient for activation of the UPR^{mt}

- UPR^{mt} is required for increased lifespan due to *jmjd-1.2* or *jmjd-3.1* overexpression

- JMJD and UPR^{mt} expression is correlated with murine lifespan in inbred BXD lines

2.4 Introduction

Aging is a deleterious and complex process characterized by the progressive decline of cellular and organismal homeostasis amid constantly increasing levels of entropy [74] and represents the primary risk factor in major human pathologies including cancer, diabetes, cardiovascular disorders, and neurodegenerative diseases [75]. Aging, however, is not only a response to experiences incurred toward the end of an organism's life: it is shaped and determined by experiences that have accumulated from the earliest stages of development, and even during the generations that came before it. The organism's perpetuation of historic cues – how its patterns of gene expression change and become cemented in response to stresses that may have occurred long in the past or in parental populations – have proven to significantly affect long-term health and longevity, the mechanistic details of which are only beginning to emerge. It is thus that we now know, for example, that the transgenerational inheritance of chromatin marks can increase lifespan for multiple generations in *C. elegans* [75-78] underscoring the importance of understanding not only the genetic but also the epigenetic contributions to the complex and disordered aging process.

One of the most dramatic examples in which early events have effects on longevity is found in the nematode *C. elegans*, in which mitochondrial stress during development can cause nearly a doubling of the animal's lifespan [79]. The timing and degree of mitochondrial dysfunction is highly selective: it must occur during a specific L3/L4 larval transition in order to cause lifespan extension, a time during which a heavy amount of germline-specific mitochondrial biogenesis also occurs [50,69]. In contrast, mitochondrial

dysfunction that is too severe or which is implemented too early or late can have a negative effect on lifespan. In many cases, titrating a level of dysfunction is absolutely required in order to observe an extension of lifespan [69]. Longevity caused by mitochondrial dysfunction also often fails to generate universal health benefits, as organisms may live longer but exhibit developmental delay and a drastic reduction in reproductive fitness [79,80]. These effects are surprisingly conserved: in yeast, flies, and mice, mitochondrial dysfunction can delay the aging process [79-85], but, when occurring later in life, has deleterious effects and is associated with age-onset neurodegenerative diseases, directly contributing to their pathologies [86].

Within mitochondria, intricate surveillance systems monitor the quality of existing and newly synthesized mitochondrial proteins to ensure mitochondrial homeostasis [87]. The mitochondrial unfolded protein response (UPR^{mt}) consists of a signaling cascade that results in upregulation of nuclear-encoded genes to alleviate the stress sensed in mitochondria. Perception of misfolding in mitochondria requires the protease ClpP, which generates a mitochondrial derived signal to activate downstream genes [54]. ClpP triggers the activation of the ubiquitin-like protein UBL-5, which acts as a coactivator of the transcription factor DVE-1. UBL-5 and DVE-1 respond to mitochondrial perturbation to increase expression of mitochondrial chaperones, including *hsp-6* and *hsp-60* [56]. In parallel, the bZIP transcription factor ATFS-1 coordinates a wide cellular response to mitochondrial stress [28,88].

Previously, several genes characterized for their role in the regulation of the UPR^{mt} were identified as specific requirements for the long lifespan of animals with reduced mitochondrial function [41,42]. The requirements for these genes in electron transport chain (ETC)-mediated longevity suggested that the function of the UPR^{mt} might have a beneficial effect on the organism and was required to maintain the longer lifespans in the mitochondrial mutants. In this model, mitochondrial dysfunction early in development was capable of imposing a mild, hormetic stress that could remodel gene expression patterns, perpetuating a beneficial effect long into adulthood [42]. In keeping with this hypothesis, induction of the UPR^{mt} during early larval stages persists long into adulthood, suggesting that the animal may possess an epigenetic mechanism to maintain the activation of stress responses and ensure increased resistance to future mitochondrial insults [42]. In yeast, mitochondrial stress generated by reactive oxygen species (ROS) causes an epigenetic remodeling that extends lifespan [89], and forced expression of UPR^{mt} genes in *Drosophila* is sufficient to preserve mitochondrial function [44].

In this study we identify two conserved histone lysine demethylases as regulators of the ETC longevity pathway. Using RNAi-based screens in *C. elegans*, we isolated the conserved histone demethylases *jmjd-1.2* and *jmjd-3.1* as potent suppressors of longevity in response to mitochondrial perturbations. We demonstrate that both *jmjd-1.2* and *jmjd-3.1* are necessary and sufficient for activation of the UPR^mt in *C. elegans*. Moreover, our experiments identify *jmjd-1.2* and *jmjd-3.1* as positive regulators of a longevity response that genetically requires UPR^mt signaling. Using transcriptome analysis, we demonstrate that *jmjd-1.2* and *jmjd-3.1* coordinate the transcriptional response to mitochondrial stress. Furthermore, using a systems genetics approach, we find that the mammalian orthologs exhibit positive genetic correlations with UPR^mt core components in the BXD mouse genetic reference population [31,90]. Together, these data reveal a conserved epigenetic mechanism that determines longevity and stress signaling in response to mitochondrial dysfunction.

2.5 Results

2.5.1 Mitochondrial ETC-mediated longevity requires the histone lysine demethylases *jmjd-1.2* and *jmjd-3.1*

We performed an RNAi-based screen to identify genes specifically required for the ETC-mediated longevity in *C. elegans*. Through these analyses, we identified a putative histone lysine demethylase of the JumonjiC (JmjC)-domain-containing protein family, *jmjd-1.2 (F29B9.2)* [91], as a potent suppressor of the ETC longevity pathway (Figure 2:1A and Table 2:S1). We hypothesized that other JmjC domain containing demethylases may have similar effects on the regulation of lifespan. From the JmjC orthologs found in *C. elegans*, we identified a second histone lysine demethylase, *jmjd-3.1 (F18E9.5)*, that was also an effective suppressor of ETC-mediated longevity (Figure 2:1B and Table 2:S1). In their roles as demethylases, *jmjd-1.2* and *jmjd-3.1* have both distinct and overlapping specificity for histone modifications, most notably against H3K27me2/3 [92,93]. We found that both *jmjd-1.2* and *jmjd-3.1* were required for the extended lifespan caused by point mutation in the Rieske iron-sulfur protein (complex III), *isp-1(qm150)* [83] (Figures 2:1C, D). Downregulation of the closely related H3K27me2/3 demethylases *jmjd-3.2*, *jmjd-3.3* and *utx-1*, however, did not significantly affect lifespan extension by *cco-1* RNAi (Figure 2:S1A), highlighting a specific role of *jmjd-1.2* and *jmjd-3.1* for ETC-mediated longevity.
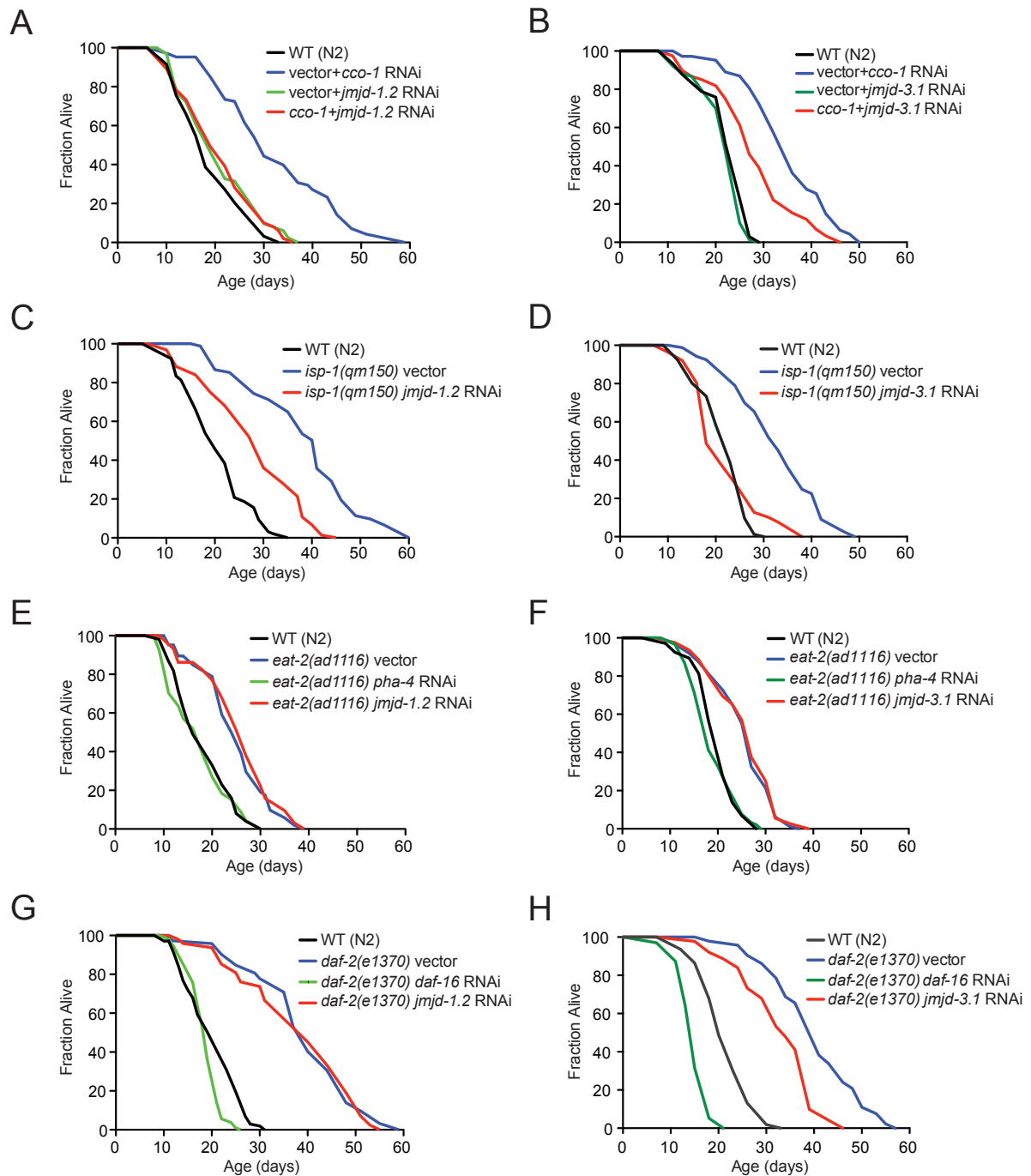
Figure 2:1 Lifespan extension by mitochondrial ETC perturbation requires the histone demethylases *jmjd-1.2* and *jmjd-3.1*.

(A) and (B) Knockdown of *jmjd-1.2* (A) or *jmjd-3.1* (B) suppresses *cco-1*-mediated lifespan extension. (C) *jmjd-1.2* is partially required for longevity of *isp-1(qm150)* mutant animals. (D) *jmjd-3.1* is required for longevity of *isp-1(qm150)* mutant animals. (E) and (F) Dietary restriction-mediated longevity of *eat-2(ad1116)* animals is not affected by *jmjd-1.2* (E) or *jmjd-3.1* (F) knockdown. (G) Longevity of *daf-2(e1370)* mutant animals is not affected by *jmjd-1.2* knockdown. (H) Longevity of *daf-2(e1370)* mutant animals partially depends on *jmjd-3.1*. See also Figure 2:S1 and Table 2:S1 for lifespan statistics.

Next, we assessed whether *jmjd-1.2* and *jmjd-3.1* were specific to lifespan extension in response to mitochondrial perturbation. The mitochondrial ETC longevity pathway acts in parallel to several other lifespan extending paradigms, including the insulin/IGF longevity response [4], dietary restriction (DR) [94], and germline-mediated longevity [95]. Neither *jmjd-1.2* nor *jmjd-3.1* downregulation altered longevity of dietary restricted *eat-2(ad1116)* animals (Figures 2:1E, F). We further found that *jmjd-1.2* had no effect on the lifespan of animals in which stress responses of the ER or cytosol were constitutively activated [96,97] (Figures 2:S1B-D) while transcription factors FoxO/*daf-16* and FoxA/*pha-4* successfully suppressed lifespan in our analyses (Figures 2:1E-H, Table 2:S1). In contrast, while *jmjd-1.2* RNAi did not affect the extended longevity seen in *daf-2(e1370)* mutant animals or germline deficient *glp-1(e2141)* animals (Figures 2:1G, S1B), we observed that the long lifespan *daf-2(e1370)* mutant worms depended on *jmjd-3.1*, albeit partially (Figure 2:1H). Recently *jmjd-3.1* was also reported to be required for the lifespan extension of germline-deficient *glp-1* animals [98]. Collectively, these data indicate that while *jmjd-3.1* is involved in several lifespan extension paradigms, both histone demethylases are required for ETC-mediated longevity.

2.5.2 Overlapping temporal requirements of jmjc demethylase activity and etc-mediated longevity

One of the most remarkable features of ETC-mediated longevity in C. elegans lies in its precise temporal requirements: Reduction of ETC function during a narrow window of development is sufficient to extend lifespan throughout life [49,69]. In contrast, loss of ETC function in adulthood is sufficient to reduce ATP production but can no longer affect lifespan. We reasoned that the activity of histone demethylases might be required during development and therefore performed RNAi shifting experiments in which we reduced ETC activity during development and restored them during adulthood by shifting young adults to Dicer (*dcr-1*) RNAi to inhibit the RNAi machinery [49,79]. We found that reduction of *jmjd-1.2* during larval development was sufficient to block *cco-1* mediated longevity (Figure 2:S1E). *jmjd-1.2* RNAi during adulthood, in contrast, reduced *cco-1* lifespan partially (Figure 2:S1F). *jmjd-3.1* was partially required for *cco-1* mediated longevity during larval development but had only a minor effect during adulthood (Figures 2:S1G, H). These data suggest that both *jmjd-1.2* and *jmjd-3.1* are required for an initial response to ETC deficiency during development that is maintained into adulthood.

2.5.3 JMJD-1.2 and JMJD-3.1 regulate the Mitochondrial Unfolded Protein Response (UPR^mt)

Previously, the UPR[mt] was found to be required for the extended longevity of mitochondrial mutants [42]. We therefore asked whether *jmjd-1.2* and *jmjd-3.1* had any effect on the induction of the UPR[mt] in *C. elegans*. In these analyses, *cco-1* RNAi was used as a potent inducer of both *hsp-6* and *hsp-60* endogenous transcripts, robustly turning on the transcriptional *hsp-6p::gfp* reporter [30]. As reported, *cco-1* mediated UPR[mt] activation required the ClpP protease *clpp-1* and the homeodomain transcription factor *dve-1* [54] (Figures 2:2A and 2:S2B). Similarly, RNAi of either *jmjd-1.2* or *jmjd-3.1* suppressed the *hsp-6p::gfp* reporter activation elicited by *cco-1* [42] (Figures 2:2A and 2:S2A), *spg-7* [30] (Figures 2:2B and 2:S2C) or *mrps-5* [41] knockdowns (Figure 2:S2D).

We tested additional JmjC-containing proteins for their effects on UPR[mt] following mitochondrial stress (Figure 2:S2A). Interestingly, RNAi against the H3K27 demethylase family members *jmjd-3.2*, *jmjd-3.3* and *utx-1* also substantially decreased UPR[mt] activation, while other JmjC-domain containing demethylases had no significant effect on UPR[mt] activation (Figures 2:2B, 2:S2A). As an alternative approach, we used the H3K27 demethylase inhibitor GSK-J4 [99] to examine potential activity towards UPR[mt] induction. GSK-J4 treatment of *hsp-6p::gfp* reporter animals grown on *mrps-5* RNAi suppressed UPR[mt] activation (Figure 2:S2E) indicating that H3K27 demethylase activity was required for the perpetuation of mitochondrial stress signaling. As H3K27 methylation can be established by the Polycomb repressive complex 2 (PRC2) in *C. elegans* [100], we asked whether reduction of polycomb components is sufficient to trigger the UPR[mt]. However, knockdown of individual PRC2 components *mes-2*, *mes-3* and *mes-6* in *C. elegans* did not activate UPR[mt] signaling (Figure 2:S2F).

We next examined a potential contribution of *jmjd-1.2* and *jmjd-3.1* on additional cellular stress responses including the unfolded protein response of the endoplasmic reticulum (UPR[er]) (Walter and Ron, 2011) and the cytosolic heat shock response (HSR) [19]. RNAi against *jmjd-1.2* did not affect induction of UPR[er] target genes, including the ER chaperone BiP (*hsp-4),* in response to UPR[er] stimulation with tunicamycin (Figures 2:2C, 2:S3A). In contrast, *jmjd-3.1* RNAi revealed minor but statistically significant effects on several UPR[er] target genes, which became evident only upon monitoring gene expression independent of the *hsp-4p::gfp* reporter (Figure 2:2D, 2:S3B), consistent with recent findings [98]. Moreover, RNAi against *jmjd-1.2* or *jmjd-3.1* did not affect the heat shock-induced expression of the HSR chaperone *hsp-16.2* (Figures 2:2E, F; 2:S3C, D). Finally, *jmjd-1.2* and *jmjd-3.1* had no effect on the expression of the antioxidant enzyme *sod-3*, which is induced by reduced insulin/IGF-1 signaling (Figure 2:2G, H). Collectively, these data
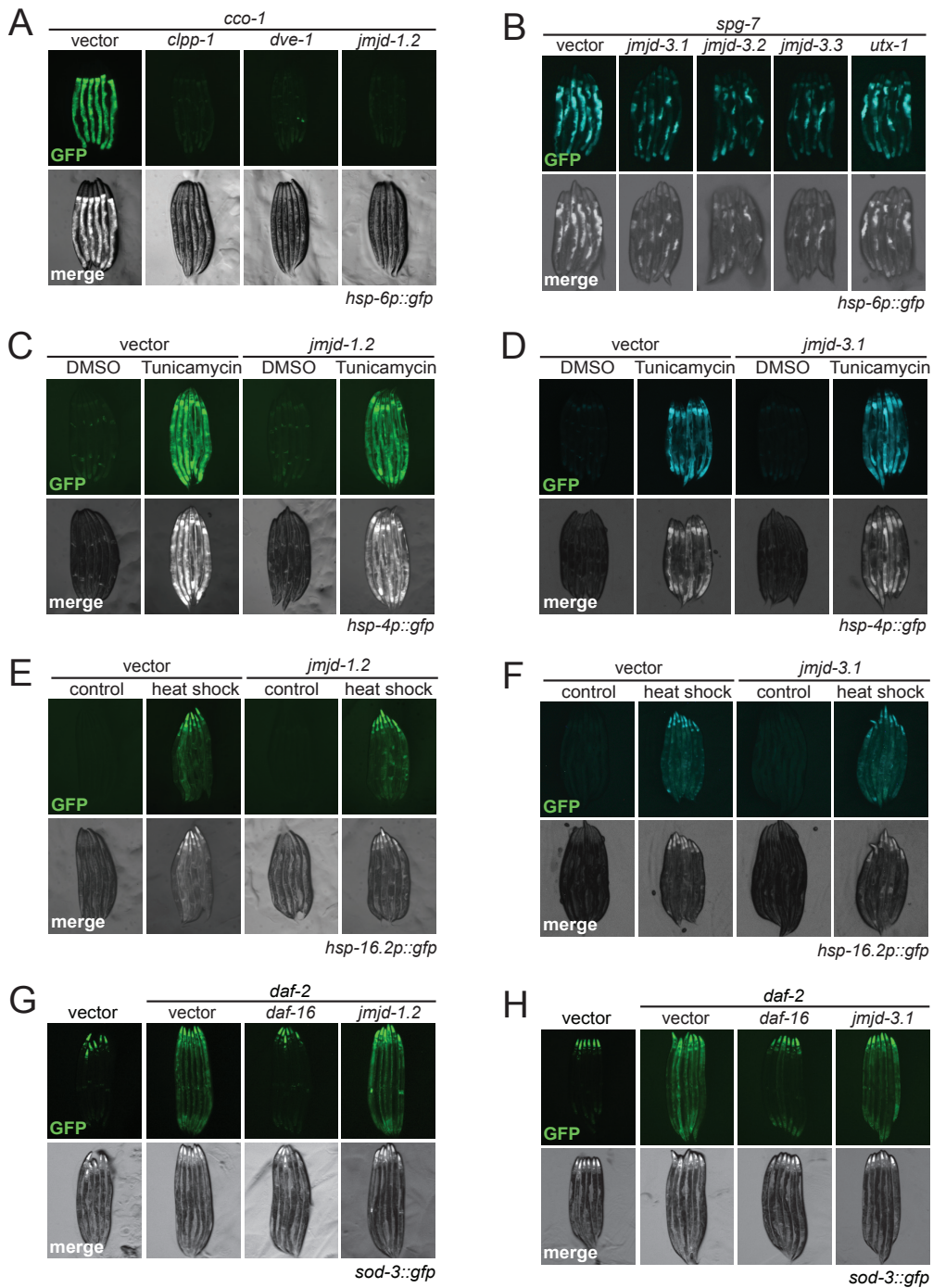
Figure 2:2 *jmjd-1.2* and *jmjd-3.1* are necessary and specific for induction of the UPR^{mt}.

(A) Fluorescent micrographs of *hsp-6p::gfp* UPR^{mt} reporter animals treated with the indicated RNAi at day 1 of adulthood. Knockdown of *jmjd-1.2* suppresses *cco-1*-mediated UPR^{mt} induction in *hsp-6p::gfp* reporter animals. (B) Knockdown of *jmjd-3* histone demethylase family members suppresses *spg-7*-mediated UPR^{mt} induction. (C) and (D) Fluorescent micrographs of *hsp-4p::gfp* UPR^{er} reporter animals. Induction of the UPR^{er} response in *hsp-4p::gfp* UPR^{er} reporter animals by tunicamycin treatment is not affected by neither *jmjd-1.2* (C) or *jmjd-3.1* (D) RNAi. (E) and (F) Fluorescent micrographs of *hsp-16.2p::gfp* reporter animals. Induction of the heat shock response in *hsp-16.2p::gfp* reporter animals occurs independently of *jmjd-1.2* (E) or *jmjd-3.1* (F) RNAi. (G) and (H) Fluorescent micrographs of *sod-3::gfp* reporter animals treated with the indicated RNAi. *daf-16* RNAi was used as a positive control. See also Figures 2:S2 and 2:S3.

35

indicate that *jmjd-1.2* specifically modulates the UPR^{mt}, while *jmjd-3.1* appears to be moderately involved in the transcriptional response to ER stress.

2.5.4 Overexpression of *jmjd-1.2* or *jmjd-3.1* is sufficient for lifespan extension and UPR^{mt} induction

The results of the previous experiments indicated that both *jmjd-1.2* and *jmjd-3.1* were required for ETC-mediated longevity and UPR^{mt} induction. We next tested their sufficiency to extend lifespan and increase mitochondrial stress signaling. We generated transgenic strains expressing *jmjd-1.2* under control of the ubiquitous *sur-5* promoter and monitored lifespan. For control, we generated an enzymatically inactive version of *jmjd-1.2* that harbors a point mutation in the catalytic histidine of the JmjC domain (*jmjd-1.2^{H508A}*). *jmjd-1.2* overexpression significantly increased longevity when compared to wild type animals (Figure 2:3A), while the catalytically-inactive *jmjd-1.2^{H508A}* had no effect (Figure 2:S4A). We also generated strains overexpressing *jmjd-3.1* under the control of its endogenous promoter (*jmjd-3.1p::jmjd-3.1::UTR*) and found these animals to be long-lived (Figure 2:3B), in agreement with previous reports [98].

Intriguingly, overexpression of either *jmjd-1.2* or *jmjd-3.1* was sufficient to induce the UPR^{mt} (Figures 2:3C-F). To identify the tissues in which expression was required, we generated transgenic strains expressing *jmjd-1.2* in either neurons or the intestine. Neuronal overexpression of *jmjd-1.2* was sufficient for lifespan extension and UPR^{mt} activation, while expression in the intestine did not (Figures 2:3G, H, 2:S4B). Similarly, overexpression of the catalytically inactive *jmjd-1.2^{H508A}* variant failed to activate the UPR^{mt} (Figure 2:S4B). Moreover, *jmjd-1.2* overexpression had no effect on mRNAs levels of UPR^{er} and HSR target genes indicating that *jmjd-1.2* selectively modulates the UPR^{mt} (Figures 2:S4C, D). *jmjd-3.1* overexpression, however, lead to a significant increase in expression of some UPR^{er} target genes, but not of the HSR (Figures 2:S4E, F).

2.5.5 The UPR^{mt} is a genetic requirement for JmjC demethylase-mediated longevity

The ubiquitin-like protein UBL-5 is required for increased longevity of the ETC mutant *isp-1(qm150)* [42] (Figure 2:S4G). Therefore, we tested whether the long lifespan of *jmjd-1.2* and *jmjd-3.1* overexpressing animals depended upon *ubl-5*. Intriguingly, *ubl-5* RNAi fully suppressed increased longevity of both *jmjd-1.2* and *jmjd-3.1*, as well as neuron-specific *jmjd-1.2* overexpressing animals.(Figures 2:4A-C). Notably, *ubl-5* was not required for increased longevity of animals ubiquitously expressing heat shock factor-1 (HSF-1) [96] (Figure 2:S4H) and had no effect on wild type lifespan [42]. These data   strongly suggest
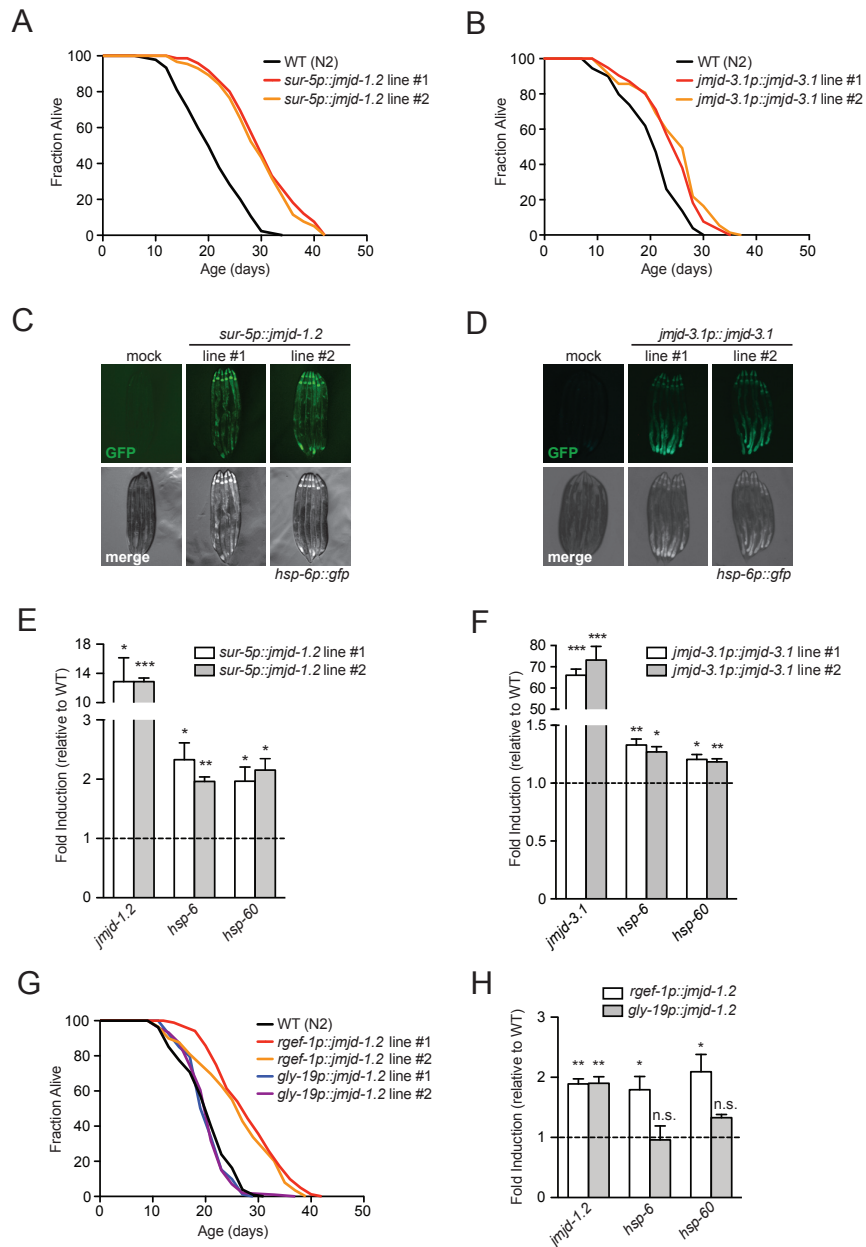
Figure 2:3 *jmjd-1.2* and *jmjd-3.1* overexpression is sufficient for lifespan extension and UPR^mt induction.

(A) and (B) Overexpression of *jmjd-1.2* and *jmjd-3.1* extends *C. elegans* lifespan. Lifespan analysis of two independent transgenic lines of *sur-5p::jmjd-1.2* (A) or *jmjd-3.1p::jmjd-3.1* (B) expressing animals compared to WT (N2) animals. (C) and (D) Fluorescent micrographs of *hsp-6p::gfp* UPR^mt reporter animals expressing either *sur-5p::jmjd-1.2* (C) or *jmjd-3.1p::jmjd-3.1* (D) transgenes in two independent lines analyzed at day 1 of adulthood. (E) and (F) Transcript levels in two independent lines of *sur-5p::jmjd-1.2* (E) or *jmjd-3.1p::jmjd-3.1* (F) expressing animals at day 1 of adulthood were measured by qRT-PCR. Results are shown relative to transcript levels in WT (N2) animals, with error bars indicating mean ± SEM. *** denotes $p < 0.001$, **$p < 0.01$, *$p < 0.05$. (G) Neuron-specific overexpression of *jmjd-1.2* is sufficient to extend lifespan. Lifespan analysis of two independent lines expressing either pan-neuronal (*rgef-1p::jmjd-1.2) or intestinal (gly-19p::jmjd-1.2)* transgenes compared to WT (N2) animals. (H) Transcript levels in animals expressing either pan-neuronal (*rgef-1p::jmjd-1.2)* or intestinal (*gly-19p::jmjd-1.2)* transgenes at day 1 of adulthood were measured by qRT-PCR. Results are shown relative to transcript levels in WT (N2) animals, with error bars indicating mean ± SEM. ** denotes $p < 0.01$, *$p < 0.05$, n.s. = $p > 0.05$. See also Figure 2:S4 and Table 2:S1 for lifespan statistics.

that the UPR^{mt} is an essential and specific requirement in H3K27 demethylase *gain-of-function* models. Since both *jmjd-1.2* and *jmjd-3.1* overexpression induced the UPR^{mt}, we also tested the requirement of the UPR^{mt} core components *clpp-1* and *atfs-1* for UPR^{mt} activation in response to demethylase overexpression. RNAi against *atfs-1* and *clpp-1* in strains overexpressing *jmjd-1.2* or *jmjd-3.1* efficiently abrogated UPR^{mt} signaling, suggesting that *jmjd-1.2* and *jmjd-3.1* function upstream of the core transcriptional UPR^{mt} machinery in *C. elegans* (Figure 2:4D-I).
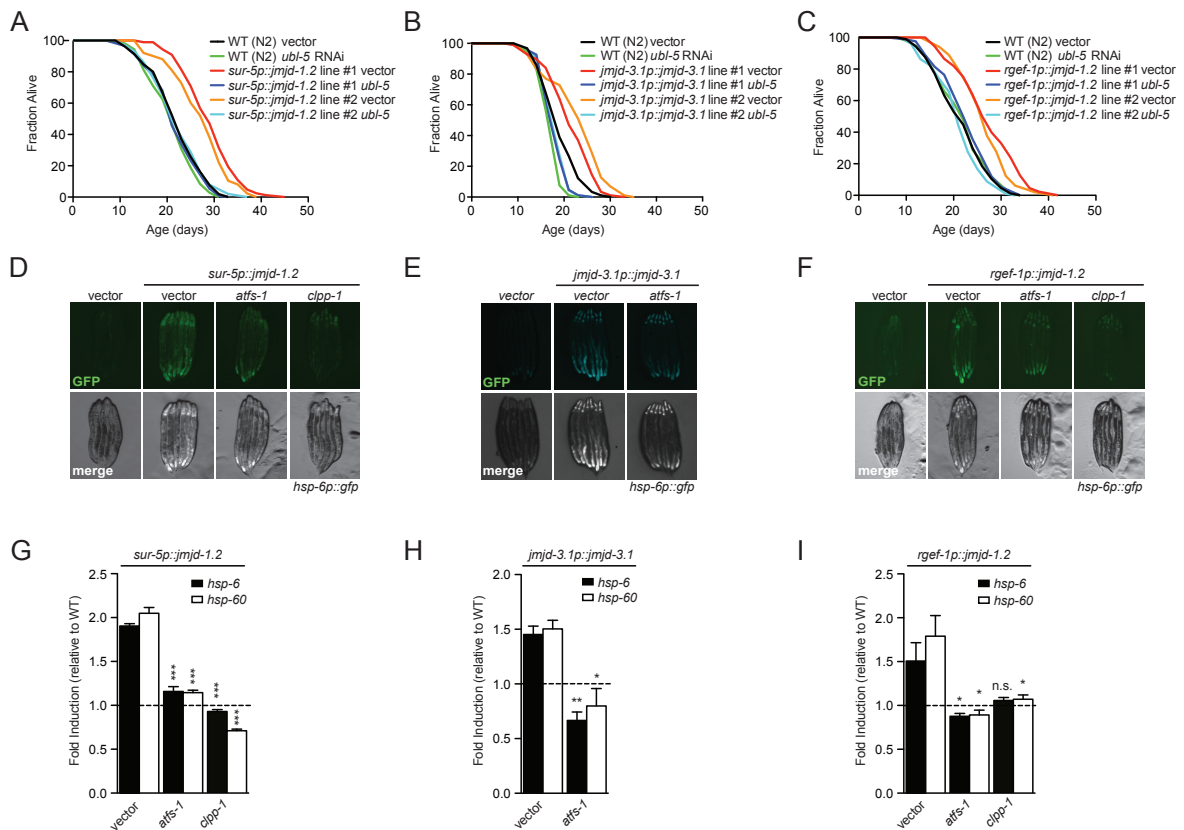
Figure 2:4 The UPR^{mt} is a genetic requirement for the pro-longevity response upon *jmjd-1.2* and *jmjd-3.1* overexpression.
(A), (B) and (C) *ubl-5* RNAi suppresses lifespan extension upon *jmjd-1.2*, *jmjd-3.1* or neuronal *jmjd-1.2* overexpression. Lifespan analysis of two independent lines of *sur-5p::jmjd-1.2* (A), *jmjd-3.1p::jmjd-3.1* (B), neuronal *rgef-1p::jmjd-1.2* (C) and WT (N2) animals grown on empty vector control or *ubl-5* RNAi. (D), (E) and (F) Fluorescent micrographs of *hsp-6p::gfp* UPR^{mt} reporter animals expressing the indicated transgenes treated with the indicated RNAi, at day 1 of adulthood. (G), (H) and (I) Transcript levels of canonical UPR^{mt} targets assessed by qRT-PCR in *sur-5p::jmjd-1.2* (G), *jmjd-3.1p::jmjd-3.1* (H) or neuronal *rgef-1p::jmjd-1.2* (I) transgenic animals at day 1 of adulthood treated with the indicated RNAi. Results are shown relative to transcript levels in WT (N2) animals grown on the indicated RNAi, with error bars indicating mean ± SEM. *** denotes $p < 0.001$, **$p < 0.01$, *$p < 0.05$, n.s. = $p > 0.05$. See also Figure 2:S4 and Table 2:S1 for lifespan statistics.

2.5.6 JMJD-1.2 and JMJD-3.1 overexpression recapitulates the transcriptional response to mitochondrial stress.

To understand the molecular mechanisms that underlie the extended longevity in response to mitochondrial ETC perturbation and histone demethylase overexpression on a whole genome level, we performed RNA-seq analysis of strains ubiquitously overexpressing *jmjd-3.1* or *jmjd-1.2*, or neuronally-expressed *jmjd-1.2,* and compared them to *cco-1* RNAi treated animals. Our analysis identified ~3,000-7,500 differentially expressed genes (DEGs) in each condition (adjusted p-value < 0.05), with the greatest number of changes observed in the *jmjd-3.1p::jmjd-3.1* strain (Figure 2:5A). Strikingly, almost half the genes differentially expressed upon *cco-1* RNAi treatment (1405/2979) were also significantly differentially expressed in all three demethylase overexpression strains, and 84% (2505/2979) were in common with at least one of the examined overexpression strains (Figure 2:5A). Among the overlapping DEGs, 99% (1385/1405) of gene expression changes go in the same direction in all 4 conditions (Figure 2:5E). These data indicate that an overwhelming majority of the gene expression changes induced by *cco-1* RNAi are recapitulated by overexpression of *jmjd-1.2* or *jmjd-3.1*. Furthermore, an examination of all nine JmjC-domain encoding genes revealed that *jmjd-1.2* and *jmjd-3.1* were specifically upregulated in response to *cco-1* RNAi treatment (Figure 2:5B). These data place *jmjd-1.2* and *jmjd-3.1* downstream of mitochondrial stress and support a model in which a majority of the transcriptional response to mitochondrial stress is mediated by *jmjd-1.2* and *jmjd-3.1*.

The 1405 overlapping genes were subjected to Gene Ontology (GO) analysis using the DAVID database [101]. Among the upregulated genes, signaling and cell communication related terms were enriched (Figure 2:5D). Importantly, larval development and growth, as well as multiple protein processing pathways, such as translation and proteasome were extensively downregulated, consistent with global remodeling of the proteome in response to stress (Figure 2:5D). Whereas the majority of mitochondrial genes were significantly reduced in all examined conditions (Figure 2:5F, G), many of the UPRmt components, such as the chaperone hsp-6, the proteases ymel-1 and spg-7 as well as the transcriptional regulator dve-1 were induced (Figure 2:5C). Remarkably, OXPHOS genes in jmjd-1.2 and jmjd-3.1 overexpression strains were downregulated to a similar extent as in cco-1 RNAi treated animals (Figure 2:5G). Surprisingly, there were only a few OXPHOS components that were significantly upregulated in all conditions, specifically cyc-1 from complex III and mtDNA encoded nduo-2, nduo-4 and nduo-5. Intriguingly, this finding is
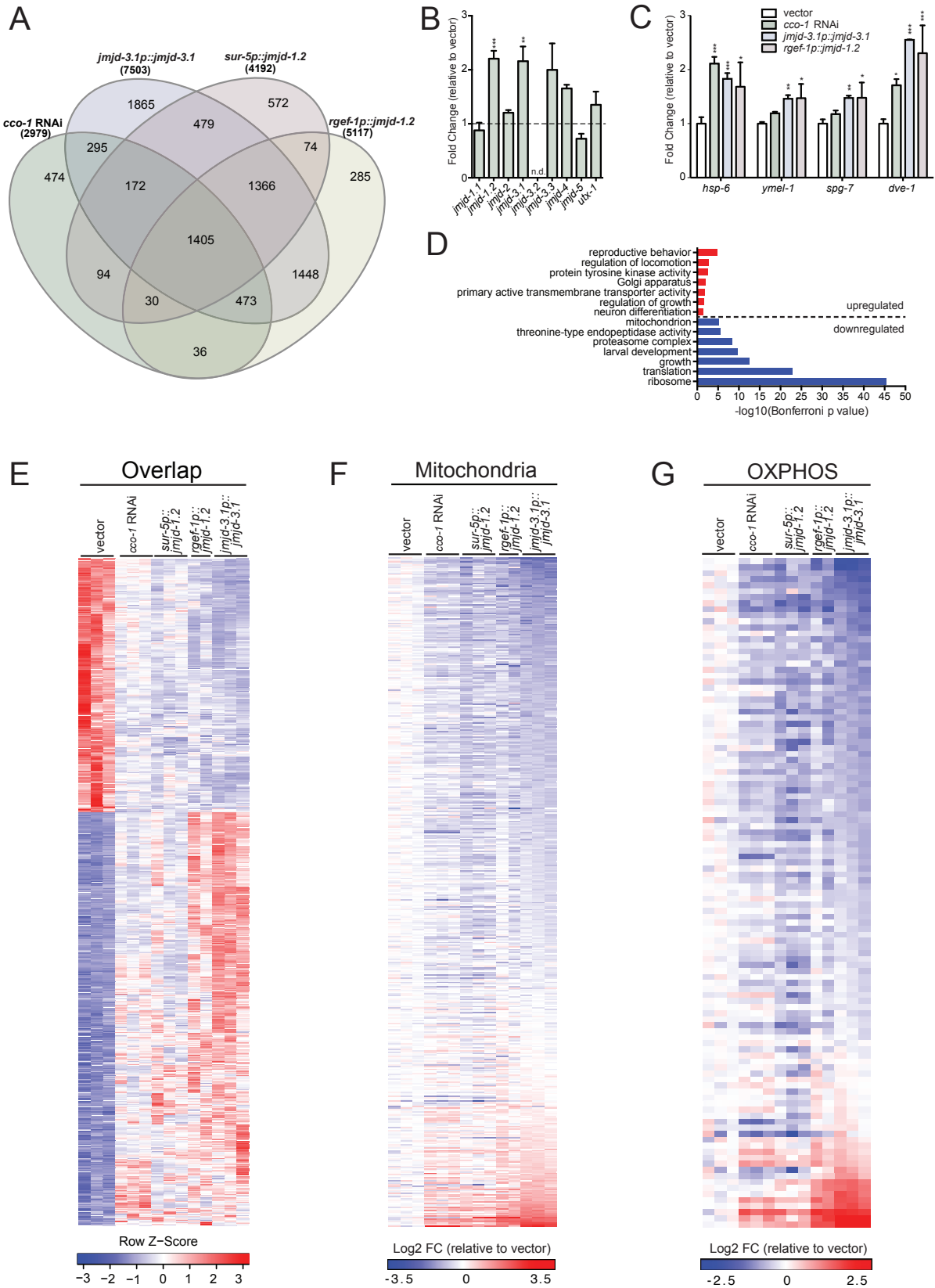
Figure 2:5 ETC perturbation and JMJD overexpression share common lifespan extension mechanisms

(A) Venn diagram of differentially expressed genes (DEGs) in *cco-1* RNAi treated worms and transgenic overexpression lines *jmjd-3.1p::jmjd-3.1*, *sur-5p::jmjd-1.2*, *rgef-1p::jmjd-1.2*, compared to wild type N2 worms on empty vector control, as measured by RNA-seq (Benjamini-Hochberg adjusted p value < 0.05). (B) Transcriptional upregulation of *jmjd-1.2* and *jmjd-3.1* upon *cco-1* RNAi. Gene expression analysis of all nine JmjC domain encoding genes in RNA-seq samples, expressed as fold change relative to wild type N2 on empty vector control. Results are expressed as mean ±SEM of normalized count values (n=3, Benjamini-Hochberg adjusted p values (padj) calculated by DESeq2, *jmjd-1.2* padj=6.93E-09, *jmjd-3.1* padj=0.002, *jmjd-3.3* padj=0.452, *jmjd-4* padj=0.085. n.d.= not detected, ** denotes p < 0.01, ***p < 0.001). (C) UPR^{mt} gene expression in RNA-seq samples, expressed as fold change relative to wild type N2 on empty vector control. Results are expressed as mean ±SEM of normalized count values. * denotes p < 0.05, **p < 0.01, ***p < 0.001). (D) Representative top GO terms of upregulated and downregulated genes in the 1405 overlapping DEGs (Bonferroni adjusted p value<0.05). (E) Gene expression heatmap of 1405 overlapping DEGs in all 4 conditions described in (A). DESeq2-normalized count values were used for calculations. The indicated Row Z-scores reflect the number of standard deviations each replicate is apart from the mean gene expression value over all conditions. (F) Heatmap of 470 mitochondrial genes from GO cellular component category mitochondrion (GO:0005739). Fold change (FC) was calculated by comparing normalized count values of each condition to wild type N2 empty vector control, then transformed to log2 scale. (G) Heatmap of 111 OXPHOS genes from GO biological process category oxidative phosphorylation (GO:0006119) and manual annotation.

reminiscent of mito-nuclear protein imbalance, a phenomenon of contrasting expression between nuclear- and mtDNA encoded OXPHOS components which tightly couples UPR^{mt} activation with longevity across organisms [41].

2.5.7 Mammalian PHF8 and JMJD3 correlate with lifespan and UPR^{mt} activation

To assess the potential roles of *jmjd-1.2* and *jmjd-3.1* in regulating UPR^{mt} and longevity in mammals, we investigated their murine homologs *Phf8* and *Jmjd3*, respectively, in the GeneNetwork database (www.genenetwork.org), which contains a vast collection of clinical and molecular (transcript and protein expression) phenotypes from the BXD mouse genetic reference panel (GRP) [31,90]. Importantly, variations within these datasets reflect mild, natural variations in gene expression patterns found in isogenic populations and are not reliant upon more deleterious genetic manipulations of mitochondrial function.

Both the transcripts for *Phf8* and *Jmjd3* showed high levels of variability in expression across the tissues and strains examined (Figure 2:6A). In tissue-specific datasets, natural variations in *Phf8* expression in the hypothalamus, spleen, and amygdala positively correlated with *Jmjd3* expression (Figure 2:6B), suggesting a correlative genetic interaction between the two enzymes. Importantly, expression levels of both histone demethylases were also positively correlated with UPR^{mt} related genes, including *Hspd1* (encoding the mitochondrial chaperone HSP60), *Satb1*, *Satb2* (orthologs of the *C. elegans* UPR^{mt} regulator *dve-1*), *Abcb10* (ortholog of the mitochondrial peptide exporter *haf-1*) [55] and *Ubl5* (ortholog of *ubl-5*) across an array of tissues (Figures 2:6C, D). The strongest associations were observed in the hypothalamus, in which UPR^{mt} related genes in addition to *Phf8* and *Jmjd3* formed a connected correlation network (Figure 2:6E).
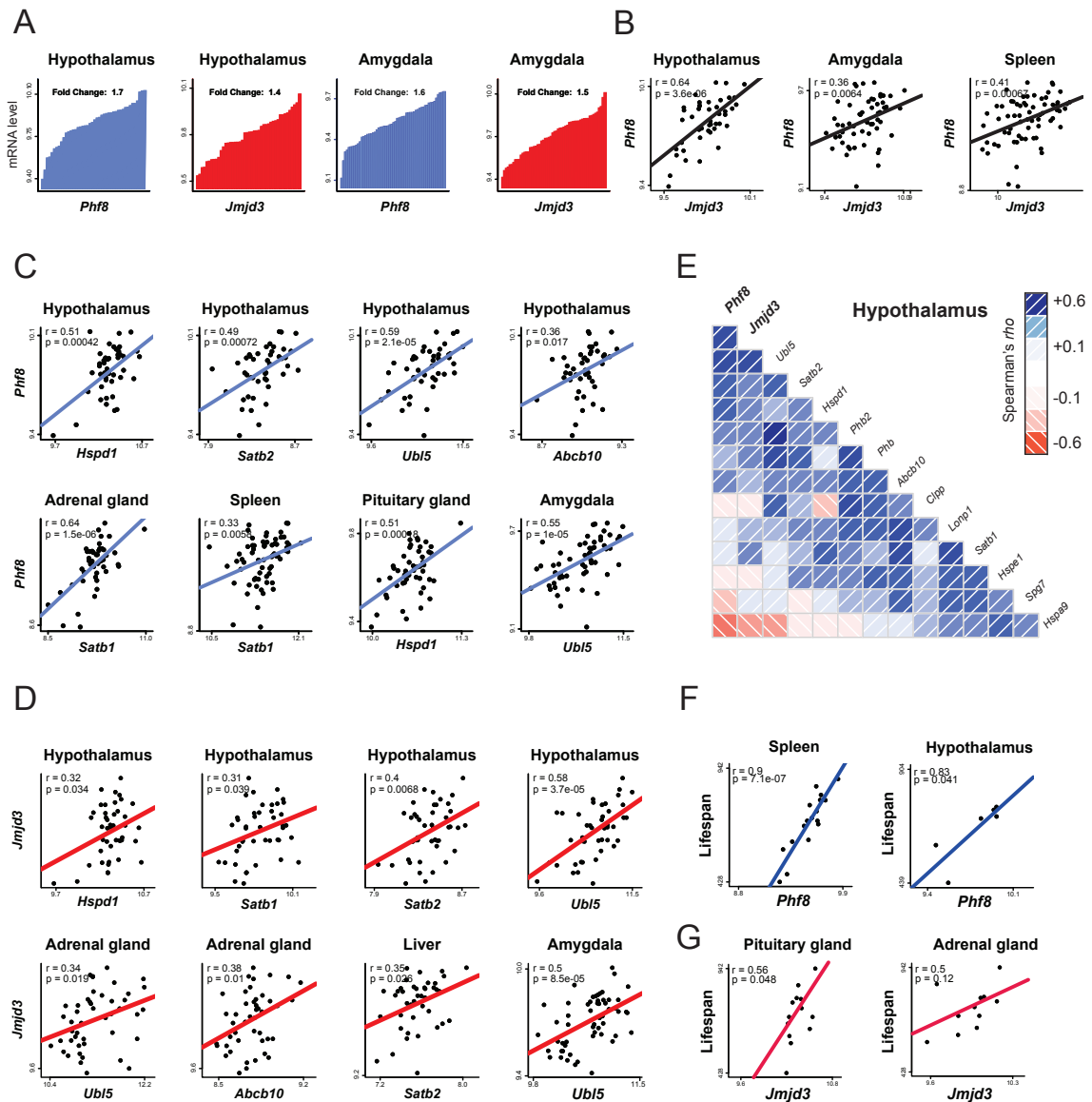
Figure 2:6 Positive correlations between *Phf8*, *Jmjd3*, lifespan and UPR^{mt} transcripts in the BXD Mouse Genetic Reference Population.

(A) Variation of *Phf8* and *Jmjd3* mRNA levels in hypothalamus (n=44) and amygdala (n=56) across BXD mouse strains. Each bar represents mRNA levels from a pool of approximately five animals per strain. (B) Positive correlations between *Phf8* (y-axis) and *Jmjd3* (x-axis) expression in hypothalamus (n=44), amygdala (n=56) and spleen (n=67). (C) Positive correlations between *Phf8* (y-axis) and selected UPR^{mt} genes (x-axis) transcripts in various tissues (n=46 for adrenal gland, n=49 for pituitary gland). (D) Positive correlations between *Jmjd3* (y-axis) and selected UPR^{mt} genes (x-axis) transcripts in various tissues (n=46 for liver). (E) Spearman's correlation co-expression network for *Phf8*, *Jmjd3* and UPR^{mt} genes in hypothalamus. Blue correlations are positive, red correlations are negative – intensity of the colors corresponds to correlation coefficients. (F) Pearson correlations of Lifespan versus *Phf8* transcript levels in either spleen (left) or hypothalamus (right) of BXD mice. (G) Pearson correlations of Lifespan versus *Jmjd3* transcript levels in either pituitary gland (left) or adrenal gland (right) of BXD mice.

In accordance with the impact of *jmjd-1.2* and *jmjd-3.1* on lifespan regulation in *C. elegans*, we observed correlations between *Phf8* and *Jmjd3* expression and lifespan in the spleen and hypothalamus or pituitary and adrenal glands of mice, respectively (Figure 2:6F, G).

Across strains expressing variable levels of *Phf8* mRNA, using immunoblotting, we found a correlative change of PHF8 protein, which was paralleled by a reduction of global H3K27me2 levels (Figure 2:7A). Increased PHF8 protein levels were also associated with higher abundance of UPR[mt] marker proteins, such as the chaperones mtHSP70 and HSP60 (Figure 2:7B), reminiscent of the transcript correlations (Figure 2:6C). Similarly, higher JMJD3 levels were associated with an increase of HSP60 protein (Figure 2:7C).

We hypothesized that a relationship between the expression of markers of UPR[mt], *Phf8*, and *Jmjd3* also might be detectable in mammalian *Jmjd3 loss-of-function* experiments, which have been published previously (GEO datasets GSE40332, GSE56696) [102]. Consistent with our prediction, in *Jmjd3* knockout mouse embryos (GSE40332), the expression of various UPR[mt] related transcripts was decreased (Figure 2:7D). Likewise, knockdown of JMJD3 by shRNA in two human T-cell lymphoma cell lines (CUTLL1 and CEM) decreased the expression levels of multiple transcripts related to the UPR[mt] (Figure 2:7E). Similarly, treatment of CUTLL1 cell line with the H3K27 demethylase inhibitor GSK-J4 (GSE56696) [102] also decreased the levels of multiple UPR[mt] transcripts in a time-dependent fashion (Figure 2:7F). Overall, these data in both the murine GRP, mice with *loss-of-function* alleles, or cell lines with modified levels or activity of PHF8 and/or JMJD3 collectively suggest that expression levels of these demethylases positively correlate with UPR[mt] expression.

Finally, we examined ChIP-seq analysis of CUTLL1 cells treated with shJMJD3 (GSE56696) for evidence of direct JmjC regulation of chromatin at coding regions of UPR[mt] target genes. In these analyses, we found that H3K27me3 enrichment on *HSPD1*, *HSPE1*, and *SATB1* genes was increased upon JMJD3 knockdown (Figure 2:7G), indicating that the repressive H3K27me3 mark may be actively removed from the coding regions of these genes by JMJD3, thereby allowing for their expression. In another independent ChIP-seq dataset (GSE20725) [103], PHF8 was found to bind to coding regions of UPR[mt] genes *HSPD1*, *HSPE1* and *UBL5* in both HeLa and 293T cells (Figure 2:7H). In addition to these *in silico* analyses, we examined H3K27me3 occupancy at coding regions of UPR[mt] regulators during mitochondrial stress in larval stage *C. elegans* by ChIP-qRT-PCR. We observed a substantial decrease in H3K27me3 abundance on *hsp-6*, *clpp-1* and *atfs-1* genes upon *cco-1* RNAi during early larval development (Figure 2:7I). Taken together, these data suggest that PHF8 and JMJD3 may be conserved positive regulators of UPR[mt] and lifespan from *C. elegans* to mammals, through the modulation of the H3K27 methylation status at coding regions of key UPR[mt] genes.
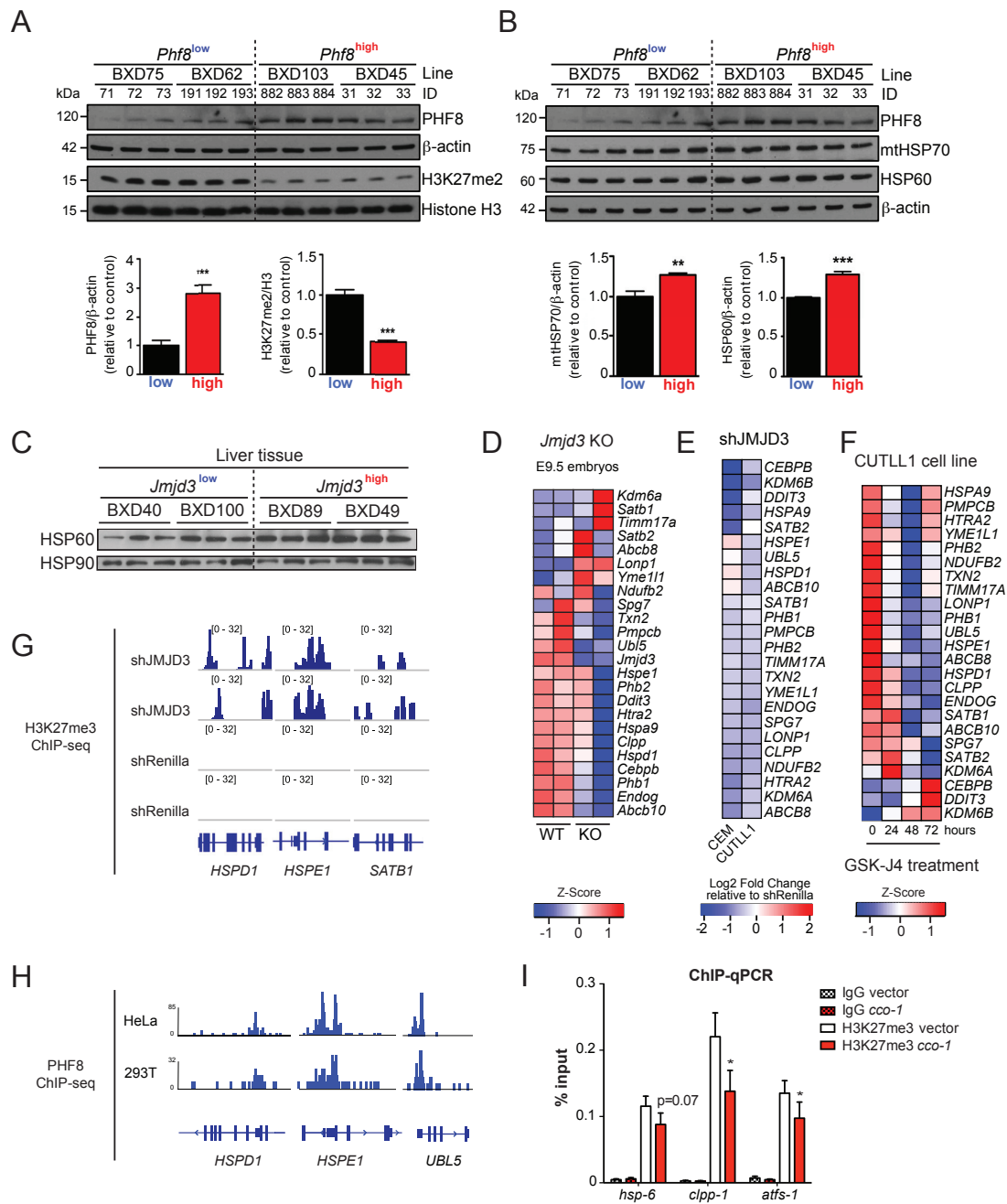
Figure 2:7 Conserved UPR^mt gene regulation mechanisms through H3K27 demethylases.

(A) and (B) Immunoblot analysis of tissue protein lysates using the indicated antibodies. Increased *Phf8* expression correlates with reduced H3K27me2 (A) and higher levels of mitochondrial chaperones (B) in the hypothalamus of the indicated BXD mouse strains. β-actin and Histone H3 were used as loading controls (upper panels). Densitometric quantifications of immunoblot signals normalized to either β-actin or Histone H3 (lower panels). Data represent the mean ± SEM. *** denotes p < 0.001, **p < 0.01. (C) Immunoblot analysis of BXD liver tissue protein lysates using the indicated antibodies. HSP90 was used as a loading control. (D) Heatmap of selected UPR^mt transcripts in WT and *Jmjd3* KO mice embryos at E9.5 (GSE40332). Low expression is shown in blue, while high expression is in red. (E) Heatmap of fold change in UPR^mt transcripts upon shJMJD3 treatment relative to shRenilla in human T-cell lymphoblastic leukemia CEM and CUTLL1 cell lines (GSE56696). (F) Heatmap of selected UPR^mt transcripts in the human T-cell lymphoblastic leukemia CUTLL1 cell line upon treatment with the H3K27 demethylase inhibitor GSK-J4 (GSE56696). (G) ChIP-Seq profiles of H3K27me3 enrichment at selected UPR^mt genes in the CUTLL1 cell

line upon shJMJD3 and shRenilla treatments (GSE56696). (H) ChIP-Seq profiles of PHF8 binding at selected UPR[mt] gene promoters in HeLa and 293T cells (GSE20725). (I) ChIP-qRT-PCR analysis of H3K27me3 enrichment at UPR[mt] genes at L3 stage of *cco-1* RNAi treated worms compared to empty vector control. IgG antibody was used as a control. Results are expressed as percent of input, with error bars indicating mean ± SEM (n=7, * denotes p < 0.01).

2.6 Discussion

The distinct timing requirements of lifespan extension due to mild mitochondrial dysfunction during larval development led to the early proposal of an epigenetic mechanism that determines ETC-mediated longevity of *C. elegans* [42,49]. Remarkably, the discovery that the UPR[mt] is not only a genetic requirement but also shares these overlapping timing requirements with ETC-mediated longevity reinforces the idea that primary mitochondrial perturbations establish an epigenetic memory which sets the rate of aging of the entire organism and protects its mitochondrial proteome from future insults [42]. The identification of *jmjd-1.2/PHF8* and *jmjd-3.1/JMJD3* provides a molecular explanation for these observations and suggests the epigenetic regulation of transcriptional outputs during mitochondrial stress. We find *jmjd-1.2* to be not only necessary and specific, but also sufficient for both induction of the UPR[mt] and extension of lifespan. *jmjd-3.1* is also necessary and sufficient for UPR[mt] induction and lifespan extension, but has overlapping roles in ER stress regulation [98].

The two histone demethylases differ in their substrate specificity: While *jmjd-3.1/*JMJD3 is associated with the removal of H3K27me2/3 epigenetic marks [92], *jmjd-1.2/*PHF8 has activity towards a wider range of substrates, including H3K9me1/2, H3K27me2 and H4K20me1 [93,103-106]. Both genes are associated with the positive regulation of gene expression and the removal of repressive marks. This raises the intriguing possibility that both enzymes might function in a linear pathway to sequentially demethylate H3K27me3 and thereby activate gene expression in response to mitochondrial perturbations. This hypothesis is supported by the mitochondrial stress-induced reduction of H3K27me3 occupancy at UPR[mt] response genes during larval development in worms (Figure 2:7I). Our results are therefore consistent with the idea that removal of repressive marks might allow access of the core UPR[mt] transcriptional machinery to induce mitochondrial stress signalling [28,55].

How is mitochondrial stress sensed by *jmjd-1.2*/PHF8 and *jmjd-3.1*/JMJD3? An attractive idea is that both *jmjd-1.2* and *jmjd-3.1* themselves are targets of the transcriptional response to mitochondrial stress as indicated in our transcriptomics analyses (Figure 2:5B). Another possibility is that acute adaptations in mitochondrial metabolism may

promote activity of JmjC demethylases. Since both JMJD3 and PHF8 belong to the family of 2-oxoglutarate dependent oxygenases, it appears likely that elevated levels of the TCA cycle intermediate alpha-ketoglutarate (α-KG) might contribute to their increased activity [107]. Intriguingly, the exogenous supplementation of α-KG has recently been found to extend lifespan of *C. elegans* [108]. While RNAi knockdown experiments for both *jmjd-1.2* and *jmjd-3.1* revealed robust suppression of ETC-mediated longevity and UPR^{mt} induction, we did not find strong effects on lifespan and *hsp-6* transcriptional induction in the analysis of the respective mutant strains suggesting that an acute depletion of the enzymes during larval development rather than chronic deficiency is necessary to unmask their role for these phenotypes (Figure 2:S5).

In this work, we identify neurons as a key tissue to promote longevity and UPR^{mt} induction upon neuron-specific *jmjd-1.2* overexpression. Neuronal *jmjd-1.2* is not only sufficient to mediate a robust UPR^{mt} induction but also extends *C. elegans* lifespan in an UPR^{mt}-dependent manner. These findings were corroborated in mice and appear to be conserved in the BXD mouse reference population. Across various neuronal subregions, high levels of PHF8 and JMJD3 correlate with increased expression of mammalian UPR^{mt} core components (CLPP, ABCB10, SATB1/2, UBL5) and downstream mitochondrial chaperones HSP60 (HSPD1) and mtHSP70 (HSPA9) illustrating that both demethylases might control an integrated transcriptional network promoting mammalian longevity.

We previously demonstrated that mito-nuclear protein imbalance induces a robust UPR^{mt} and is linked to increased lifespan, both in nematodes and in BXD mice [41]. Interestingly, mito-nuclear imbalance might also play a role in longevity mediated by overexpression of *jmjd-1.2* and *jmjd-3.1*, as suggested by our RNA-seq analysis (Figure 2:5G). As further proof of concept that similar stressors could activate the UPR^{mt} across species, we recently found that expression of *Cox5b* and *Spg7* correlate negatively with the UPR^{mt} network, indicating that their low abundance likely triggers the UPR^{mt} in mammals [31]. These data indicate that the UPR^{mt} pathway is active *in vivo* in mammals under physiological, non-stress conditions. Based on the observed positive correlations between PHF8, JMJD3 and UPR^{mt} in multiple tissues, we suggest that the regulation of UPR^{mt} by the H3K27 demethylases PHF8 and JMJD3 is also conserved in BXD mice under basal conditions. Of note, this association between histone demethylases and UPR^{mt} seems in certain tissues linked to mouse lifespan regulation, although further mechanistic work is required to ascertain this relation. Our bioinformatics analysis and literature discussed above suggests that PHF8 and JMJD3 regulate UPR^{mt} genes by removing repressive

H3K27 methylation marks from their coding regions. Identifying the exact mechanism of regulation and whether there is a developmental aspect of the UPR^{mt} pathway in mammals, as demonstrated in *C. elegans* [42], remains an important direction for future work.

Collectively, our data corroborate the increasing body of literature in which epigenetic marks that control chromatin states, including histone methylation, represent a hallmark of aging [75-78]. Mitochondrial perturbations early in life have long-lasting effects on gene expression, and within this work we provide a mechanistic understanding of how this might be achieved. Our results thus reveal a conserved mode for the regulation of stress response and lifespan dependent on mitochondrial function.

2.7 Materials and methods

Lifespan Analysis

Lifespan experiments were conducted at 20ºC as previously described [42]. Lifespans were performed on nematodes fed HT115 bacteria expressing the indicated RNAi, using the pre-fertile period of adulthood as day 0. Animals were transferred to fresh plates every other day until day 12. Prism 5 software was used for statistical analysis to determine significance calculated using the log-rank (Mantel-Cox) method. Lifespan experiments involving RNAi shifting to *Dicer (dcr-1)* RNAi were performed as described [49,79]. Briefly, for lifespans with selective RNAi only during development, animals were grown on *cco-1+jmjd-1.2* or *cco-1+jmjd-3.1* RNAi bacteria and transferred to *dcr-1* dsRNA expressing bacteria at L4 stage. For lifespans with RNAi during adulthood, animals were grown on empty vector RNAi control bacteria and transferred to *cco-1+jmjd-1.2* or *cco-1+jmjd-3.1* RNAi bacteria at L4 stage.

Gene Expression Analysis

C. elegans were age synchronized by egg bleaching and cultivated on nematode growth media (NGM) plates containing HT115 bacteria expressing the indicated RNAi constructs at 20°C and harvested at day 1 of adulthood. Animals were collected in M9 buffer, centrifuged at 1000 x g for 30 sec, resuspended in Trizol (Life Technologies) and snap frozen in liquid nitrogen. After several freeze-thaw cycles, total RNA was isolated using the RNeasy Mini Kit (Qiagen) according to the manufacturer´s instructions. 1 µg of total RNA was subjected to cDNA synthesis using the QuantiTect Reverse Transcription Kit (Qiagen). Quantitative Real-Time PCR reactions were performed with the SYBR Select

Master Mix (Applied Biosystems) in Optical 384-well MicroAmp plates (Applied Biosystems) using a QuantStudio 6 Flex (Applied Biosystems).

Fluorescence Microscopy

For fluorescence microscopy, animals were blindly chosen under the light microscope (at random) from a population, immobilized with 100 µg/ml levamisole (Sigma) and images were then captured using a Leica M250FA automated fluorescent stereo microscope equipped with a Hamamatsu ORCA-ER camera.

Immunoblot Analysis

Mouse tissue extracts were prepared in modified RIPA buffer using a hand-held homogenizer (UltraTurrax). Crude lysates were centrifuged at 10,000 x g at 4°C for 10 min and total protein amount was determined with the DC Protein Assay (BioRad). Supernatants were supplemented with 4x SDS sample buffer, boiled for 5 min at 95°C and resolved by standard SDS-PAGE. Proteins were transferred to PVDF membranes (Immobilon). Equal loading was assessed with anti-β-actin (Abcam) antibodies.

Accession numbers

RNA-sequencing data have been deposited in the Gene Expression Omnibus (GEO) database under accession number GSE78990.

2.8 Author contributions

C.M., V.J., J.A. and A.D. conceived the study and wrote the manuscript with input from all co-authors. C.M. performed *C. elegans* RNAi screens, lifespan assays, RNA-seq sample preparations, fluorescence microscopy, qRT-PCR experiments, immunoblots related to *jmjd-1.2*/PHF8 and analyzed data. V.J. performed RNA-seq analysis, *C. elegans* lifespan assays, fluorescence microscopy, qRT-PCR experiments and immunoblots related to *jmjd-3.1*/JMJD3 and analyzed data. J.D. generated transgenic *C. elegans* lines by microinjection. O.M. performed some of the *C. elegans* experiments and generated *jmjd-3.1* overexpressing *C. elegans* strains. S.D.J. performed qRT-PCR experiments and analyzed data. P.M.Q. performed mammalian microarray and ChIP-seq analyses. K.K.S. helped with the RNA-seq sample preparations and performed RNA-seq gene expression analysis. S.N.U. performed *C. elegans* crosses, backcrosses and strain integrations of *jmjd-1.2* overexpressing lines. E.G.W. performed initial bioinformatic analyses on BXD mouse tissues. L.M. and C.M. identified *jmjd-3.1* as a UPR^mt regulator in a screening campaign. V.M. conducted the *C. elegans* lifespan suppressor screen. S.C.W. conceived

the high-throughput *C. elegans* RNAi screens and wrote the manuscript. R.J.S. provided intellectual input and supported the early phase of the project.

2.9 Acknowledgements

2.10 Supplementary materials and methods

Strains

The Bristol strain (N2) was used as the wild type strain. The following strains were obtained from the *Caenorhabditis* Genetics Center (Minneapolis, MN). MQ887 (*isp-1(qm150)IV*), CB1370 (*daf-2(e1370)III*), DA1116 (*eat-2(ad1116)II*), CF1903 (*glp-1(e2141)III*), SJ4100 (zcIs13[*hsp-6p::GFP*]), SJ4058 (zcIs9[*hsp-60p::GFP*]), SJ4005 (zcIs4[*hsp-4p::GFP*]), CL2070 (dvIs[*hsp-16.2::GFP*; *pRF4(rol-6)*]), CF1553 muIs84[pAD76(sod-3::GFP)], VC936 (*jmjd-3.1(gk384)X*). Strains were backcrossed at least three times prior to experimental analysis. Strains AGD710 (*sur-5p::hsf-1*) (Baird et

al., 2014) and AGD927 (*rab-3p::xbp-1s*) [97] have been described, *F29B9.2(tm3713)IV* was a gift from A.E. Salcini [93].

Strain generation

For generation of overexpression strains the all-tissue promoter *sur-5* (Gu et al., 1998)*,* pan-neuronal promoter *rgef-1* [109] or intestinal promoter *gly-19* [110] were used. The *jmjd-1.2* ORF was amplified from wild-type *C. elegans* cDNA. Full length DNA plasmid constructs were injected at 50 ng/µl along with a coinjection marker (*myo-2p*::tdTomato) at 10 ng/µl to generate transgenic overexpression nematodes. Extra-chromosomal arrays were integrated by gamma irradiation and backcrossed to N2 ten times as previously described. The *jmjd-3.1* promoter and coding sequence were amplified from *C. elegans* genomic DNA. Sequences were cloned into the pPD30_38 expression vector (kind gift of Dr. Carina Holmberg) between *Pci*I and *Nhe*I restriction sites (the *unc-54* promoter and enhancer were replaced). *jmjd-3.1* overexpression plasmid was coinjected with pharyngeal CFP marker (*myo-2p::cfp*, kind gift of Dr. Carina Holmberg). Extra-chromosomal arrays were integrated using gamma irradiation and backcrossed five times to N2. Two independent lines carrying integrated transgenes were used in experiments.

RNA interference

Bacterial feeding RNAi experiments were performed as described [111] RNAi clones were used from either the Ahringer or Vidal libraries and sequence-verified. Double RNAi experiments were carried out by mixing bacterial cultures normalized to their optical densities (OD600) before seeding onto NGM plates.

UPR^er and HSR stress assays

ER stress was induced in day 1 adults with 25 ng/µL tunicamycin in M9 for 4 hours on a rotating platform at 20°C. Worms were then washed with M9 and collected for further analysis. Heat shock was induced in day 1 adults by incubation in M9 submerged into 34°C water bath for 15 min. Worms were allowed to recover on solid NGM plates for 1.5 h at 20°C and collected for further analysis.

RNA-sequencing

Wild type N2 and transgenic overexpression strains *jmjd-3.1p::jmjd-3.1*, *sur-5p::jmjd-1.2* and *rgef-1p::jmjd-1.2* were used for the experiment. Synchronized eggs were plated on empty vector (EV) or EV + *cco-1* RNAi bacteria, grown at 20ºC and collected by washing with M9 at the L4 stage, then snap frozen in liquid nitrogen. Pellets were grinded with mortar and pestle on dry ice and the resulting powder was thawed in the presence of lysis

buffer (50 mM Tris-HCl, 50 mM NaCl, 10 mM MgCl$_2$, 5 mM CaCl$_2$ 200 μg/ml cycloheximide, 200 μg/ml heparin, 1% (v/v) Triton X-100, 0.1% (w/v) sodium deoxycholate) and incubated on ice for 10 minutes prior to centrifugation at 4°C, 16,000 x g for 10 minutes. Poly-A RNA was purified from clarified lysate using olig-dT25 Dynabeads (Ambion) and Trizol-LS (Life Technologies) extraction, each according to manufacturer's instructions. Sequencing libraries were prepared using the Epicentre ScriptSeq v2 according to manufacturer's instructions. Illumina HiSeq 2500 reads were pre-processed and mapped to a set of noncoding RNAs before mapping the remaining reads to an index containing the longest single isoform ± 30nt for each gene in the *C. elegans* WS230 genome using Bowtie version 0.12.7 [112] with the following settings: -m 1 -v 2 -a --norc --best –strata, which allows up to two mismatches and requires a single best alignment. In-house Python scripts were used to count reads mapping to each transcript and the count data were used for statistical analysis by DESeq2 [113], where pairwise comparisons were evaluated by the negative binomial method. Three biological replicates of each condition were used for analysis, except for the *rgef-1p::jmjd-1.2* strain, for which one of the three replicates did not pass quality control and was removed from the analysis. Differentially expressed genes (DEGs) relative to the N2 EV condition were defined by a Benjamini-Hochberg adjusted p-value of less than 0.05. Venn diagrams were generated with InteractiVenn [114]. GO terms of overlapping genes were determined with DAVID [101], using Bonferroni and Benjamini-Hochberg adjusted p value < 0.05. DESeq2-determined normalized count values were used for generating gene expression bar graphs and heatmaps. Fold change was calculated by dividing to average of normalized count values for N2 EV condition. Heatmaps were generated using heatmap.2 function from the gplots R package or GENE-E (Broad Institute). The set of 470 mitochondrial genes used in Figure 2:5F was retrieved from GO:0005739. The set of 111 OXPHOS genes in Figure 2:5G was retrieved from GO:0006119 and manual annotation. For mitochondria and OXPHOS heatmaps, genes with 0 counts in at least one condition were removed. RNA-sequencing data described in this study have been deposited in the Gene Expression Omnibus (GEO) database [115] under accession number GSE78990.

ChIP-qPCR

Chromatin immunprecipitation (ChIP) assays were performed essentially as described [116] with minor modifications. Briefly, wild type N2 worms were synchronized by bleaching and grown on solid NGM plates at 20°C until L3 stage, exposed to either empty vector or *cco-1* RNAi. Crosslinking was performed by treatment with 1% (w/v)

formaldehyde for 20 min at room temperature. Worms were then lysed and sonicated with Bioruptor (Diagenode) to obtain 500–1,000 bp DNA fragments. H3K27me3 was then immunoprecipitated from 500 μg lysate using rabbit H3K27me3 ChIP-grade (07-449, Abcam) or rabbit IgG (sc2027, Santa Cruz) antibodies and protein A sepharose beads (sc2003, Santa Cruz). Crosslinks were reversed by 4h incubation at 65°C. DNA fragments were extracted with phenol-chlorophorm-isoamylalcohol and precipitated with ethanol. Standard quantitative RT-PCR experiments were performed as described above. Primers used for qRT-PCR were *hsp-6* (fw, gccagaaagggacttcagac, rv, cttttgggcccatagtgaca), *clpp-1* (fw, tctccgcagagaagtgtgaa, rv, cccaaagcgagaatcatacc) and *atfs-1* (fw, agcttacaggaccagcttcg, rv, gttccagctcgtctgatggt).

Bioinformatic analyses

All BXD transcriptome data sets for bioinformatic analyses were downloaded from GeneNetwork (http://www.genenetwork.org) and performed as described in previous studies [31,90]. BXD transcriptome datasets used to establish genetic correlations were INIA Hypothalamus Affy MoGene 1.0 ST (Nov10) Male, INIA Amygdala Affy MoGene 1.0 ST (Nov10) RMA Male, UTHSC Affy MoGene 1.0 ST Spleen (Dec10) RMA Males, INIA Adrenal Affy MoGene 1.0ST (Jun12) RMA Males, INIA Pituitary Affy MoGene 1.0ST (Jun12) RMA and EPFL/LISP BXD CD Liver Affy Mouse Gene 1.0 ST (Apr13) RMA, Lifespan datasets ID 10148 and 12564. The correlations are Pearson's *r* or Spearman's *rho*, depending on the distribution of data. The correlation matrix was constructed using corrgram package in R. Publicly available microarray, RNA-seq and ChIP-seq data were retrieved from the GEO database (http://www.ncbi.nlm.nih.gov/geo). H3K27me3 ChIP-seq raw data (GSE56696) were re-analyzed using Galaxy [117] with the same parameters as previously described [102]. PHF8 ChIP-Seq data was obtained from GSE20725 [103]. Binding of UPR^{mt} genes were explored using IGV [118]. Heatmaps of UPR^{mt} genes from *Jmjd3*-knockout embryos (GSE40332) and human T-cell lymphoblastic leukemia cell lines CUTLL1 and CEM (GSE56696) [102] were made using heatmap.2 function from the gplots R package.

2.11 Supplementary data
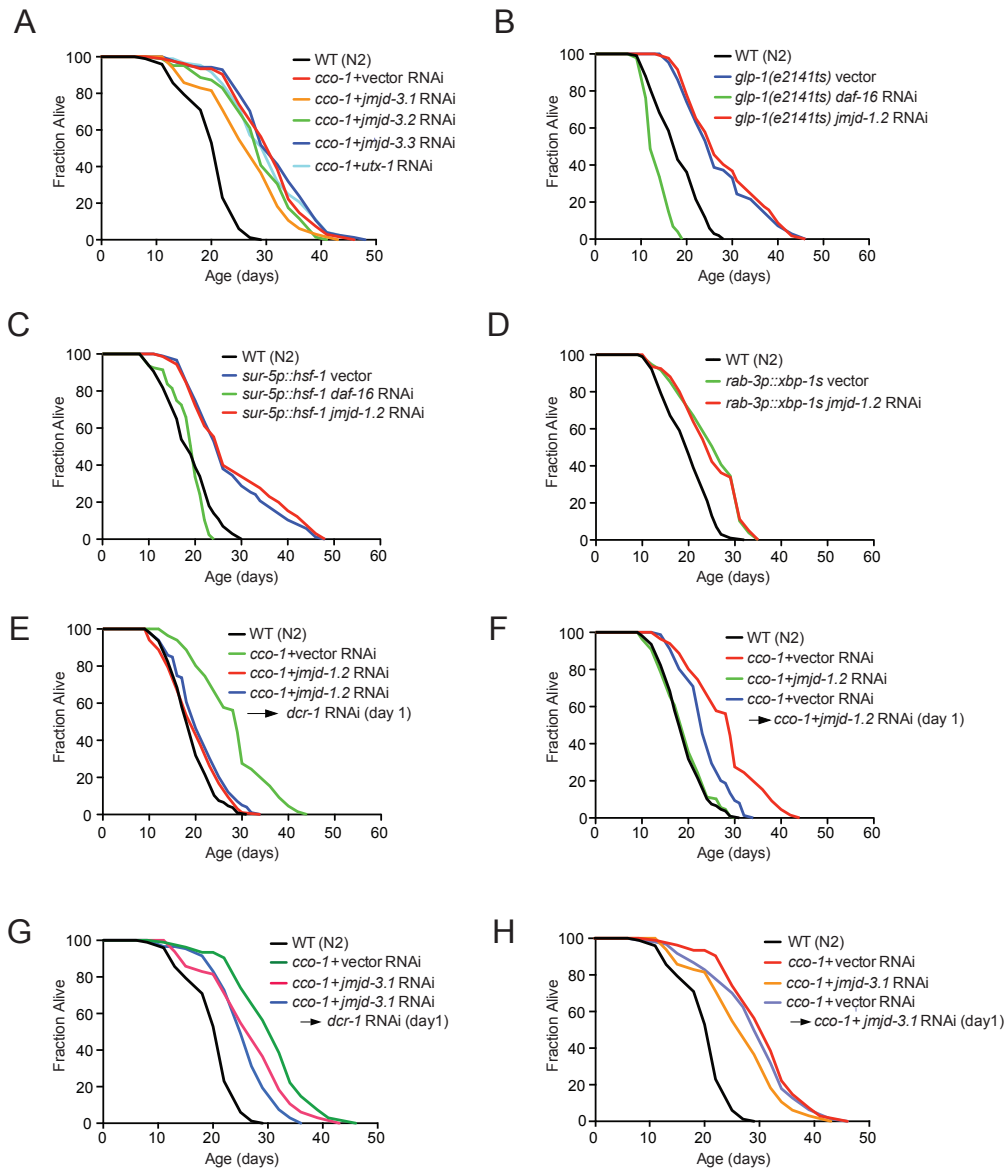
Figure 2:S1 Temporal requirements of *jmjd-1.2* activity and specificity for ETC-mediated longevity, related to Figure 2:1.

(A) Among the *C. elegans* H3K27me3 demethylases, only *jmjd-3.1* is required for *cco-1* RNAi mediated lifespan extension. (B) Germ-cell loss-mediated longevity (*glp-1(e2141)* strain) occurs independently on *jmjd-1.2*.(C) Heat Shock Factor-1 (HSF-1)-mediated lifespan extension occurs independently of *jmjd-1.2*. (D) Longevity due to neuronal expression of *xbp-1s* (*rab-3p::xbp-1s* strain) is unaffected by *jmjd-1.2*. (E) Knockdown of *jmjd-1.2* selectively during larval development is sufficient to suppress *cco-1*-mediated lifespan extension. Lifespan analysis of N2 animals grown on *cco-1* dsRNA bacteria mixed with *jmjd-1.2* dsRNA bacteria during development and then moved to *dcr-1* dsRNA expressing bacteria at the L4 larval stage, to disrupt the RNAi machinery. (F) *jmjd-1.2* RNAi selectively during adulthood partially suppresses *cco-1*-mediated longevity. Lifespan analysis of N2 animals grown on *cco-1* dsRNA bacteria mixed with empty vector control bacteria during development and then moved to *cco-1* dsRNA bacteria mixed with *jmjd-1.2* dsRNA bacteria at the L4 larval stage. (G) Knockdown of *jmjd-3.1* selectively during larval development is sufficient to suppress *cco-1*-mediated lifespan extension. (H) *jmjd-3.1* RNAi selectively during adulthood does not suppress *cco-1*-mediated longevity. See also Table 2:S1 for lifespan statistics.
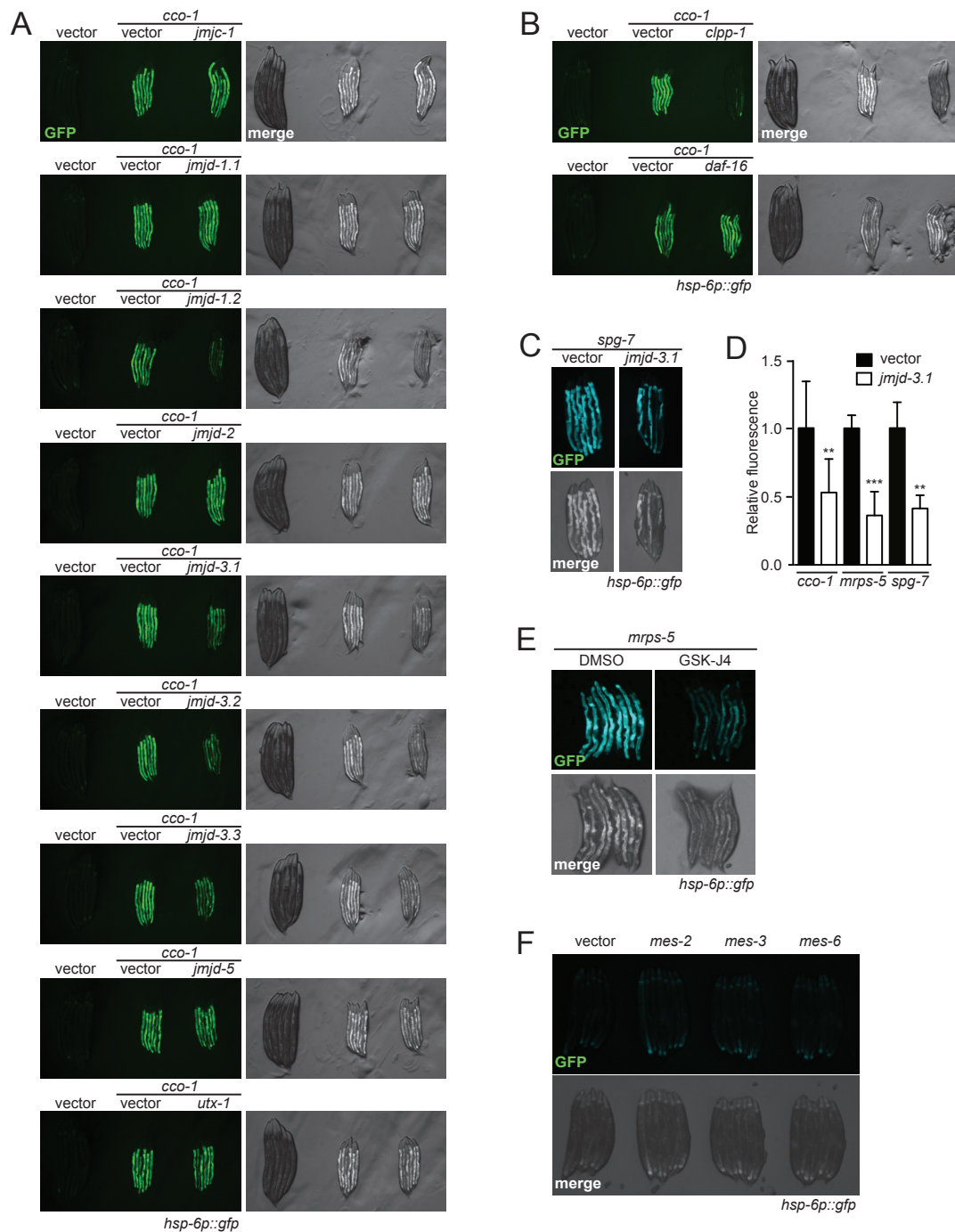
Figure 2:S2 Specificity of *jmjd-1.2* and *jmjd-3.1* for UPR^mt induction, related to Figure 2:2.

(A) Fluorescent micrographs of *hsp-6p::gfp* reporter animals treated with the indicated RNAi. (B) Fluorescent micrographs of *hsp-6p::gfp* reporter animals treated with the indicated RNAi. *clpp-1* RNAi represents positive control (upper panel), *daf-16* RNAi negative control (lower panel). (C) Fluorescent micrographs of *hsp-6p::gfp* reporter animals treated with the indicated RNAi. (D) Quantification of fluorescent intensities of *hsp-6p::gfp* reporter animals treated with the indicated RNAi. Data represent mean ± SEM. *** denotes p < 0.001, **p < 0.01. (E) Fluorescent micrographs of *hsp-6p::gfp* reporter animals grown on *mrps-5* RNAi treated with the demethylase inhibitor GSK-J4 or DMSO as control. (F) Fluorescent micrographs of *hsp-6p::gfp* reporter animals grown on RNAi of Polycomb components *mes-2, mes-3* and *mes-6*.
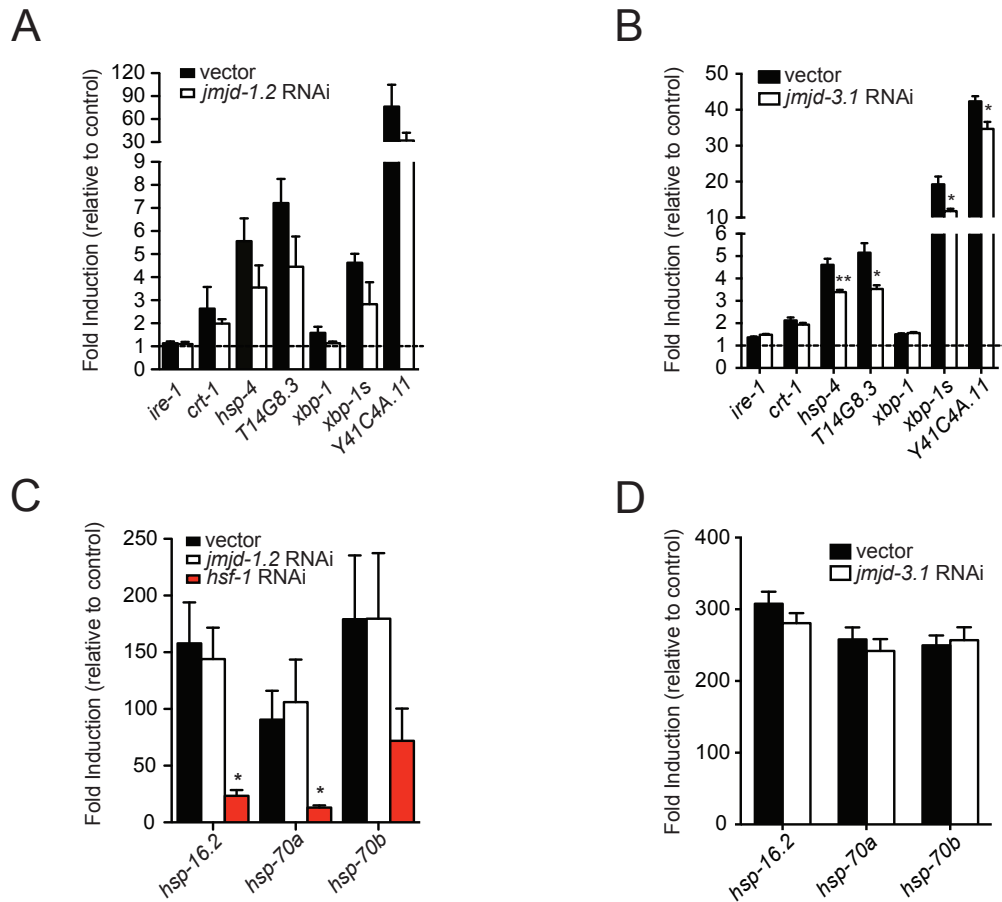
Figure 2:S3 Effect of *jmjd-1.2* and *jmjd-3.1* loss- or gain-of-Function on UPR^ER^ and HSR, related to Figure 2:3.

(A) *jmjd-1.2* is not required for induction of the UPR^er^. Transcript levels of UPR^er^ target genes were measured by quantitative RT-PCR in day 1 adults grown on vector or *jmjd-1.2* RNAi bacteria. Day 1 worms were treated with 25ng/µL tunicamycin in M9 or DMSO in M9 as control for 4 hours. Results are shown relative to transcript levels in empty vector control treated animals, with error bars indicating mean ± SEM. A Student's t test was used to assess significance. (B) *jmjd-3.1* is partially required for induction of the UPR^er^. Transcript levels of UPR^er^ target genes were measured by quantitative RT-PCR in day 1 adults grown on vector or *jmjd-3.1* RNAi bacteria. Day 1 worms were treated with 25ng/µL tunicamycin in M9 or DMSO in M9 as control for 4 hours. Results are shown relative to transcript levels in empty vector control treated animals, with error bars indicating mean ± SEM. ** denotes p < 0.01, *p < 0.05. (C) *jmjd-1.2* is not required for induction of the HSR. Transcript levels of HSR target genes were measured by quantitative RT-PCR in day 1 adults grown on either vector or *jmjd-3.1* RNAi bacteria. *hsf-1* RNAi was used as a positive control. Day 1 worms were exposed to 34°C for 15 min. Results are shown relative to transcript levels in empty vector control treated animals, with error bars indicating mean ± SEM. * denotes p < 0.05. (D) *jmjd-3.1* is not required for induction of the HSR. Transcript levels of HSR target genes were measured by quantitative RT-PCR in day 1 adults grown on vector or *jmjd-3.1* RNAi bacteria. Day 1 worms were exposed to 34°C for 15 min. Results are shown relative to transcript levels in empty vector control treated animals, with error bars indicating mean ± SEM. A Student's t test was used to assess significance.
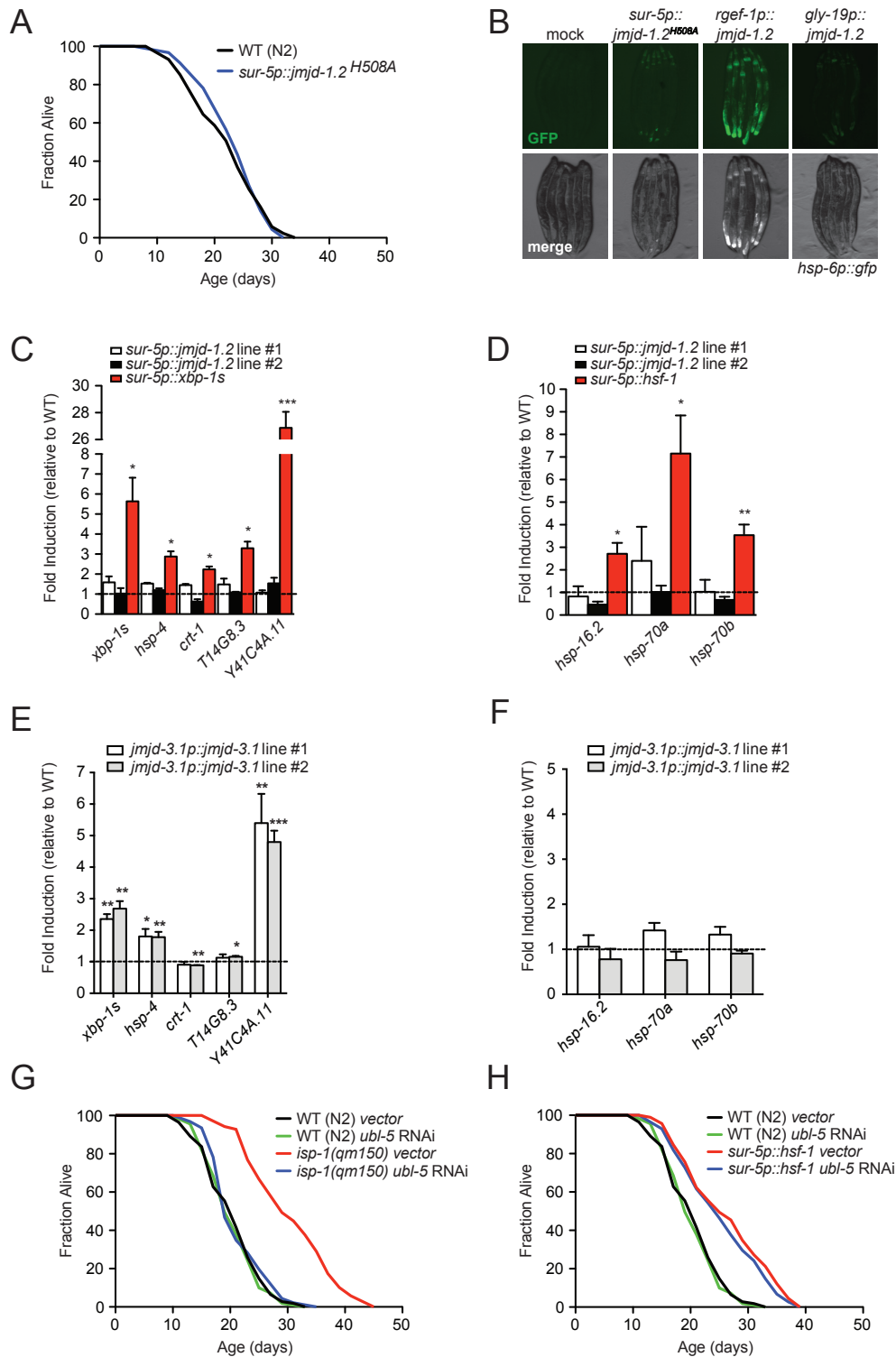
Figure 2:S4 *ubl-5* is a specific genetic requirement for ETC- and *jmjd-1.2*-mediated longevity, related to Figures 2:3 and 2:4.

(A) Overexpression of *jmjd-1.2* in all tissues extends *C. elegans* lifespan in a catalytic site-dependent manner. Lifespan analysis of wild type N2 and JmjC domain mutant strain *sur-5p::jmjd-1.2*[H508A]. (B) Neuron-specific overexpression of *jmjd-1.2* is sufficient for UPR[mt] induction. Fluorescent micrographs of SJ4100 *hsp-6p::GFP* UPR[mt] reporter animals expressing *sur-5p::jmjd-1.2*[H508A], *rgef-1p::jmjd-1.2*, and *gly-*

19p::jmjd-1.2 transgenes at day 1 of adulthood. (C) *jmjd-1.2* overexpression does not affect expression of selected UPR^{er} target genes. Transcript levels of UPR^{er} target genes were measured by quantitative RT-PCR in day 1 adults of N2 and two independent lines of *sur5p::jmjd-1.2*. *sur5p::xbp-1s* worms were used as a positive control. Results are shown relative to transcript levels in N2 animals, with error bars indicating mean ± SEM. *** denotes $p<0.001$, *$p < 0.05$. (D) *jmjd-1.2* overexpression does not affect expression of selected HSR target genes. Transcript levels of UPR^{er} target genes were measured by quantitative RT-PCR in day 1 adults of N2 and two independent lines of *sur5p::jmjd-1.2*. *sur5p::hsf-1* worms were used as a positive control. Results are shown relative to transcript levels in N2 animals, with error bars indicating mean ± SEM. ** denotes $p<0.01$, *$p < 0.05$. (E) *jmjd-3.1* overexpression increases expression of selected UPR^{er} target genes. Transcript levels of UPR^{er} target genes were measured by quantitative RT-PCR in day 1 adults of N2 and two independent lines of *jmjd-3.1::jmjd-3.1*. Results are shown relative to transcript levels in N2 animals, with error bars indicating mean ± SEM. * denotes $p < 0.05$, **$p<0.01$, ***$p<0.001$. (F) *jmjd-3.1* overexpression does not change expression of HSR markers. Transcript levels of HSR markers were measured by quantitative RT-PCR in day 1 adults of N2 and two independent lines of *jmjd-3.1::jmjd-3.1*. Results are shown relative to transcript levels in N2 animals, with error bars indicating mean ± SEM. A Student's t test was used to assess significance. (G) *ubl-5* is required for increased longevity of *isp-1(qm150)* mutant animals. (H) *ubl-5* is not required for extended longevity of *sur-5p::hsf-1* animals.
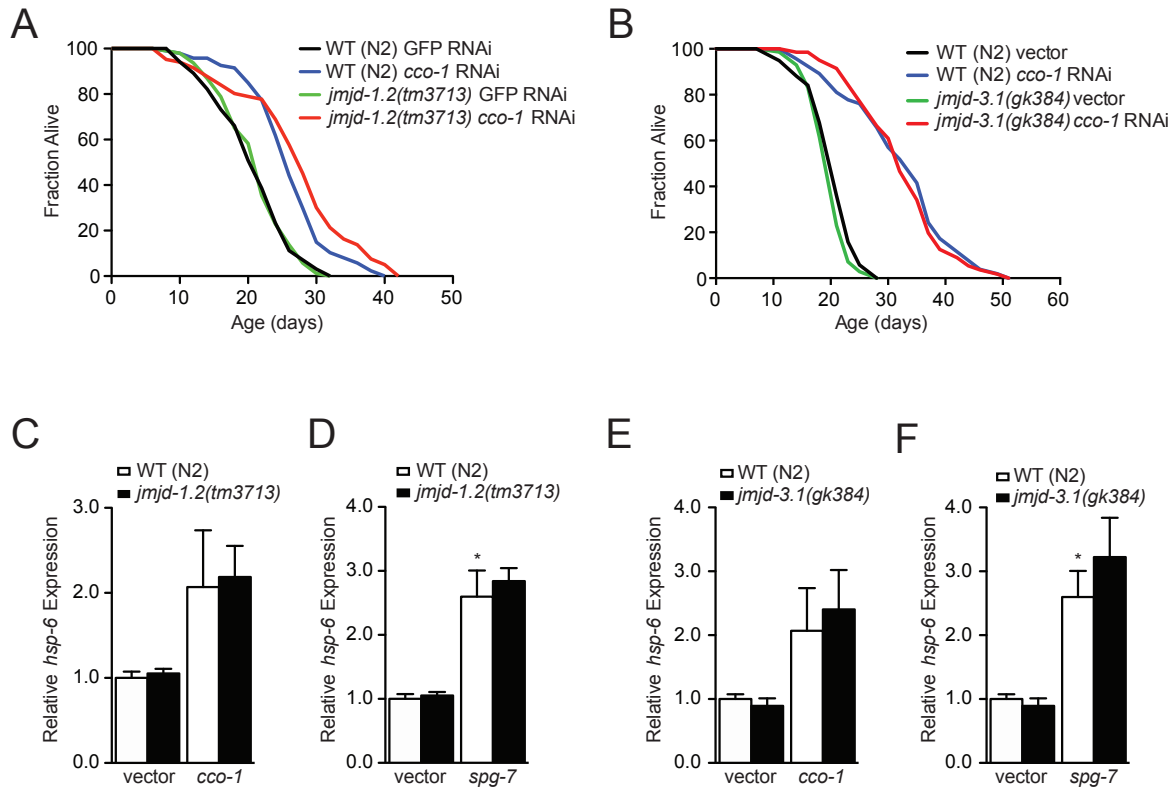
Figure 2:S5 Mutant alleles of *jmjd-1.2* and *jmjd-3.1* do not suppress *cco-1*-mediated longevity and UPR^{mt} induction, related to Figures 2:1 and 2:2.

(A) Lifespan analysis of wild type N2 and *jmjd-1.2(tm3713)* mutant strain on *cco-1* RNAi or GFP RNAi as control. (B) Lifespan analysis of wild type N2 and *jmjd-3.1(gk384)* mutant strain on empty vector or *cco-1* RNAi. (C) Transcript levels of *hsp-6* in wild type N2 and *jmjd-1.2(tm3713)* animals at day 1 of adulthood grown on the indicated RNAi were measured by quantitative RT-PCR. (D) Transcript levels of *hsp-6* in wild type N2 and *jmjd-1.2(tm3713)* animals at day 1 of adulthood grown on the indicated RNAi were measured by quantitative RT-PCR. (E) Transcript levels of *hsp-6* in wild type N2 and *jmjd-3.1(gk384)* animals at day 1 of adulthood grown on the indicated RNAi were measured by quantitative RT-PCR. (F) Transcript levels of *hsp-6* in wild type N2 and *jmjd-3.1(gk384)* animals at day 1 of adulthood grown on the indicated RNAi were measured by quantitative RT-PCR. Results are shown relative to transcript levels in N2 animals, with error bars indicating mean ± SEM. A Student's t test was used to assess significance. *$p < 0.05$. See also Table 2:S1.

Table 2:S1 Lifespan statistics

Corresponding Figure	Strain, Treatment	Mean Lifespan ± SEM [days]	Median [days]	# Deaths/# Total	% Change in Mean Lifespan	p-value Log-rank (Mantel-Cox)
1A	N2, vector RNAi	18.8 ± 0.6	18	104/110	na	na
	N2, vector+*cco-1* RNAi	32.5 ± 1.2	30	88/110	72.9	< 0.0001
	N2, vector+*jmjd-1.2* RNAi	20.9 ± 0.8	19	92/111	11.2	0.0118
	N2, *cco-1+jmjd-1.2* RNAi	21.0 ± 0.8	19	99/109	10.5	0.018
	Statistical comparison:					
	N2, vector+*cco-1* RNAi vs. *cco-1+jmjd-1.2* RNAi					< 0.0001
	N2, vector+*jmjd-1.2* RNAi vs. *cco-1+jmjd-1.2* RNAi					0.9779
Repeat	N2, GFP RNAi	20.9 ± 0.5	21	101/120	na	na
	N2, GFP+*cco-1* RNAi	33.8 ± 0.9	35	98/120	61.7	< 0.0001
	N2, GFP+*jmjd-1.2* RNAi	20.6 ± 0.5	21	97/120	-1.4	0.8042
	N2, *cco-1+jmjd-1.2* RNAi	23.7 ± 0.7	25	100/120	13.3	0.0023
	Statistical comparison:					
	N2, GFP+*cco-1* RNAi vs. *cco-1+jmjd-1.2* RNAi					< 0.0001
1B	N2, vector RNAi	22.2 ± 0.6	25	67/90	na	na
	N2, vector+*cco-1* RNAi	32.5 ± 0.8	34	48/90	46.4	0
	N2, vector+*jmjd-3.1* RNAi	21.8 ± 0.5	22	71/90	1.8	0.25
	N2, cco-1+*jmjd-3.1* RNAi	27.3 ± 1.0	27	60/90	23.0	< 0.0001
	Statistical comparison:					
	N2, vector+*cco-1* RNAi vs. *cco-1+jmjd-3.1* RNAi					< 0.0001
1C	N2, vector RNAi	20.4 ± 0.6	20	98/108	na	na
	isp-1(qm150), vector RNAi	38.6 ± 1.3	41	65/110	89.2	< 0.0001
	isp-1(qm150), jmjd-1.2 RNAi	28.1 ± 1.0	30	80/111	37.7	< 0.0001
	Statistical comparison:					
	isp-1(qm150), vector *RNAi vs. jmjd-1.2 RNAi*					< 0.0001
1D	N2, vector RNAi	21.8 ± 0.5	23	86/100	na	na
	isp-1(qm150), vector RNAi	31.2 ± 1.0	33	47/100	43.1	< 0.0001
	isp-1(qm150), jmjd-3.1 RNAi	21.8 ± 1.0	18	47/100	0.0	0.3
	Statistical comparison:					
	isp-1(qm150), vector RNAi *vs. jmjd-3.1* RNAi					< 0.0001
1E	N2, vector RNAi	17.8 ± 0.6	16	101/114	na	na
	eat-2(ad1116), vector RNAi	24.8 ± 0.8	24	63/111	39.3	< 0.0001
	eat-2(ad1116), pha-4 RNAi	17.1 ± 0.6	18	93/108	-3.9	0.6571
	eat-2(ad1116), jmjd-1.2 RNAi	25.6 ± 0.8	27	76/115	43.8	< 0.0001
	Statistical comparison:					
	eat-2(ad1116), vector RNAi vs. *pha-4* RNAi					< 0.0001
	eat-2(ad1116), vector RNAi vs. *jmjd-1.2* RNAi					0.3683
Repeat	N2, GFP RNAi	22.8 ± 0.5	23	85/100	na	na
	eat-2(ad1116), GFP RNAi	28.4 ± 0.9	29	66/100	24.5	< 0.0001
	eat-2(ad1116), pha-4 RNAi	23.7 ± 0.8	25	85/100	3.9	0.284
	eat-2(ad1116), jmjd-1.2 RNAi	29.0 ± 0.8	31	69/100	27.2	< 0.0001
	Statistical comparison:					
	eat-2(ad1116), GFP RNAi vs. *pha-4* RNAi					< 0.0001
	eat-2(ad1116), GFP RNAi vs. *jmjd-1.2* RNAi					0.4974
1F	N2, vector RNAi	17.5 ± 0.5	18	61/70	na	na
	eat-2(ad1116), vector RNAi	23 ± 0.7	25	81/100	31.4	< 0.0001
	eat-2(ad1116), pha-4 RNAi	16.7 ± 0.5	15	92/100	-4.6	0.59
	eat-2(ad1116), jmjd-3.1 RNAi	23.2 ± 0.7	25	73/100	32.6	< 0.0001
	Statistical comparison:					
	eat-2(ad1116), vector RNAi vs. *pha-4* RNAi					< 0.0001
	eat-2(ad1116), vector RNAi vs. *jmjd-3.1* RNAi					0.64
1G	N2, vector RNAi	20 ± 0.6	21	103/111	na	na
	daf-2(e1370), vector RNAi	40.1 ± 1.3	40	74/113	100.5	< 0.0001
	daf-2(e1370), daf-16 RNAi	18.4 ± 0.3	19	107/121	-8.0	< 0.0001
	daf-2(e1370), jmjd-1.2 RNAi	39.7 ± 1.9	40	46/112	98.5	< 0.0001
	Statistical comparison:					
	daf-2(e1370), vector RNAi vs. *daf-16* RNAi					< 0.0001
	daf-2(e1370), vector RNAi vs. *jmjd-1.2* RNAi					0.7368
Repeat	N2, GFP RNAi	22.2 ± 0.6	23	82/100	na	na
	daf-2(e1370), GFP RNAi	47.7 ± 1.2	49	85/100	114.9	< 0.0001
	daf-2(e1370), daf-16 RNAi	20.8 ± 0.4	21	89/100	-6.7	< 0.0001
	daf-2(e1370), jmjd-1.2 RNAi	46.7 ± 1.2	49	90/100	110.3	0.0389
	Statistical comparison:					
	daf-2(e1370), GFP RNAi vs. *daf-16* RNAi					< 0.0001
	daf-2(e1370), GFP RNAi vs. *jmjd-1.2* RNAi					0.7891
1H	N2, vector RNAi	21.6 ± 0.6	20	56/100	na	na
	daf-2(e1370), vector RNAi	36.2 ± 0.5	39	92/100	67.6	< 0.0001

	daf-2(e1370), daf-16 RNAi	15.0 ± 0.3	15	67/100	-30.6	< 0.0001
	daf-2(e1370), jmjd-3.1 RNAi	32.5 ± 0.8	34	75/100	50.5	< 0.0001
	Statistical comparison:					
	daf-2(e1370), vector RNAi vs. *daf-16* RNAi					< 0.0001
	daf-2(e1370), vector RNAi vs. *jmjd-3.1* RNAi					< 0.0001
3A	N2, vector RNAi	21.1 ± 0.5	20	87/100	na	na
	sur-5p::jmjd-1.2 line #1, vector *RNAi*	30.4 ± 0.8	30	67/100	44.1	< 0.0001
	sur-5p::jmjd-1.2 line #2, vector *RNAi*	29.5 ± 0.7	30	79/100	39.8	< 0.0001
3B	N2	20.7 ± 0.6	21	78/100	na	na
	jmjd-3.1p::jmjd-3.1 line #1	24 ± 0.5	26	76/100	16.0	< 0.0001
	jmjd-3.1p::jmjd-3.1 line #2	24.1 ± 0.6	26	77/100	16.4	< 0.0001
3G	N2, vector RNAi	20.4 ± 0.5	21	105/120	na	na
	rgef-1p::jmjd-1.2 line #1, vector RNAi	28.1 ± 0.7	28	92/120	37.7	< 0.0001
	rgef-1p::jmjd-1.2 line #2, vector RNAi	26.1 ± 0.8	27	89/120	27.9	< 0.0001
	gly-19p::jmjd-1.2 line #1, vector RNAi	20.3 ± 0.4	21	92/120	-0.4	0.7486
	gly-19p::jmjd-1.2 line #2, vector RNAi	20.5 ± 0.4	21	101/120	0.5	0.7929
4A	N2, vector RNAi	22.2 ± 0.5	23	105/120	na	na
	N2, *ubl-5* RNAi	21.3 ± 0.5	21	107/120	-4.5	0.2192
	sur-5p::jmjd-1.2 line #1 vector RNAi	29.2 ± 0.6	29	84/120	31.5	< 0.0001
	sur-5p::jmjd-1.2 line #1, ubl-5 RNAi	21.8 ± 0.5	21	112/120	-1.8	0.5952
	sur-5p::jmjd-1.2 line #2 vector RNAi	27.3 ± 0.6	29	90/120	23.0	< 0.0001
	sur-5p::jmjd-1.2 line #2, ubl-5 RNAi	22.3 ± 0.6	21	101/120	0.4	0.9766
	Statistical comparison:					
	sur-5p::jmjd-1.2 line #1, vector vs. *ubl-5* RNAi					< 0.0001
	sur-5p::jmjd-1.2 line #2, vector vs. *ubl-5* RNAi					< 0.0001
Repeat	N2, vector RNAi	21.7 ± 0.5	22	86/100	na	na
	N2, *ubl-5* RNAi	22.8 ± 0.4	24	90/100	5.1	0.1934
	sur-5p::jmjd-1.2 line #1 vector RNAi	30.5 ± 0.6	30	73/100	40.6	< 0.0001
	sur-5p::jmjd-1.2 line #1, ubl-5 RNAi	24.5 ± 0.7	26	84/100	12.9	0.0022
	sur-5p::jmjd-1.2 line #2 vector RNAi	29.0 ± 0.7	28	80/100	33.6	< 0.0001
	sur-5p::jmjd-1.2 line #2, ubl-5 RNAi	23.8 ± 0.7	24	90/100	9.7	0.0343
	Statistical comparison:					
	sur-5p::jmjd-1.2 line #1, vector vs. *ubl-5* RNAi					< 0.0001
	sur-5p::jmjd-1.2 line #2, vector vs. *ubl-5* RNAi					< 0.0001
4B	N2, vector RNAi	19.4 ± 0.4	19	90/100	na	na
	N2, *ubl-5* RNAi	17.4 ± 0.3	19	92/100	-10.3	< 0.0001
	jmjd-3.1p::jmjd-3.1 line #1 vector RNAi	21.8 ± 0.5	21	90/100	12.4	< 0.0001
	jmjd-3.1p::jmjd-3.1 line #1 *ubl-5* RNAi	18.2 ± 0.3	19	90/100	-6.2	< 0.0001
	jmjd-3.1p::jmjd-3.1 line #2 vector RNAi	22.6 ± 0.6	26	91/100	16.5	< 0.0001
	jmjd-3.1p::jmjd-3.1 line #2 *ubl-5* RNAi	18.3 ± 0.3	19	93/100	-5.7	< 0.0001
4C	N2, vector RNAi	21.7 ± 0.6	22	87/100	na	na
	N2, *ubl-5* RNAi	22.0 ± 0.6	22	94/100	1.3	0.7146
	rgef-1p::jmjd-1.2 line #1 vector RNAi	27.4 ± 0.7	28	88/100	26.3	< 0.0001
	rgef-1p::jmjd-1.2 line #1 ubl-5 RNAi	22.7 ± 0.6	24	77/100	4.6	0.2252
	rgef-1p::jmjd-1.2 line #2 vector RNAi	26.5 ± 0.5	27	88/100	22.1	< 0.0001
	rgef-1p::jmjd-1.2 line #2 ubl-5 RNAi	21.1 ± 0.5	21	82/100	-2.8	0.5568
	Statistical comparison:					
	rgef-1p::jmjd-1.2 line #1, vector vs. *ubl-5* RNAi					< 0.0001
	rgef-1p::jmjd-1.2 line #2, vector vs. *ubl-5* RNAi					< 0.0001
S1A	N2, vector RNAi	20.3 ± 0.5	22	89/100	na	na
	N2, *cco-1*+vector RNAi	30.4 ± 0.7	32	63/100	50.0	< 0.0001
	N2, *cco-1*+*jmjd-3.1*	26.7 ± 0.6	27	66/100	31.5	< 0.0001
	N2, *cco-1*+*jmjd-3.2*	28.9 ± 0.8	29	69/100	42.4	< 0.0001
	N2, *cco-1*+*jmjd-3.3*	31.1 ± 0.7	32	68/100	53.2	< 0.0001
	N2, *cco-1*+*utx-1*	30 ± 0.7	32	69/100	47.8	< 0.0001
	Statistical comparison:					
	N2, vector+*cco-1 vs. cco-1*+*jmjd-3.1* RNAi					< 0.01
	N2, vector+*cco-1 vs. cco-1*+*jmjd-3.2* RNAi					0.15
	N2, vector+*cco-1 vs. cco-1*+*jmjd-3.3* RNAi					0.39
	N2, vector+*cco-1 vs. cco-1*+*utx-1* RNAi					0.88
S1B	N2, vector RNAi	18.6 ± 0.5	18	106/121	na	na
	glp-1(e2141), vector RNAi	27.4 ± 0.9	26	75/120	47.3	< 0.0001
	glp-1(e2141), daf-16 RNAi	13.6 ± 0.3	12	81/120	-26.9	< 0.0001
	glp-1(e2141), jmjd-1.2 RNAi	28.4 ± 1.0	26	66/120	52.7	< 0.0001
	Statistical comparison:					
	glp-1(e2141), vector RNAi vs. *daf-16* RNAi					< 0.0001
	glp-1(e2141), vector RNAi vs. *jmjd-1.2* RNAi					0.5772
Repeat	N2, GFP RNAi	21.4 ± 0.5	23	84/100	na	na
	glp-1(e2141), GFP RNAi	28.7 ± 0.8	29	99/100	34.1	< 0.0001

	glp-1(e2141), daf-16 RNAi	17.2 ± 0.4	17	61/100	-24.4	< 0.0001
	glp-1(e2141), jmjd-1.2 RNAi	28.6 ± 0.8	29	88/100	33.6	< 0.0001
	Statistical comparison:					
	glp-1(e2141), GFP RNAi vs. *daf-16* RNAi					< 0.0001
	glp-1(e2141), GFP RNAi vs. *jmjd-1.2* RNAi					0.9373
S1C	N2, vector RNAi	19.1 ± 0.5	19	101/121	na	na
	sur-5p::hsf-1, vector RNAi	27.5 ± 0.9	26	87/123	44.0	< 0.0001
	sur-5p::hsf-1, daf-16 RNAi	18.7 ± 0.4	20	89/120	-2.1	0.0522
	sur-5p::hsf-1, jmjd-1.2 RNAi	28.4 ± 1.2	26	68/120	48.7	< 0.0001
	Statistical comparison:					
	sur-5p::hsf-1, vector RNAi vs. *sur-5p::hsf-1, jmjd-1.2* RNAi					0.4452
S1D	N2, vector RNAi	20.1 ± 0.5	20	100/123	na	na
	rab-3p::xbp-1s, vector RNAi	25.1 ± 0.7	27	85/120	24.9	< 0.0001
	rab-3p:xbp-1s, jmjd-1.2 RNAi	24.8 ± 0.7	25	84/120	23.4	< 0.0001
	Statistical comparison:					
	rab-3p::xbp-1s, vector RNAi vs. *rab-3p:xbp-1.2* RNAi					0.9078
S1E	N2, vector RNAi	19.2 ± 0.4	18	107/120	na	na
	N2, *cco-1*+vector RNAi	28.2 ± 0.9	29	69/126	46.9	< 0.0001
	N2, *cco-1*+*jmjd-1.2* RNAi	21.1 ± 0.6	20	99/122	9.9	0.001
	N2, *cco-1*+*jmjd-1.2* RNAi (*dcr-1* RNAi @day1)	20.1 ± 0.6	21	96/124	4.7	0.0404
	Statistical comparison:					
	N2, vector+*cco-1* vs. *cco-1*+*jmjd-1.2* RNAi (*dcr-1* RNAi @day1)					< 0.0001
	N2, vector vs. *cco-1*+*jmjd-1.2* RNAi (*dcr-1* RNAi @day1)					0.2186
Repeat	N2, GFP RNAi	21.1 ± 0.6	21	79/100	na	na
	N2, *cco-1*+*GFP* RNAi	32.5 ± 1.0	33	77/100	54.0	< 0.0001
	N2, *cco-1*+*jmjd-1.2* RNAi (*dcr-1* RNAi @day1)	20.4 ± 0.8	21	40/100	-3.4	0.5789
	Statistical comparison:					
	N2, *cco-1*+GFP RNAi vs. *cco-1*+*jmjd-1.2* RNAi (*dcr-1* RNAi @day1)					< 0.0001
S1F	N2, vector RNAi	19.3 ± 0.5	20	107/120	na	na
	N2, *cco-1*+vector RNAi	29.5 ± 1.0	29	89/111	52.8	< 0.0001
	N2, *cco-1*+*jmjd-1.2* RNAi	20.3 ± 0.5	21	113/121	5.2	0.1069
	N2, *cco-1*+vector RNAi (*cco-1*+*jmjd-1.2* @day1)	23.8 ± 0.5	23	75/124	23.3	< 0.0001
	Statistical comparison:					
	N2, *cco-1*+vector RNAi vs. *cco-1*+vector RNAi (*cco-1*+*jmjd-1.2* @day1)					< 0.0001
Repeat	N2, GFP RNAi	21.2 ± 0.6	21	73/100	na	na
	N2, *cco-1*+GFP RNAi	35.9 ± 1.0	37	80/100	69.3	< 0.0001
	N2, *cco-1*+GFP RNAi (*cco-1*+*jmjd-1.2* @day1)	22.0 ± 0.8	23	58/100	3.8	0.8317
	Statistical comparison:					
	N2, *cco-1*+GFP RNAi vs. *cco-1*+*vector* RNAi (*cco-1*+*jmjd-1.2* @day1)					< 0.0001
	N2, GFP RNAi vs. *cco-1*+*vector* RNAi (*cco-1*+*jmjd-1.2* @day1)					0.5789
S1G	N2, vector RNAi	20.3 ± 0.5	22	89/100	na	na
	N2, *cco-1*+vector RNAi	30.4 ± 0.7	32	63/100	50.0	< 0.0001
	N2, *cco-1*+*jmjd-3.1* RNAi	26.7 ± 0.8	27	66/100	31.5	< 0.0001
	N2, *cco-1*+*jmjd-3.1* RNAi (*dcr-1* RNAi @day1)	25.8 ± 0.6	25	69/100	27.1	< 0.0001
	Statistical comparison:					
	N2, vector+*cco-1* vs. *cco-1*+*jmjd-3.1* RNAi (*dcr-1* RNAi @day1)					< 0.0001
S1H	N2, vector RNAi	20.3 ± 0.5	22	89/100	na	na
	N2, *cco-1*+vector RNAi	30.4 ± 0.7	32	63/100	50	< 0.0001
	N2, *cco-1*+*jmjd-3.1* RNAi	26.7 ± 0.8	27	66/100	31.5	< 0.0001
	N2, *cco-1*+vector RNAi (*cco-1*+*jmjd-3.1* @day1)	28.9 ± 0.8	29	74/100	42.4	< 0.0001
	Statistical comparison:					
	N2, *cco-1*+vector RNAi vs. *cco-1*+vector RNAi (*cco-1*+*jmjd-3.1* @day1)					0.43
S4A	N2, vector RNAi	22.2 ± 0.7	24	87/100	na	na
	sur-5p::jmjd-1.2 H508A, vector RNAi	23.2 ± 0.6	24	92/100	4.5	0.2573
Repeat	N2, vector RNAi	18.5 ± 0.5	18	111/121	na	na
	sur-5p::jmjd-1.2 H508A, vector RNAi	18.2 ± 0.7	16	76/133	-1.6	0.9773
S5A	N2, vector RNAi	20.6 ± 0.5	21	109/120	na	na
	N2, *ubl-5* RNAi	20.5 ± 0.4	19	111/125	-0.5	0.6683
	isp-1(qm150), vector RNAi	30.7 ± 0.9	29	69/120	49.0	< 0.0001
	isp-1(qm150), *ubl-5* RNAi	21.4 ± 0.5	19	92/120	3.9	0.1919
S5B	N2, vector RNAi	20.6 ± 0.5	21	109/120	na	na
	N2, *ubl-5* RNAi	20.5 ± 0.4	19	111/125	-0.5	0.6683
	sur-5p::hsf-1, vector RNAi	26.2 ± 0.8	25	77/122	27.2	< 0.0001
	sur-5p::hsf-1, *ubl-5* RNAi	25.5 ± 0.7	25	87/122	23.8	< 0.0001

Chapter 3   TCA cycle perturbation and its relation to UPR^{mt} and lifespan regulation in *C. elegans*

Adapted from

This chapter investigates relation between UPR^{mt} and TCA cycle. With J.A., I conceived the study and wrote the manuscript. I performed the majority of the experiments and analysed the microarray data.

3.1 Summary

The TCA cycle is composed of a series of chemical reactions in the mitochondria that oxidize nutrients for subsequent ATP harvesting and that provide intermediates for biosynthetic reactions. In this study we investigated the effects of genetic perturbations of the TCA cycle on cellular stress response mechanisms in *C. elegans*, with a particular focus on their impact on the mitochondrial unfolded protein response (UPR[mt]) and lifespan. Downregulation of citrate synthase, α-ketoglutarate dehydrogenase and fumarase all induce the UPR[mt], but they have divergent effects on lifespan. Restricting the knockdown of these genes to early larval development stages had positive effects on longevity, which were shown to be dependent on the UPR[mt]. Analysis of the transcriptome of *C. elegans* with loss-of-function (LOF) of these TCA cycle genes revealed some common mechanisms. When we compared gene expression profiles after LOF of these TCA cycle genes with those obtained after the knockdown of other mitochondrial genes, such as *spg-7*, *mrps-5* and *cco-1*, we identified a core set of transcripts, which change in common and which likely represent a signature of mitochondrial dysfunction. This data could potentially be used for further understanding of molecular mechanisms involved in mitochondrial diseases and development of treatment strategies.

3.2 Introduction

Mitochondria perform multiple essential functions in the cell, the main of which is the production of ATP from nutrients through the tricarboxylic acid (TCA) cycle and oxidative phosphorylation [16]. The TCA cycle is a cyclic set of enzymatic reactions, occurring in the mitochondrial matrix, which oxidizes the acetyl-CoA derived from carbohydrates, amino acids and lipids [119]. Importantly, this cycle generates the reducing agents NADH and FADH$_2$, and TCA cycle chemical intermediates, which are precursors for various biosynthetic reactions. Genetic defects in some of the TCA cycle genes are associated with cancer, while others manifests themselves as multisystem disorders with similarity to defects in oxidative phosphorylation [120]. Contributions of the TCA cycle enzymes to organismal physiology and their potential connection to mitochondrial and/or general cellular stress responses have not yet been well studied.

One of the main stress response pathways in mitochondria is the mitochondrial unfolded protein response (UPR[mt]). The UPR[mt] pathway detects mitochondrial proteotoxic stress, such as the accumulation of unfolded or unassembled proteins, and activates a

transcriptional response, which induces not only the expression of chaperones and proteases, needed to reestablish mitochondrial proteostasis, but also activates other cellular adaptive mechanisms, such as glycolysis, to deal with the transient mitochondrial dysfunction [18,28,121]. The main UPR[mt] effectors and markers in *C. elegans* are the chaperones *hsp-6* (the ortholog of mouse mtHsp70), *hsp-60* (the ortholog of Hsp60) [30], and the protease *clpp-1*. Their induction is coordinated by the transcriptional regulators *atfs-1* [28], *ubl-5* [56], *dve-1* [54], as well as by the epigenetic regulators, *jmjd-3.1* and *jmjd-1.2* [122]. UPR[mt] activation has been associated with lifespan extension in mice and worms [41]. For the UPR[mt] induction to have an effect on lifespan in *C. elegans*, it has to occur during the early developmental stages invoking the involvement of epigenetic changes to exert long-lasting effects on stress response and longevity [42,122].

In this study we examined the effects of TCA cycle perturbations induced by feeding worms with RNAi targeting specific TCA cycle enzymes. We analyzed the impact of these genetic perturbations on general mitochondrial health, stress responses and worm longevity. In addition, we compared gene expression profiles of three TCA cycle disruption conditions, associated with the induction of UPR[mt], with the changes induced by other mitochondrial perturbations to distill a common gene expression signature of mitochondrial stress.

3.3 Results

3.3.1 Effect of TCA cycle perturbation on *C. elegans* stress responses

The TCA cycle is composed of 8 chemical reactions performed by either single enzymes (e.g. citrate synthase) or by multiprotein enzyme complexes (e.g. succinate dehydrogenase) (Figure 3:1A). We perturbed TCA cycle function in *C. elegans* by a loss of function (LOF) strategy targeting all 8 enzymatic reactions by specific RNAis. First, we measured basal oxygen consumption rate (OCR) in wild type N2 worms with downregulation of TCA cycle enzymes by RNAi starting from egg development, using Seahorse respirometry at first day of adulthood (Figure 3:1B). Worms treated with most of the RNAi clones had similar basal OCR. The LOF of aconitase (*aco-2*)*,* α-ketoglutarate dehydrogenase (*dlst-1*) and fumarase (*fum-1*), however, resulted in lower basal OCR. RNAi of almost all TCA cycle enzymes did not increase maximal respiratory capacity after uncoupling with carbonyl cyanide-p-trifluoromethoxyphenylhydrazone (FCCP) injection, with the exception of the LOF of succinyl-CoA synthetase (*sucg-1*) (Figure 3:1B).
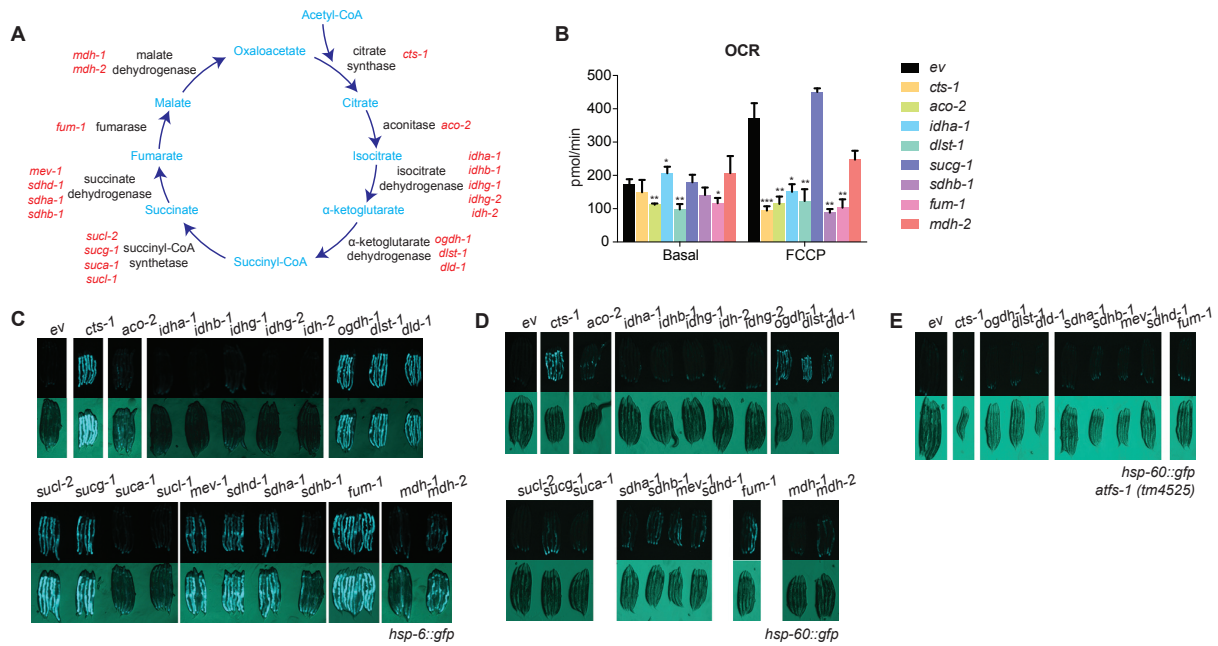
Figure 3:1 Effect of TCA cycle perturbation on UPR^{mt} in *C. elegans*.

Scheme of TCA cycle reactions, metabolites and enzymes. (B) Oxygen consumption rate (OCR) of animals treated with the TCA cycle enzyme RNAi during the whole life and assessed at day 1 of adulthood (n=6). Values are mean ± s.e.m.; *$p \leq 0.05$, **$p \leq 0.01$, ***$p \leq 0.001$. (C) Fluorescent micrographs of UPR^{mt} reporter *hsp-6::gfp* treated with the TCA cycle enzyme RNAi during the whole life and imaged at day 1 of adulthood. (D) Fluorescent micrographs of UPR^{mt} reporter *hsp-60::gfp* animals, treated with the TCA cycle enzyme RNAi. (E) Fluorescent micrographs of UPR^{mt} reporter *hsp-60::gfp* crossed into mutant *atfs-1(tm4525)*, treated with RNAi of those TCA cycle enzymes, which knockdown induces UPR^{mt}.

We then examined whether the knockdown of TCA cycle genes induced specific stress responses in *C. elegans*, such as the UPR^{mt}, the oxidative stress response, the ER stress and heat shock response (HSR). RNAi was applied starting from egg development and stress reporters were scored at the first day of adulthood. RNAi against the TCA cycle enzymes was first tested in *hsp-6::gfp* (SJ4100), UPR^{mt} reporter worms, expressing GFP under the control of the promoter of the mitochondrial chaperone *hsp-6, a* UPR^{mt} marker. LOF of citrate synthase (*cts-1*), α-ketoglutarate dehydrogenase (*ogdh-1, dlst-1, dld-1*), fumarase (*fum-1*) induced a robust UPR^{mt} (Figure 3:1C). Reduced succinyl-CoA synthetase (*sucl-2, sucg-1*) and succinate dehydrogenase (*mev-1, sdhd-1, sdha-1*) activity also induced the UPR^{mt} albeit to a lower extent. Finally, a very mild *hsp-6::gfp* induction was observed after RNAi of one of the malate dehydrogenase components, *mdh-2*. No change in UPR^{mt} was detected with RNAis targeting aconitase (*aco-2*) or isocitrate dehydrogenase (*idha-1, idhb-1, idhg-1, idhg-2, idh-2*). Similar, although less pronounced, results were obtained when we used another UPR^{mt} reporter, i.e. the *hsp-60::gfp* strain (SJ4058), which expresses GFP under mitochondrial chaperone *hsp-60* promoter. The strongest induction of UPR^{mt} was visible after LOF of citrate synthase (*cts-1*), α-ketoglutarate dehydrogenase (*ogdh-1, dlst-1, dld-1*) and fumarase (*fum-1*) RNAi (Figure
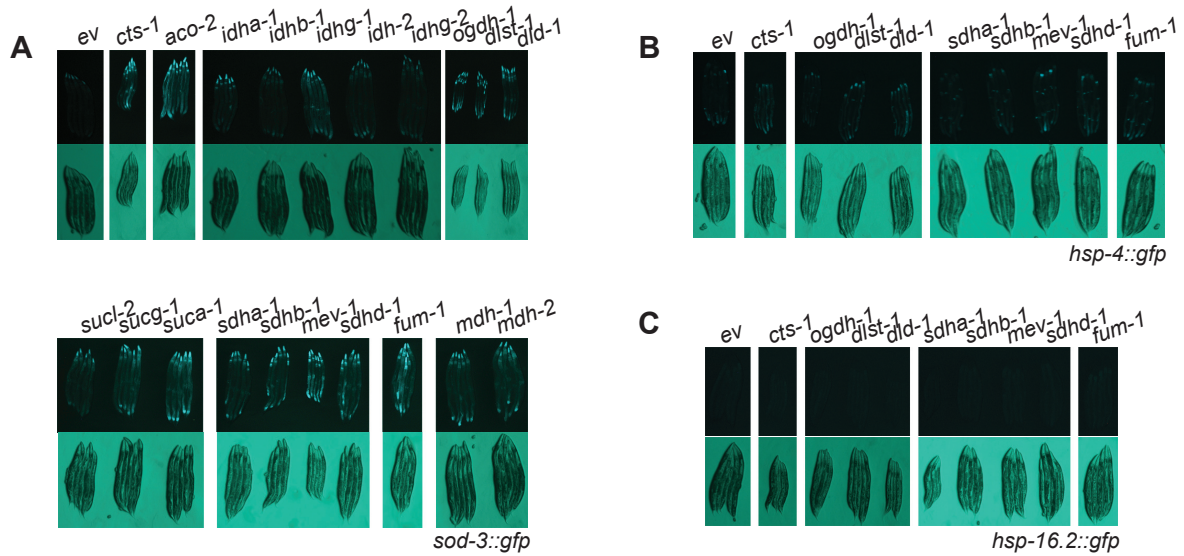
Figure 3:2 Effect of TCA cycle perturbation on *C. elegans* stress responses.
(A) Fluorescent micrographs of oxidative stress reporter *sod-3::gfp* animals, treated with the TCA cycle enzyme RNAi during the whole life and imaged at day 1 of adulthood. (B) Fluorescent micrographs of ER stress reporter *hsp-4::gfp* animals, treated with RNAi of those TCA cycle enzymes, which knockdown induces UPR^mt. (C) Fluorescent micrographs of heat shock response reporter *hsp-60::gfp* animals, treated with RNAi of those TCA cycle enzymes, which knockdown induces UPR^mt.

3:1D). The induction of the UPR^mt by LOF of these TCA cycle enzymes was dependent on the main transcriptional regulator of the UPR^mt, *atfs-1*, as no increased fluorescence was present upon RNAi of these enzymes in the *hsp-60::gfp* strain, which was backcrossed into *atfs-1(tm4526)* mutant background (Figure 3:1E).

We then tested whether LOF of TCA cycle enzymes also affected other stress response pathways. Basically all RNAi conditions induced some activity in the *sod-3::gfp* worms (KN259) in which the expression of GFP is under the control of the promoter of the oxidative stress responsive iron/manganese superoxide dismutase *sod-3*, indicating that interference with the TCA cycle induces ROS production and subsequent activation of adaptive antioxidant responses (Figure 3:2A). In the RNAi conditions, which resulted in the induction of the two UPR^mt reporters *hsp-6::gfp* and *hsp-60::gfp*, there was no apparent increase in GFP expression when we used the *hsp-4::gfp* worms (SJ4005), a reporter strain for ER stress (Figure 3:2B). In addition, no heat shock response (HSR) was induced by RNAis against these TCA cycle enzymes, as determined using the specific *hsp-16.2::gfp* (CL2070) HSR reporter strain (Figure 3:2C).

3.3.2 Effect of TCA cycle perturbation on *C. elegans* lifespan

Next, we assessed the effect of LOF of the different TCA cycle enzymes during the whole life of *C. elegans* on its longevity. As previously reported [123], aconitase *aco-2* RNAi
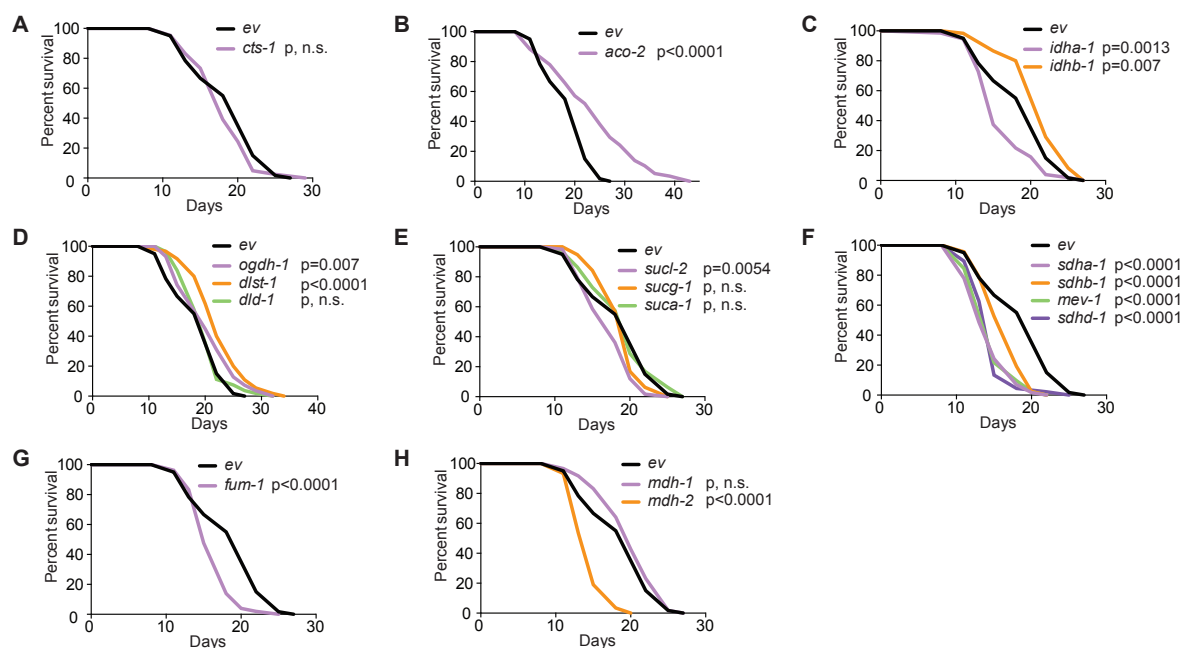
Figure 3:3 Effect of TCA cycle perturbation on *C. elegans* lifespan.
Lifespan of wild type N2 animals treated throughout the whole life with RNAi for different TCA cycle components. Figure panels are arranged according to the flow through the cycle. (A) citrate synthase *cts-1*, (B) aconitase *aco-2*, (C) isdocitrate dehydrogenase enzyme complex components *idha-1, idhb-1*, (D) α-ketoglutarate dehydrogenase enzyme complex components *ogdh-1, dlst-1, dld-1*, (E) succinyl-CoA synthetase enzyme complex components *sucl-2, sucg-1, suca-1*, (F) succinate dehydrogenase enzyme complex components *sdha-1, sdhb-1, mev-1, sdhd-1*, (G) fumarase *fum-1*, (H) malate dehydrogenase *mdh-1, mdh-2*. p values represent comparison with empty vector (*ev*) RNAi control, calculated using log rank test.

increases worm lifespan (Figure 3:3B). In addition, LOF of α-ketoglutarate dehydrogenases, especially with *dlst-1* RNAi, also increases longevity (figure 3:3D). In contrast, the downregulation of succinyl-CoA dehydrogenase (*sdha-1, sdhb-1, mev-1, sdhd-1*), which is also part of complex II of OXPHOS (Figure 3:3F), as well as of fumarase *fum-1* (Figure 3:3G) reduced lifespan. RNAi of citrate synthase *cts-1* (Figure 3:3A) as well as of succinyl-CoA synthetase (*sucl-2, sucg-1, suca*-1) (Figure 3:3E) generally did not change worm longevity. Finally, the lifespan effects for RNAi of isocitrate dehydrogenase (*idha-1, idhb-1*) (Figure 3:3C) and malate dehydrogenase (*mdh-1, mdh-2*) (Figure 3:3H) were not consistent and were dependent on the individual enzyme targeted in the enzymatic complex.

We then determined whether these effects on *C.elegans* lifespan correlated with the induction of the UPR^{mt}. There was no apparent correlation between the activation of the UPR^{mt} and lifespan. In fact, upon LOF of *fum-1* and complex II components lifespan decreased, after *cts-1* RNAi lifespan did not change, whereas after α-ketoglutarate dehydrogenase RNAi the lifespan increased, even though all those conditions induce a robust UPR^{mt} (Figures 3:1C, 3:3A, 3:3D, 3:3G).
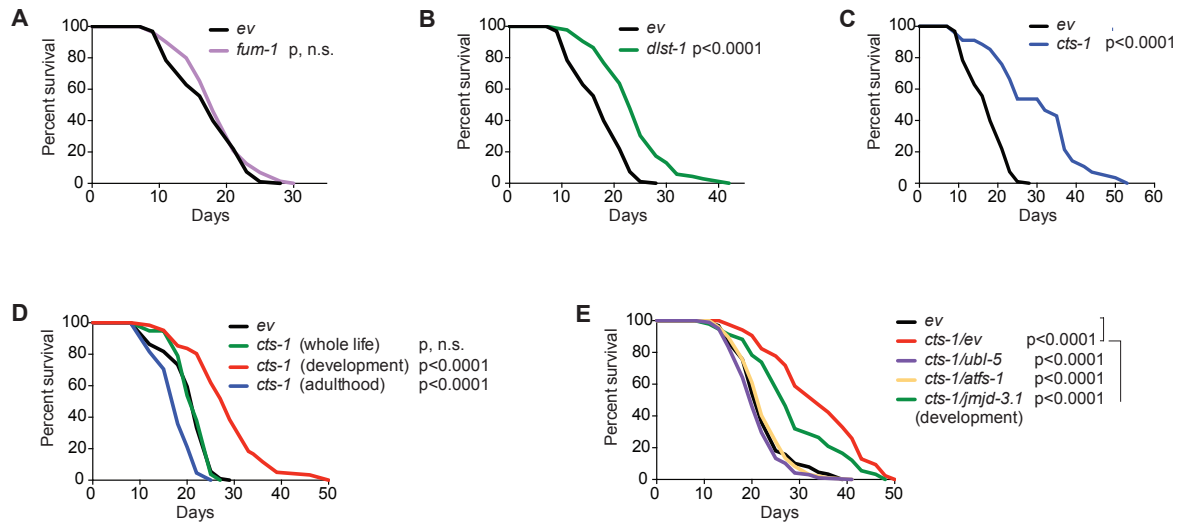
Figure 3:4 Developmental effects on lifespan by perturbation of UPR^{mt} associated TCA cycle enzymes.

Lifespan of wild type N2 animals, treated only during worm larval stages from egg development until L4, with RNAi of (A) fumarase *fum-1*, (B) α-ketoglutarate dehydrogenase *dlst-1* or (C) citrate synthase *cts-1*. (D) Lifespan of animals treated with *cts-1* RNAi during the whole life, only during larval development until L4 stage, or only during adulthood. (E) Lifespan of animals treated only during development with *cts-1* RNAi mixed with an empty vector (*ev*) RNAi control or RNAi targeting the UPR^{mt} regulators *ubl-5*, *atfs-1* or *jmjd-3.1*. p values represent comparison with empty vector (*ev*) RNAi control, or in (E), with *cts-1/ev* RNAi condition, calculated using log rank test.

As the positive effects of the induction of the UPR^{mt} on lifespan occur during early larval development stages [42], we next treated *C. elegans* with *fum-1*, *dlst-1* and *cts-1* RNAi, which all robustly induce UPR^{mt} but have divergent effects on lifespan, only during worm development until L4 stage. Interestingly, in all the cases restricting RNAi to this time window resulted in positive effects on worm lifespan, compared to RNAi feeding throughout the entire life (Figures 3:4A, 3:4B, 3:4C). Upon developmental restriction of *fum-1* RNAi, lifespan became similar to that of control worms treated with empty vector (*ev*), which was a significant improvement compared to the decreased lifespan seen in worms in which *fum-1* was knocked down throughout life (compare Figure 3:4A with Figure 3:3G). Developmentally restricted *dlst-1* LOF increased lifespan to a similar extent as whole life RNAi (compare Figure 3:4B and Figure 3:3D). Surprisingly, while *cts-1* RNAi during the entire life did not change the lifespan (Figure 3:3A), RNAi restricted to development strongly increased worm longevity (Figure 3:4C). Of note, testing the effects of *cts-1* RNAi during the different life stages of the worm revealed that RNAi fed only during adulthood actually reduced the lifespan (Figure 3:4D). Presumably, RNAi during development is of benefit to worm physiology, but continuing RNAi throughout adulthood has negative effects. Thus the lifespan extension, visible with developmental restricted RNAi can no longer be observed, explaining why *cts-1* RNAi during whole life appears to

have no effect on lifespan. Increased longevity by *cts-1* RNAi only during worm development was dependent on UPR^{mt}, as lifespan extension was completely suppressed by RNAi targeting the UPR^{mt} transcriptional regulators, *ubl-5* and *atfs-1*, and partly blocked by RNAi against the epigenetic regulator of the UPR^{mt}, *jmjd-3.1* (Figure 3:4E).

3.3.3 Gene expression analysis of *fum-1*, *dlst-1* and *cts-1* RNAi treated animals

To gain further mechanistic insight into how TCA cycle perturbation impact on *C. elegans* homeostasis, we performed microarray analysis of worms fed with *fum-1*, *dlst-1* and *cts-1* RNAi, the three TCA enzymes that robustly induce the UPR^{mt}. Animals were treated with RNAi during larval development and collected at L4 stage. A threshold of 1.5-fold change compared to empty vector (*ev*) control and a Bonferroni adjusted p value of 0.05 was used to determine the differentially expressed genes (DEG) for each condition. In total, 72 genes were differentially expressed after *fum-1* RNAi (Figure 3:5A), 1685 after *dlst-1* RNAi (Figure 3:5B) and 3817 after *cts-1* RNAi (Figure 3:5C). RNAi-mediated knockdowns of those 3 genes were efficient and specific (Figure 3:5D). There was no apparent
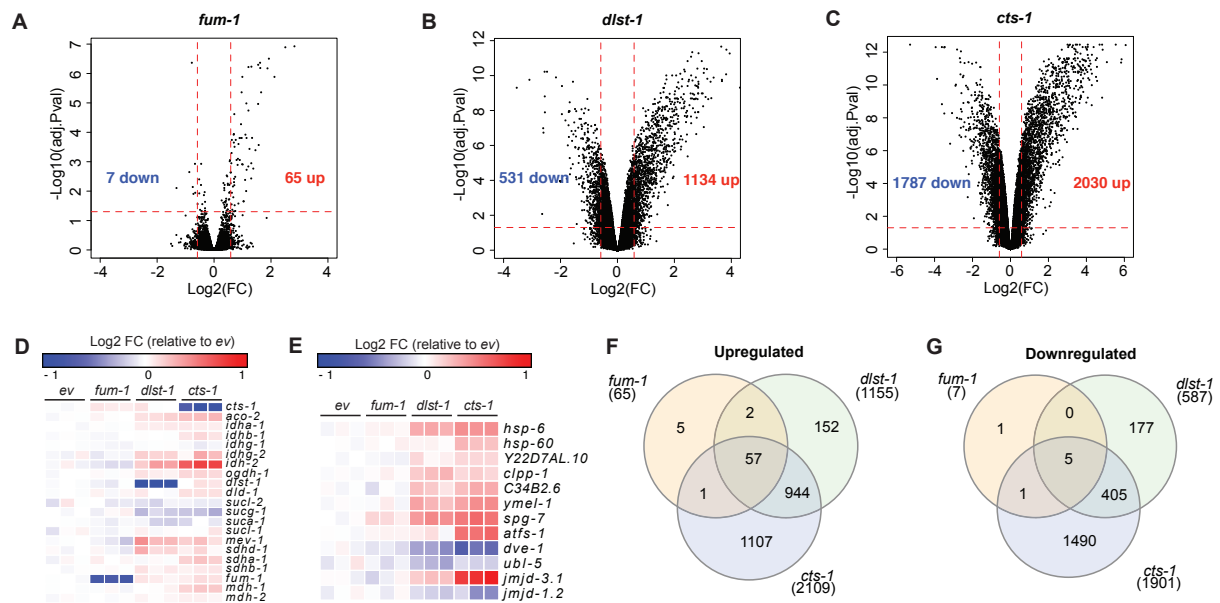
Figure 3:5 Gene expression analysis of animals treated with *fum-1*, *dlst-1* and *cts-1* RNAi .

Volcano plots of gene expression changes of wild type N2 worms treated only during development with (A) fumarase *fum-1*, (B) α-ketoglutarate dehydrogenase *dlst-1* and (C) citrate synthase *cts-1* RNAi compared to *ev* RNAi control. Fold change>1.5, Benjamini-Hochberg adjusted p value < 0.05. (D) Heatmap of gene expression of TCA cycle enzymes in animals treated with the *fum-1, dlst-1 and cts-1* RNAi compared to *ev* RNAi control. Fold change (FC) was calculated by comparing normalized expression values of each condition to *ev* control and then transformed to log2 scale. (E) Heatmap of gene expression of key UPR^{mt} indicators in animals treated with the *fum-1, dlst-1 and cts-1* RNAi compared to *ev* RNAi control. (F) Venn diagram of upregulated differentially expressed genes (DEGs) in animals treated with the *fum-1, dlst-1 and cts-1* RNAi. (G) Venn diagram of downregulated DEGs in animals treated with the *fum-1, dlst-1 and cts-1* RNAi.

compensation by an increase of other TCA cycle genes after *fum-1* RNAi, although some TCA cycle genes were moderately induced after *dlst-1* and *cts-1* RNAi, as illustrated by *idh-2* expression, which was induced by ~1.3-fold and ~1.7-fold upon *dlst-1* and *cts-1* RNAi, respectively (Figure 3:5D). Some of the UPR^{mt} signature genes, such as *hsp-6*, *hsp-60*, *atfs-1*, *jmjd-3.1*, were upregulated, with the strongest induction observed after *cts-1* RNAi (Figure 3:5E).

Most changes in gene expression were observed upon LOF of citrate synthase *cts-1*, the first enzyme of TCA cycle, less upon LOF of α-ketoglutarate dehydrogenase *dlst-1*, which functions later in the cycle, and RNAi of one of the last enzymes in the TCA cycle, fumarase *fum-1,* had a very small effect on gene expression (Figure 3:5A-C). Several of the DEGs were common among LOF of all three TCA cycle enzymes (Figures 3:5F, 3:5G). 88% (57/65) of *fum-1* RNAi upregulated genes were common with the other two conditions, and 82% (944/1155) of *dlst-1* RNAi induced genes were shared with *cts-1* RNAi condition (Figure 3:5F). Similarly, only 1 out of 7 significantly downregulated genes by *fum-1* was unique, and 69% (405/587) of *dlst-1* RNAi reduced genes were also down in *cts-1* condition (Figure 3:5G). To gain insight into specific gene expression changes, we examined gene classes, which were enriched among the DEGs of *dlst-1* and *cts-1* RNAi by performing gene functional classification by Gene Ontology (GO) categories using DAVID (Figure 3:6A-E). Various gene categories were significantly upregulated in both conditions, such as protein splicing and hedgehog receptor activity (Figure 3:6A, 3:6C).
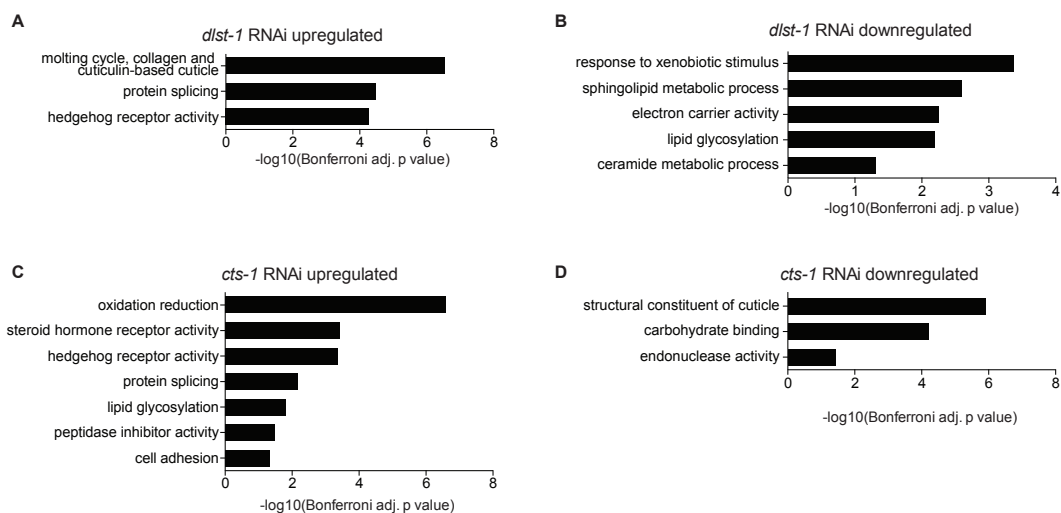
Figure 3:6 Gene classes changed after *dlst-1* and *cts-1* RNAi.
(A) Representative top GO terms of upregulated genes in the *dlst-1* RNAi treated animals. (B) Representative top GO terms of downregulated genes in the *dlst-1* RNAi treated animals. (C) Representative top GO terms of upregulated genes in the *cts-1* RNAi treated animals. (D) Representative top GO terms of downregulated genes in the *cts-1* RNAi treated animals. Bonferroni adjusted p value < 0.05.

Cuticle genes were upregulated after *dlst-1* RNAi (figure 3:6A), but downregulated after *cts-1* RNAi (Figure 3:6D). *cts-1* RNAi also induced genes involved in oxidation reduction, steroid hormone receptor, lipid glycosylation, peptidase inhibitor and cell adhesion processes (Figure 3:6C). After *dlst-1* RNAi, response to xenobiotic stimulus, electron carrier activity and several lipid metabolic processes, involving sphingolipids, ceramide and lipid glycosylation were downregulated (Figure 3:6B). After *cts-1* RNAi, genes with endonuclease activity and involved in carbohydrate binding were significantly downregulated (Figure 3:6D).

3.3.4 Comparison of gene expression profiles in *C. elegans* with TCA cycle knockdown and other mitochondrial perturbations

We next compared the changes in gene expression observed upon specific perturbation of the TCA cycle with those seen upon the induction of mitochondrial stress pathways, in particular the UPR^mt. We hence performed microarray analysis of *C. elegans* treated with
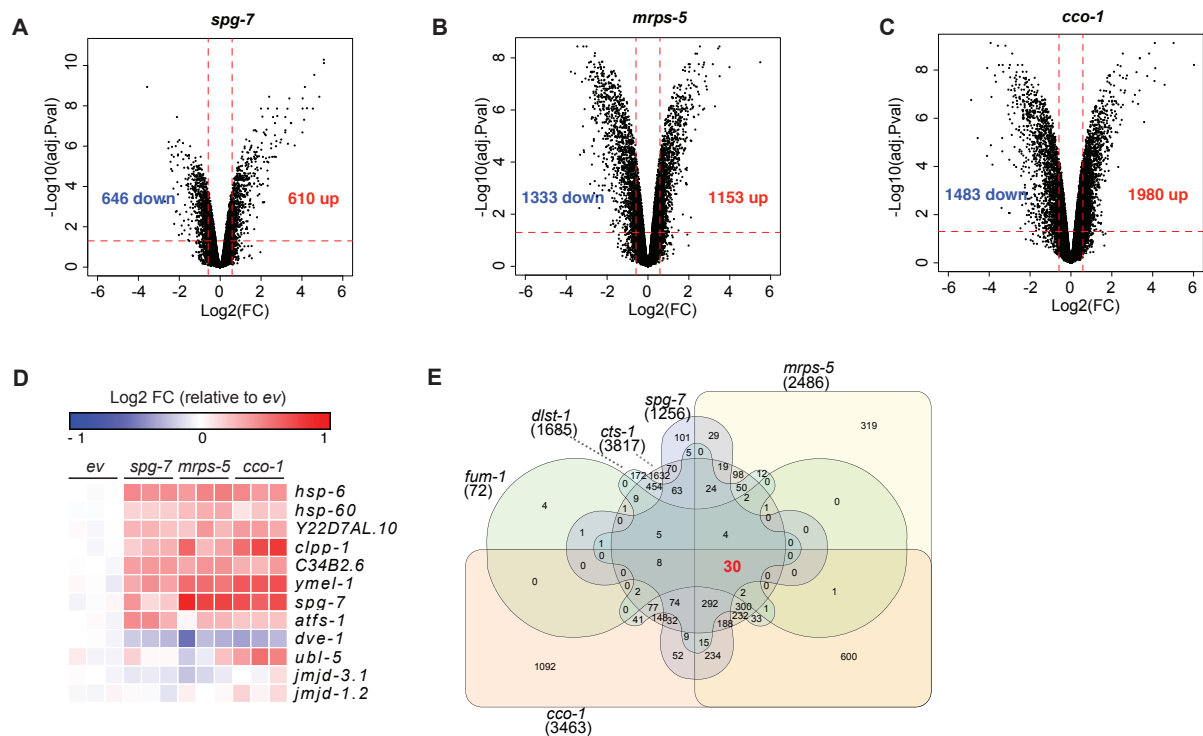
Figure 3:7 Gene expression analysis of animals treated with prototypical inducers of the UPR^mt , *spg-7, mrps-5* and *cco-1* RNAi .

Volcano plots of gene expression changes of wild type N2 worms treated only during development with (A) *spg-7*, (B) *mrps-5* and (C) *cco-1* RNAi compared to *ev* RNAi control. Fold change>1.5, Benjamini-Hochberg adjusted p value < 0.05. (D) Heatmap of UPR^mt gene expression in animals treated with RNAi targeting *spg-7*, *mrps-5* and *cco-1* compared to *ev* RNAi control. Fold change (FC) was calculated by comparing normalized expression values of each condition to *ev* control and then transformed to log2 scale. (E) Venn diagram of DEGs in animals treated with RNAi against *fum-1*, *dlst-1*, *cts-1*, *spg-7*, *mrps-5* and *cco-1*. There are 30 overlapping genes in all 6 conditions, which are indicated in red.

RNAi targeting the mitochondrial matrix protease *spg-7*, the mitochondrial ribosomal protein *mrps-5*, and the ETC complex IV component, *cco-1*. Knockdown of those 3 genes is known to induce the UPR^{mt} and is associated with longevity [41,42,124]. A total of 1256 genes were changed after *spg-7* RNAi (Figure 3:7A), 2486 after *mrps-5* RNAi (Figure 3:7B) and 3463 after *cco-1* RNAi (Figure 3:7C). Microarray data showed the activation of multiple UPR^{mt} genes, similar to the changes seen upon interference with the TCA cycle (compare Figure 3:7D and 3:5E). *spg-7* RNAi was having the weakest and *cco-1* RNAi the strongest effect on the induction of these UPR^{mt} genes (Figure 3:7D). Of note, *dve-1* expression was reduced in a similar fashion upon the induction of the UPR^{mt} as after TCA gene knockdown (Figures 3:7D and 3:5E).

After overlaying the DEGs from the 3 perturbations of the TCA cycle with those from the 3 inducers of mitochondrial proteotoxic stress (UPR^{mt}), 30 common genes were identified that were changed in all 6 conditions (Figure 3:7E). The expression of all genes, with one
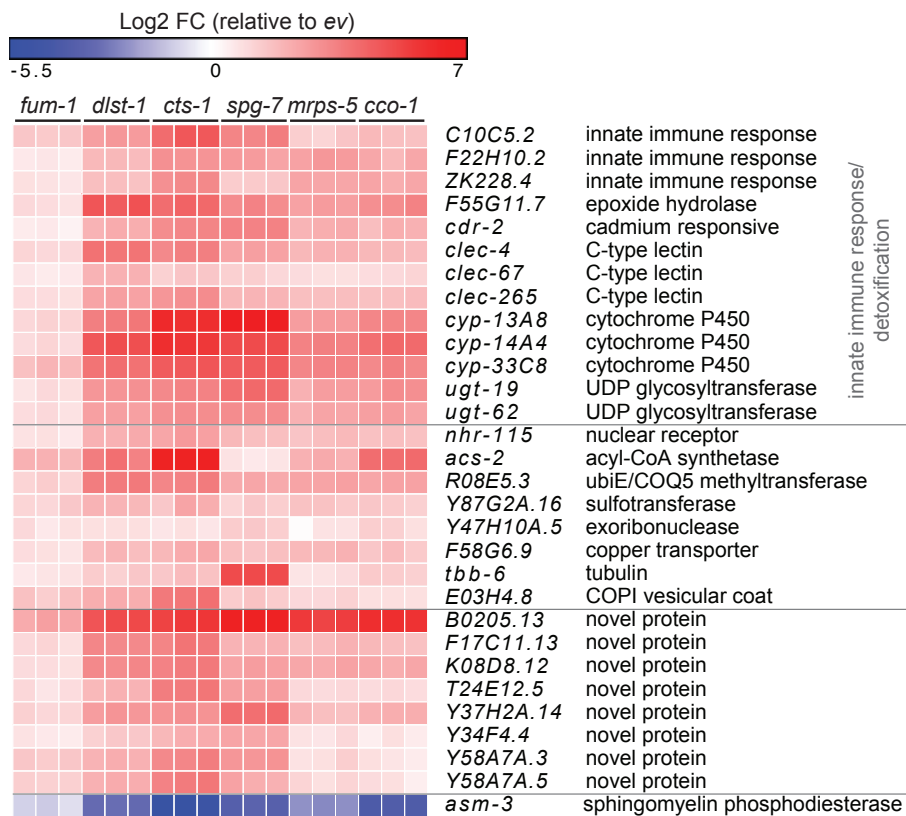
Figure 3:8 Common gene expression signature upon LOF of TCA cycle enzymes and of prototypical inducers of the UPR^{mt}.

Heatmap of expression changes and short description of the 30 common induced genes in animals treated with the RNAi against *fum-1*, *dlst-1*, *cts-1*, *spg-7*, *mrps-5* and *cco-1* compared to *ev* RNAi control. Fold change (FC) was calculated by comparing normalized expression values of each condition to *ev* control and then transformed to log2 scale.

exception, were highly increased in all 6 conditions; some of them showing an induction by more than 100-fold (Figure 3:8). A large group of 13 commonly induced genes were involved in the innate immune response or the detoxification of exogenous compounds. These genes include: the cadmium-responsive *cdr-2*, three C-type lectins, which are upregulated in response to stressors such as pathogens and ionizing radiation, three cytochrome P450s and two UDP glycosyltransferase genes that catalyze the metabolism of various exogenous compounds. Several other genes with diverse functions were also highly induced in all RNAi conditions. These include the nuclear receptor *nhr-115*, *acs-2*, involved in beta oxidation, *R08E5.3*, a homolog of ubiE-COQ5 methyltransferase, involved in biosynthesis of menaquinone and ubiqinone, the sulfotransferase, *Y87G2A.16*, the exoribonuclease *Y47H10A.5,* involved in pre-mRNA capping quality control, the copper transporter, *F58G6.9,* and structural constituents of the cytoskeleton, tubulin *tbb-6*, as well as Golgi-resident COPI vesicular coat protein, *E03H4.8*. Finally, several uncharacterized novel genes are also among the most induced in all examined mitochondrial perturbations. *asm-3*, sphingomyelin phosphodiesterase which converts sphingomyelin to ceramide, was the only gene whose expression was strongly reduced in all conditions. This set of genes likely describes a common signature of disturbed mitochondria and indicates the pleiotropic nature of the pathways affected by mitochondrial perturbations.

3.4 Discussion

We show here that LOF of enzymes involved in several TCA cycle reactions, namely citrate synthase, α-ketoglutarate dehydrogenase, fumarase, activates the *atfs-1*-dependent UPR^{mt}, as evidenced by (1) the study of two different UPR^{mt} reporter strains, (2) the UPR^{mt}-specific gene expression signatures, and (3) the typical development-restricted effects on lifespan. LOF of these TCA cycle enzymes also activated oxidative stress responses, but the stress seemed to be confined to mitochondrial stress pathways, as there was no impact on ER stress or HSR pathways. We investigated the gene expression patterns after *cts-1, dlst-1* and *fum-1* RNAi and identified several commonly changed molecular mechanisms. Finally, we also performed gene expression analysis of other prototypical genetic perturbations that are known to induce the UPR^{mt}, such as *spg-7, mrps-5, cco-1* RNAi feeding*,* and identified 30 genes, which commonly change in all examined mitochondrial perturbations.

RNAi of TCA cycle enzymes during the whole life had varying effects on lifespan. Presumably, as TCA cycle is highly interconnected with other cellular pathways, each TCA cycle perturbation had unique consequences, which impacted in a specific fashion on the

general physiology and lifespan of the worm. It is interesting to note that for the three examined TCA enzymes *fum-1, dlst-1* and *cts-1*, RNAi only during development was more beneficial than during the whole life. In case of *fum-1*, worms lived shorter with full-life RNAi, while their lifespan was similar to *ev* control when RNAi was applied only during development. Longer lifespan was also observed with *dlst-1* and *cts-1* RNAi, when RNAi-mediated knockdown was applied only during larval development, compared to the whole life treatment. As defined for *cts-1* RNAi, there was a decrease of lifespan when RNAi was applied only during adulthood. Thus likely, no change in *C. elegans* lifespan when *cts-1* RNAi is provided during the whole life is a cumulative effect on beneficial effects of RNAi during development and detrimental effects when RNAi is provided during adulthood. What mechanisms play a role in this phenomenon, most likely different depending on the *C. elegans* life stage, and whether the same can be observed for other TCA cycle enzymes, or other mitochondrial genes associated with lifespan regulation, is a future direction of investigation. Clearly, one of the regulating mechanisms positively contributing to the increased longevity when RNAi is applied during development is the UPR^{mt}. The ability to extend lifespan when RNAi treatment is restricted only during the larval development stages, has been reported for the lifespan extension by RNAi of *cco-1* [42] and *mrps-5* [41], and appears to be fully dependent on the induction of the UPR^{mt}. Consistent with these reports, the lifespan extension by one of the TCA cycle genes, *cts-1*, RNAi during development, was fully dependent on the main transcriptional UPR^{mt} regulators, *atfs-1* and *ubl-5*. Lifespan extension was also partially dependent on the histone demethylase, *jmjd-3.1*, consistent with a similar partial effect reported for *cco-1* RNAi induced longevity [122].

Presumably, the reason why specifically citrate synthase, α-ketoglutarate dehydrogenase, and fumarase RNAi strongly trigger UPR^{mt} and not RNAi of other TCA enzymes, as well as why these conditions each affect the lifespan in a distinct manner, may depend on the metabolites that accumulate after knockdown in those conditions. It has been reported that supplementation of α-ketoglutarate [108], oxaloacetate [125], malate and fumarate extend lifespan [126]. In addition, it is known that α-ketoglutarate is a cofactor for DNA and histone demethylases [127], including the Jumonji C domain (JmjC) containing demethylases such as *jmjd-1.2* and *jmjd-3.1*, which have been shown to be positive regulators of lifespan [122]. These findings may explain the lifespan increase after *cts-1* and *dlst-1* RNAi, where accumulation of their substrates, oxaloacetate and α-ketoglutarate, respectively, could occur. However, to evaluate this possibility, precise measurements of quantitative changes in TCA cycle metabolites after RNAi of different enzymes should be

performed. In addition, it should be assessed, whether the supplementation of metabolites induces UPR^{mt}.

We examined the gene expression profiles of three UPR^{mt} inducing TCA cycle RNAi conditions *fum-1, dlst-1* and *cts-1* by microarray analysis and identified that 70-90% of changed genes were common in all conditions. The most changes were triggered by *cts-1* RNAi, which is the first enzyme and entry into the cycle. Disturbance of later steps of TCA cycle by *dlst-1* or *fum-1* has less effect, possibly because less reactions of the cycle are affected and some of the intermediate metabolites can be also replenished by anaplerotic reactions, leading to smaller impact on the cellular pathways, which depend on TCA cycle. We further performed the microarray analysis of three RNAi conditions targeting mitochondrial *spg-7, mrps-5* and *cco-1* genes, which have been established as genetic UPR^{mt} inducers. The number of changed genes was similar between RNAi of *cts-1* and *cco-1*, indicating that the extent of changes invoked by repressing the function of either TCA cycle or oxidative phosphorylation are comparable, consistent also with their similar positive effects on lifespan. Induction of UPR^{mt} signature genes was clear among the majority of examined TCA cycle and other mitochondrial perturbation conditions with the exception of *fum-1* RNAi, which, perturbing the end of the TCA cycle, triggered relatively few gene expression changes. More common pathways could be identified by a deeper analysis of changed genes.

Microarray analysis of knockdowns of six different mitochondrial proteins revealed an interesting set of common genes, which could be called the core mitochondrial perturbation signature. Almost half of the induced genes are involved in innate immunity and detoxification. This is in accordance with several studies reporting such response to mitochondrial dysfunction, which is regulated by *atfs-1* [37,128]. In addition, there was a decrease of *asm-3*, and enzyme involved in ceramide synthesis, which indicates that ceramide levels are decreased after mitochondrial perturbation. The reduced ceramide content after mitochondrial stress has also been observed in the Dillin laboratory [129]. However, it has been reported that ceramide was required for the activation of the UPR^{mt}, possibly participating in an early step of mitochondrial surveillance by specifically marking outer membranes of dysfunctional mitochondria [37]. As different ceramide species have been examined in the aforementioned studies, most likely they each have specific functions in mitochondrial stress signaling. It is also possible that ceramide is required in the initial induction of UPR^{mt} and then it is downregulated in a negative feedback loop; this hypothesis hence requires further investigation. In addition, there is a significant induction

of the hedgehog receptor activity GO category in both *dlst-1* and *cts-1* RNAi conditions. It is well known that hedgehog proteins can be covalently modified with cholesterol [130]. Importantly, it has been already shown that statins, cholesterol-lowering drugs, abrogate the ability to sense mitochondrial damage and activate the UPR[mt] [37], while gain-of-function *atfs-1* mutants are protected against statin toxicity [60]. With multiple indications from previous reports and our data, lipid homeostasis and specific lipid molecules such as ceramide and cholesterol likely play an important role in resolving mitochondrial stress, which requires further studies. Several other interesting genes were exposed by our transcriptomic analysis of mitochondrial stress pathways, raising several interesting questions, e.g., what is the role of induction of primary β-oxidation enzyme *acs-2*, nuclear hormone receptor *nhr-115* or copper transporter *F58G6.9* in animals with perturbed mitochondria.

In conclusion, we identified that knockdown of three specific TCA cycle enzymes induces mitochondrial repair mechanism UPR[mt] and affects lifespan. We analysed their gene expression in comparison to other genetic mitochondrial perturbations leading to UPR[mt] and identified commonly changed gene sets. Deeper understanding of some of the described molecular mechanisms involved in mitochondrial dysfunction and their relevance in lifespan regulation might help to discover strategies for treating mitochondrial diseases and better aging.

3.5 Materials and methods

C. elegans strains

C. elegans strains were cultured at 20°C on nematode growth media (NGM) plates seeded with the HT115 bacteria expressing RNAi constructs. Strains used were wild type Bristol strain (N2), SJ4100 (zcIs13[*hsp-6*::GFP]), SJ4005 (zcIs4[*hsp-4*::GFP]), SJ4058 (zcIs9 [hsp-60::GFP + lin-15(+)]), KN259 (huIs33[*sod-3*::GFP + pRF4(*rol-6*(su1006))]), CL2070 (dvIs70 [hsp-16.2p::GFP + rol-6(su1006)]) and were provided by *Caenorhabditis* Genetics Center (University of Minnesota). The zcIs9 [hsp-60::GFP + lin-15(+) + *atfs-1(tm4525)V*] was kindly provided by Cole Haynes (MSKCC).

Lifespan analysis

Lifespan experiments were performed as previously described [122]. Briefly, 60-100 animals were used per conditions and scored every other day. Animals that crawled off the plate or had an exploded vulva phenotype were censored. For whole life RNAi experiments, animals were treated with RNAi from egg development until the end of life.

For selective RNAi only during development, animals were grown on RNAi plates from egg development until the L4 stage and then transferred to empty vector (*ev*) control plates. For selective RNAi only during adulthood, animals were treated with *ev* RNAi from egg development and transferred to plates with the indicated RNAi at L4 stage until the end of life. For lifespan experiment with RNAi mixing, indicated RNAi bacteria were mixed 1:1 before seeding on the plates. Survival analyses were performed using the Kaplan Meier method and the significance of differences between survival curves calculated using the log rank test.

Fluorescence analysis

The GFP reporter strains were treated with RNAi starting from egg development until microscopy at day 1 of adulthood. For fluorescence microscopy, animals were blindly chosen under the light microscope from a population and immobilized with 10 mM solution of tetramisole hydrochloride (Sigma) in M9 before taking their pictures.

Respiration assay

Wild type N2 worms were treated with RNAi starting from egg development until the assessment at day 1 of adulthood. Oxygen consumption was measured using the Seahorse XF96 equipment (Seahorse Bioscience Inc.). Typically, 100 animals per condition were recovered from NGM plates with M9 medium, washed three times in 2 ml M9 to eliminate residual bacteria, and resuspended in 500 ml M9 medium. Worms were transferred in 96-well standard Seahorse plates (#100777-004) (10 worms per well) and oxygen consumption was measured 6 times. Respiration rates were normalized to the protein content for each condition.

Microarray analysis

C. elegans were age synchronized by egg bleaching and cultivated on NGM plates seeded with HT115 bacteria expressing RNAi constructs at 20°C and harvested at L4 stage. Total RNA was isolated using Trizol (Life Technologies) and purified using the RNeasy Mini Kit (Qiagen) in accordance with the manufacturer's instructions. Microarray analysis was performed using Affymetrix *C. elegans* Gene 1.0ST chips in triplicates per RNAi condition. Microarray data was analyzed using Bioconductor libraries in R. A threshold of 1.5-fold change compared to empty vector (ev) control and Bonferroni adjusted p value of 0.05 was used to determine the differentially expressed genes (DEG). Volcano plots were generated with R (www.r-project.org), heatmaps with GENE-E (Broad

Institute), and Venn diagrams with InteractiVenn [114]. GO terms were determined with DAVID [101] using Bonferroni adjusted p value < 0.05.

3.6 Acknowledgements

3.7 Author contributions

V.J. and J.A. designed the study and wrote the manuscript. V.J. performed the experiments and analyzed data. A.M. contributed to microarray sample preparation. O.M. contributed to lifespan experiments. Microarray samples were processed in R.W. W. laboratory.

3.8 Supplementary data

Table 3:S1 Lifespan statistics

Figure	RNAi	Mean lifespan ± SEM (days)	Variation compared to *ev* (%)	p value compared to *ev*	p value compared to *cts-1/ ev*	Deaths/total
3:3	*ev*	18.8 ± 0.563				60/70
	cts-1	18.2 ± 0.562	-3.19	ns		41/70
	aco-2	21.5 ± 0.758	14.36	<0.0001		58/70
	idha-1	16.3 ± 0.518	-13.30	0.0013		51/70
	idhb-1	21.3 ± 0.483	13.30	0.007		47/70
	ogdh-1	20.3 ± 0.588	7.98	0.014		57/70
	dlst-1	22.1 ± 0.493	17.55	<0.0001		58/70
	dld-1	19.8 ± 0.456	5.32	ns		54/70
	sucl-2	17.3 ± 0.424	-7.98	0.0054		58/70
	sucg-1	19.1 ± 0.386	1.60	ns		47/70
	suca-1	19.2 ± 0.542	2.13	ns		57/70
	sdha-1	14.4 ± 0.373	-23.40	<0.0001		58/70
	sdhb-1	16.5 ± 0.42	-12.23	<0.0001		42/70
	mev-1	14.6 ± 0.425	-22.34	<0.0001		42/70
	sdhd-1	14.7 ± 0.388	-21.81	<0.0001		45/70
	fum-1	16.4 ± 0.381	-12.77	<0.0001		51/70
	mdh-1	20.1 ± 0.507	6.91	ns		57/70
	mdh-2	14.6 ± 0.285	-22.34	<0.0001		58/70
3:4A-C	*ev*	17.5 ± 0.493				96/100
	fum-1	18.8 ± 0.537	7.43	ns		74/100
	dlst-1	23.7 ± 0.689	35.43	<0.0001		71/100
	cts-1	28.2 ± 1.419	61.14	<0.0001		31/100
3:4D	*ev*	20.8 ± 0.434				108/112
	cts-1 (whole life)	21.6 ± 0.606	3.85	ns		30/112
	cts-1 (development)	28.4 ± 0.895	36.54	<0.0001		59/112
	cts-1 (adulthood)	17.8 ± 0.346	-14.42	<0.0001		109/112
3:4E	*ev*	22.5±0.62				89/100
	cts-1/ev	32.8±0.864	45.78	<0.0001		83/100
	cts-1/ubl-5	21.2±0.516	-5.78	ns	<0.0001	98/100
	cts-1/atfs-1	22.7±0.534	0.89	ns	<0.0001	97/100
	cts-1/jmjd-3.1	28.2±0.872	25.33	<0.0001	<0.0001	91/100

Chapter 4　Bioinformatic analysis of UPR^{mt}

This chapter presents two systemic studies of BXD genetic reference population resource and investigates UPR^{mt} as an example. I performed *C. elegans* based experiments, and contributed to conceiving ideas and writing on the parts of manuscripts related to UPR^{mt}.

4.1 Multilayered genetic and omics dissection of mitochondrial activity in a mouse reference population

The manner by which genotype and environment affect complex phenotypes is one of the fundamental questions in biology. In this study we quantified the transcriptome, a subset of the metabolome, and using targeted proteomics, a subset of the liver proteome from 40 strains of the BXD mouse genetic reference population on two diverse diets. We used the integrated molecular profiles to characterize complex pathways, as illustrated with the mitochondrial unfolded protein response (UPR^{mt}). The UPR^{mt} shows strikingly variant responses at the transcript and protein level that are remarkably conserved between *C.elegans*, mice, and humans. Overall, these examples demonstrate the value of an integrated multilayered omics approach to characterize complex metabolic phenotypes.

4.1.1 Introduction

The central dogma of molecular biology states that genetic information encoded in DNA is first transcribed by RNA polymerase, then translated by ribosomes into proteins. However, the DNA sequence of a gene provides little information for predicting when, where, and to what extent its associated RNA and protein products will be expressed. Since the advent of microarray technology, comprehensive gene expression patterns—i.e. the transcriptome—can be precisely and comprehensively quantified across large populations. Unfortunately, transcript levels generally have only modest correlation with the levels of corresponding proteins [131-133], and genetic variants similarly affecting both the transcript and peptide levels of a gene are relatively uncommon [134,135]. As proteins in most cases are more directly responsible than transcripts in the regulation of cellular pathways—and ultimately phenotypic traits—there is a critical need for efficient, large-scale and accurately quantitative proteomics methods to complement transcriptomic datasets.

Over the past decade, the development of discovery mass spectrometry ("shotgun") has allowed the first large-scale studies on quantitative proteomics. In this approach, protein extracts are cleaved into short peptide sequences, which are then chromatographically separated and analyzed by tandem mass spectrometry. This allows the untargeted discovery of thousands of peptides, but if the number of unique peptide fragments in a sample significantly exceeds the number of available sequencing cycles (as in whole proteome extracts), any individual peptide will be inconsistently sampled across repeat analyses. This reduces the technical reproducibility, but moreover means that the number

of peptides consistently quantified across all (or most) samples decreases as the study size increases [136]. Consequently, discovery mass spectrometry strategy has yielded mixed results in large population studies [131,137], particularly as specific peptides of interest cannot be targeted, and the most consistently identified peptides are biased towards those of higher abundance [138]. To overcome these hurdles, selected reaction monitoring (SRM) was developed, which perfects technical reproducibility and allows consistent multiplexed quantitation of target proteins by deploying a mass spectrometric measurement assay that is specific for each targeted peptide [139]. Thus, hundreds of target peptides can be consistently and accurately quantified across large populations of samples. Recent studies in yeast have shown that the proteins and transcripts of genes are typically controlled by different, distinct mechanisms [135,140]. However, these hypotheses have not been well tested in mammalian genetic reference populations (GRPs) through multilayered transcriptomic and proteomic strategies.

Large GRPs are frequently used to determine to which extent phenotypic variation is driven by genetic variants (i.e. heritability), and to subsequently identify genes driving such variation. These genes can be identified by genome-wide association (GWA) or by quantitative trait locus (QTL) mapping, approaches that have been applied to various species and have led to the successful identification of dozens of major allelic variants [90,141-143]. In mammals, the murine BXD family is the largest and best studied GRP, consisting of ~150 recombinant inbred strains descended from C57BL/6J (B6) and DBA/2J (D2) [90]. Using 40 strains of this population on both chow (CD) and high fat (HFD) diets, we have obtained major metabolic phenotypes and established a multilayered dataset focused on 192 metabolic genes expressed in the liver. For all genes, we know the sequence variants, transcript levels, and protein levels in all cohorts. This data is further supplemented with targeted metabolite analysis in liver and serum, generating the first large-scale multilayered quantitative picture of any cellular process in the BXD population.

4.1.2 Protein targeting across a genetically & environmentally diverse murine population

We first selected 192 metabolic proteins for study, with particular focus on genes regulating mitochondria and general energy metabolism. For each gene, synthetic peptides were generated based on established assays [144] (Figure 4:1A) to accurately quantify each protein across all cohorts. To validate peptide measurements, we compared the coefficients of variation (CV) among technical and biological peptide replicates. Both technical and biological replicates showed a high degree of reproducibility (CV ~ 0.09 and

0.12 respectively), indicating the peptides are sufficiently accurate for the quantification of targeted peptides across large, diverse populations. More importantly, the results for biological replicates reveal nearly equally high overall reproducibility ($r > 0.98$; Figure 4:1B), suggesting low biological variance within each cohort, particularly relative to cross-cohort variance (CV ~ 0.33). 82.1% of the quantified peptides are highly variable (CV > 0.20), indicating that the biological error (i.e. variation within a cohort) is much smaller than the variation induced by differences in genotypes and diet. We observed nearly complete quantification of all 192 proteins across all cohorts, with only ~60 missing peptide counts out of ~15,000 measurements (i.e. 99.6% completion; Figure 4:1C, top). This completion is similar to the level of completeness achieved by microarrays (Figure 4:1C, bottom) and a major contrast to shotgun-acquired proteomics, which typically have completeness of ~70% [136].

It has been well-established that transcriptomic networks of many metabolic processes covary quite well, e.g. within the electron transport chain or within the citric acid cycle [145]. On protein level, proteins which function in common biological processes or which localize to the same functional modules are also reported to be subject to similar regulatory process and generally covary [146]. To validate and identify which of these 192 proteins vary synchronously, we computed the robust Spearman correlation network for all protein pairs using the full SRM dataset (Figure 4:1D). The resulting network contained 82 correlated nodes (proteins) with 211 edges in 3 main enrichment clusters. As expected, many of the mitochondrial proteins and proteins involved in lipid metabolism are highly correlated (Figure 4:1D, cluster a and b). Within cluster a. are five of the six measured proteins involved in mitochondrial unfolded protein response (UPR^{mt}) (HSPD1, HSPE1, HSPA9, CLPP, and LONP1 indicated in red), along with three of the four measured NADH dehydrogenase genes (NDUFA1, NDUFB3 and NDUFS6—in blue), and four of the eight measured mitochondrial-encoded proteins (MT-CYB, MT-CO2, MT-CO3, and MT-ND3 in black). Meanwhile, proteins involved in carbohydrate metabolism are enriched in the same cluster (Figure 4:1D, cluster c). These results show that functionally-related proteins tend to be coordinately regulated at a protein level, and that coregulation of protein abundance is strongly maintained for certain processes. To validate biological significance of these function-based covariation clusters, we further investigated one, the UPR^{mt} network (elaborated in Figure 4:3).
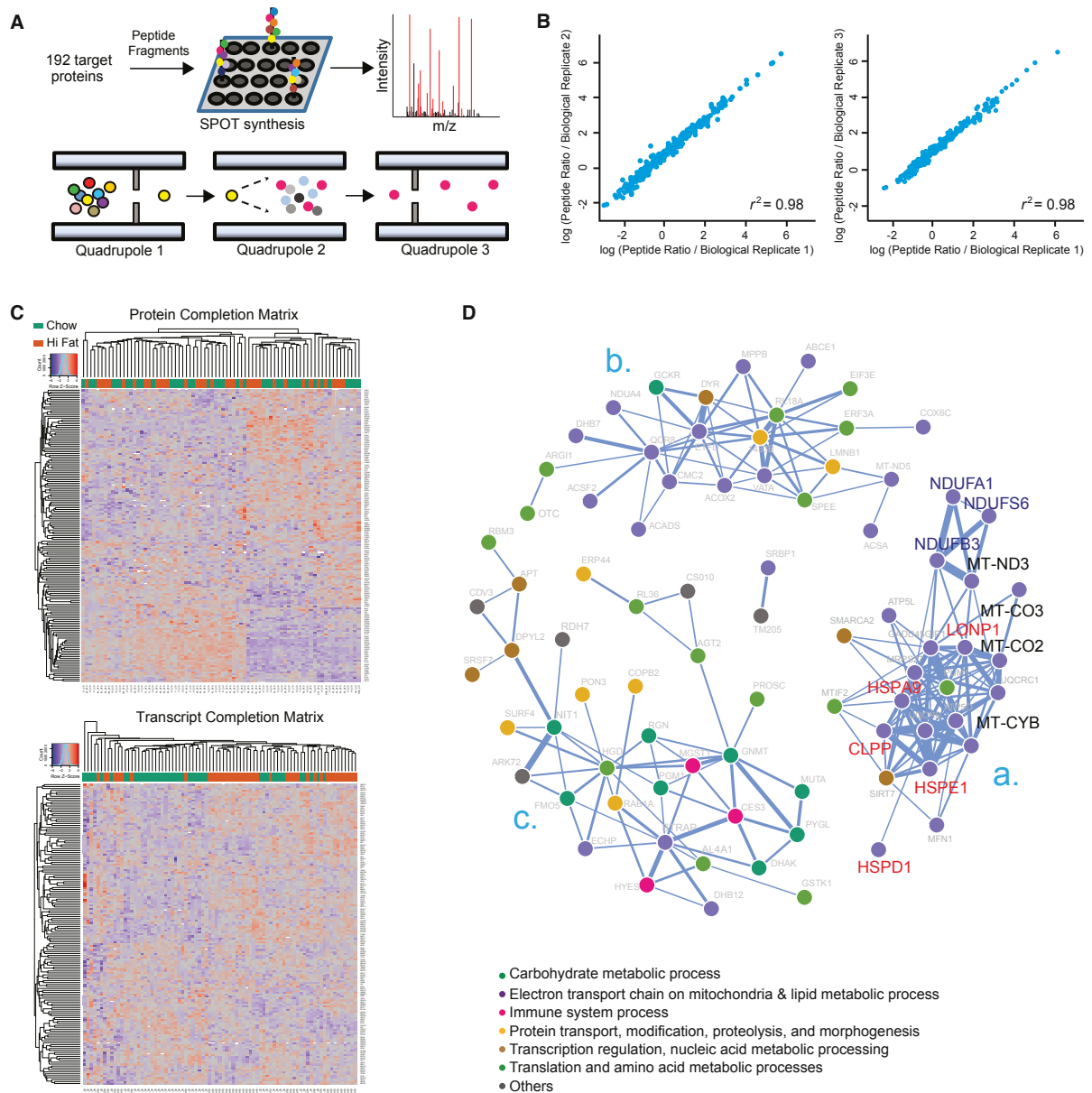
Figure 4:1. SRM-based protein quantification and covariation network

(A) SRM assay development for targeted proteomic measurements. 309 peptides corresponding to 192 genes were designed and synthesized via SPOT synthesis. Fragment ion spectra were generated on a triple-quadrupole MS with SRM-triggered MS2 mode, then ions were selected based on their relative intensities. Dot colors indicate different amino acids. m/z, mass-to-charge ratio. Mouse liver homogenate combined with the heavy reference proteome was analyzed with SRM on a triple-quadrupole MS. Different dot colors represent different peptides (Quadrupole 1) or product ions (Quadrupole 3). (B) Biological replicates had near-perfect reproducibility ($r^2 \sim 0.98$), shown here for all three biological replicates of the BXD60 CD cohort. (C) Two-way cluster analysis of protein (upper) and transcript (lower) abundances in all 77 cohorts (40 CD, 37 HFD). Columns are clustered based on samples, and rows are clustered based on gene-product abundances. Protein and transcript abundances are colored in a red-blue scale. Red: high abundance. Blue: low abundance. White: missing data. (D) Protein association network based on robust Spearman correlation measures for all protein pairs. Statistically significant and strong positive associations ($p < 0.01$ & $r > 0.6$) are edges. The largest correlation clusters are labeled "a.", "b.", and "c.". Nodes are labeled with protein names and colored according to their biological process, as reported by DAVID [101].

4.1.3 Protein and mRNA gene products generally do not correlate

With the general protein measurements validated, we generated a global overview of how genotype and diet influence differential transcript and protein expression (Figure 4:2A). At the genetic level, transcripts and proteins map to an equivalent number of significant QTLs: we detected 65 significant transcript QTLs (eQTLs—blue lines at center) and 57 significant protein QTLs (pQTLs—red lines at center). However, though the total number of eQTLs and pQTLs are roughly equivalent, the predominant type of regulation was very different: 74% of the eQTLs are *cis*-mapping (ratio of solid to dashed blue lines), versus only 31% of pQTLs (ratio of solid to dashed red lines). This indicates a closer connection between a transcript and its gene than a protein and its gene. In general, *trans*-mapping proteins and transcripts mapped evenly across the genome, not yielding any clear "hot spots" for these metabolic genes (sample magnification of QTLs mapping to chromosome 5 in Figure 4:2B).

Within each diet, we found proteins and transcripts to be nominally correlated for ~25% of genes (i.e. Spearman correlation *p*-value < 0.05; Figure 4:2C, diets considered separately), similar to findings in other species and populations [131,132,134,147]. Of the correlated transcript–peptide pairs (46 in CD, 55 in HFD), 31 correlate significantly in both diets (16%), while 70 pairs (36%) correlate in at least one diet. Correspondingly, while ~50% of genes were affected by diet, transcripts were more frequently influenced (84 of 189) than proteins (37 of 192), with only 21 genes affected at both the transcript and protein level (Figure 4:2D). Genes which were the most strongly affected by diet at the transcript level (Figure 4:2E) tend to be similarly affected at the protein level (Figure 4:2F)—e.g. *Cyp3a11* is higher in CD—though exceptions are frequent, e.g. *Srebf1* mRNA is induced by HFD, but unaffected at the protein level, while in another counter-example, the HFD cohorts have more ETFDH protein, but less of the transcript. Thus, while transcripts and proteins are moderately covarying estimations of their gene's activity and typically have covarying responses to external factors (e.g. diet), these trends are too weak to support the measurement of any one particular transcript to serve as a proxy for the protein (or vice versa) without prior knowledge.

4.1.3 The Mitochondrial Unfolded Protein Response (UPR^mt)

The UPR^{mt} is a mitochondrial stress response pathway that is activated by proteostatic stress, such as by accumulation of unassembled or unfolded proteins in the mitochondria [33], by the presence of an imbalance between mitochondrial and nuclear encoded proteins [41], transcription/translation of nuclear-encoded or by electron transport chain
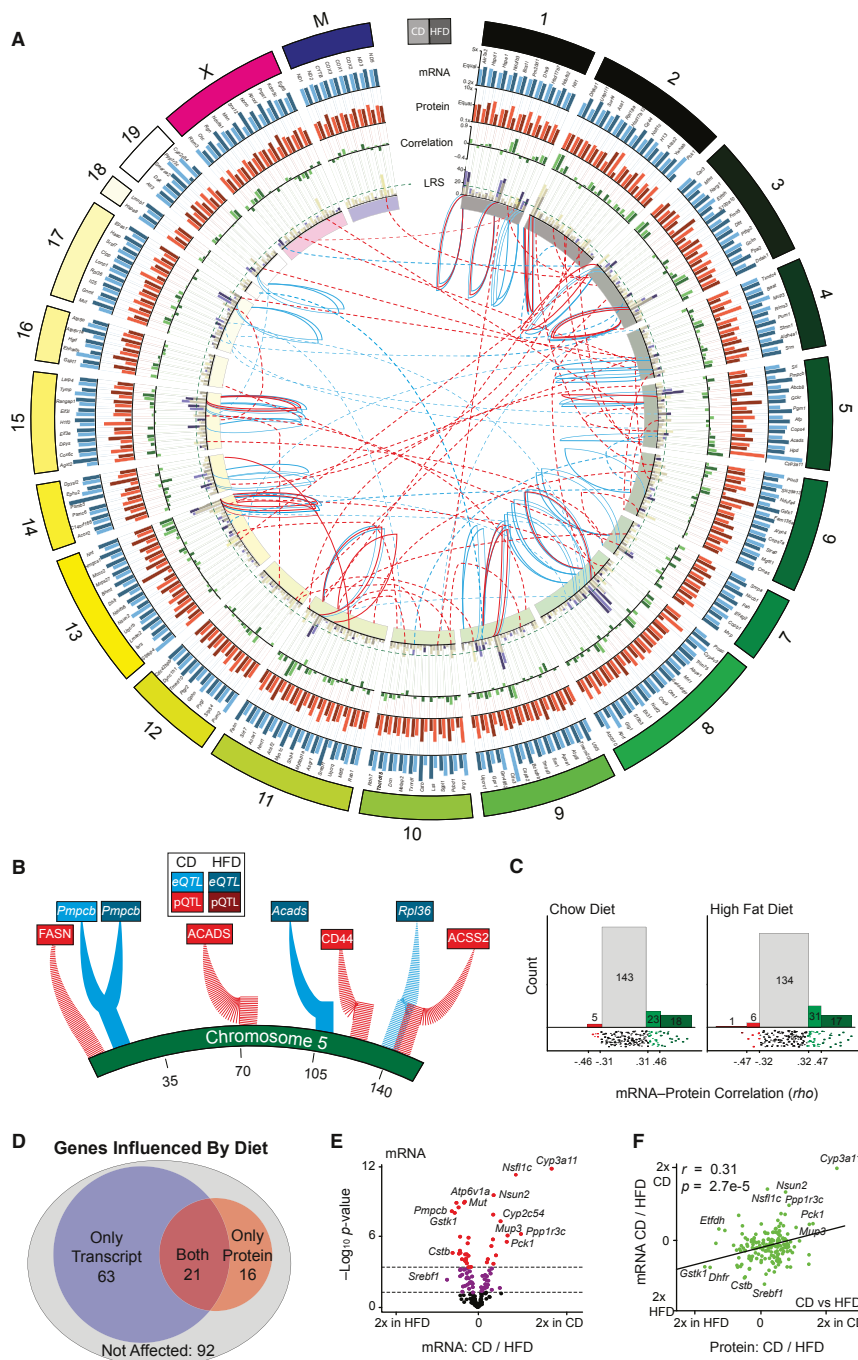
Figure 4:2. mRNA and protein overview

(A) Circos plot of mRNA and protein data for all 192 genes, labeled on outer edge. Genes are represented by two bars: light for CD, dark for HFD. Genes are arranged by relative chromosome position; chromosome length is according to number of genes measured. Blue Bars: Transcript relative expression CD vs. HFD; Orange Bars: Protein relative expression CD vs. HFD. Bars with more unequal heights indicate diet has a larger impact. Green Bars: Correlation between transcript and protein for each gene within each diet. Purple/Yellow Bars: Fuchsia bars represent the strength of the peak eQTL. Yellow bars represent the strength of the peak pQTL. The two bars are overlaid with transparency. The dashed green line represents the simplified significance cutoff (LRS ≥ 18). Inner Ring: Chromosome location. Central Lines: Blue lines for significant eQTLs, red for significant pQTLs. Solid lines represent *cis*-QTLs, dashed lines represent *trans*-QTLs. QTL lines stem from the LRS bar graph, and terminate on the inner side of the chromosome ring at the approximate QTL location. (B) Magnified view of eQTLs/pQTLs mapping to

chromosome 5. (C) In CD ~25% (left) and in HFD ~30% (right) of transcripts correlate nominally significantly with their protein. The lower strip charts show correlation distribution. Spearman correlation values corresponding to nominal significance ($p < 0.05$) and corrected significance ($p < 0.0002$) are displayed on the axis. (D) Venn diagram of genes, which are differentially regulated between CD and HFD as transcripts (blue), proteins (red), both (purple), or neither (grey). (E) Volcano plot for mRNA showing magnitude of dietary effect versus significance. ~45% vary with nominal significance ($p < 0.05$) between the dietary conditions. ~19% vary with corrected significance (raw-$p < 0.0003$). Some extreme genes are labeled. (F) Plot of the effect of diet on transcripts vs. the effect of diet on proteins. In general, transcripts and proteins are similarly affected by diet.

defects [36,148]. The activation of UPR^{mt} in turn leads to the protective genes such as mitochondrial chaperones and proteases to reestablish mitochondrial proteostasis (reviewed in [18,149,150]). The bulk of research on the UPR^{mt} has taken place using *C. elegans* and mammalian cell lines, thus little is known about when or how UPR^{mt} occurs *in vivo* in mammals. Furthermore, as the UPR^{mt} is a stress response tied to maintaining mitochondrial protein balance, we hypothesized that its protein correlation networks may be different than those generally examined at the transcriptional level.

In the worm, two "classical" approaches have been typically used to induce the UPR^{mt}: loss-of-function of *cco-1*, a nuclear encoded component of the electron transport chain [148], or loss of function of *spg-7*, a mitochondrial protein quality-control protease [30]. We confirmed that the knockdown of either gene by RNAi triggers the UPR^{mt} response in *C. elegans*, by strong induction of the mitochondrial chaperone *hsp-6* and of the proteases *lonp-1* and *clpp-1* (Figure 4:3A). Moreover, we linked this UPR^{mt} activation to specific phenotypes—a major reduction in size and mobility, as well as a decrease in oxygen consumption—which are consequences of mitochondrial stress (Figure 4:3B). However, whether this coordinated regulation of UPR^{mt} genes is conserved in mammals *in vivo*, has not been previously shown.

In the BXDs, we investigated the expression of six members of the UPR^{mt} pathway, which are well-conserved from *C. elegans*: mitochondrial chaperones (*Hspd1, Hspe1, Hspa9*), proteases (*Clpp, Lonp1*), and a transcriptional regulator involved in UPR^{mt} (*Ubl5*). These UPR^{mt} genes are also coordinately regulated at both mRNA and protein level in the BXDs, but with much stronger connections among proteins (Figure 4:3C). Moreover, the UPR^{mt} network correlates negatively with *Cox5b* and *Spg7* (mouse orthologs of worm *cco-1* and *spg-7*, respectively), indicating that low abundance of these genes amplifies UPR^{mt} in mammals as in *C. elegans* (Figure 4:3D). The network is also influenced in part by diet. While *Cox5b* expression patterns are similar between CD and HFD, *Spg7* covariation is disjointed between the dietary cohorts (Figure 4:3E). This may explain why, despite a similar overall UPR^{mt} response in both diets (Figure 4:3D & F), *Spg7* trends positively in HFD cohorts, while *Cox5* remains consistent (Figure 4:3G). Using four large
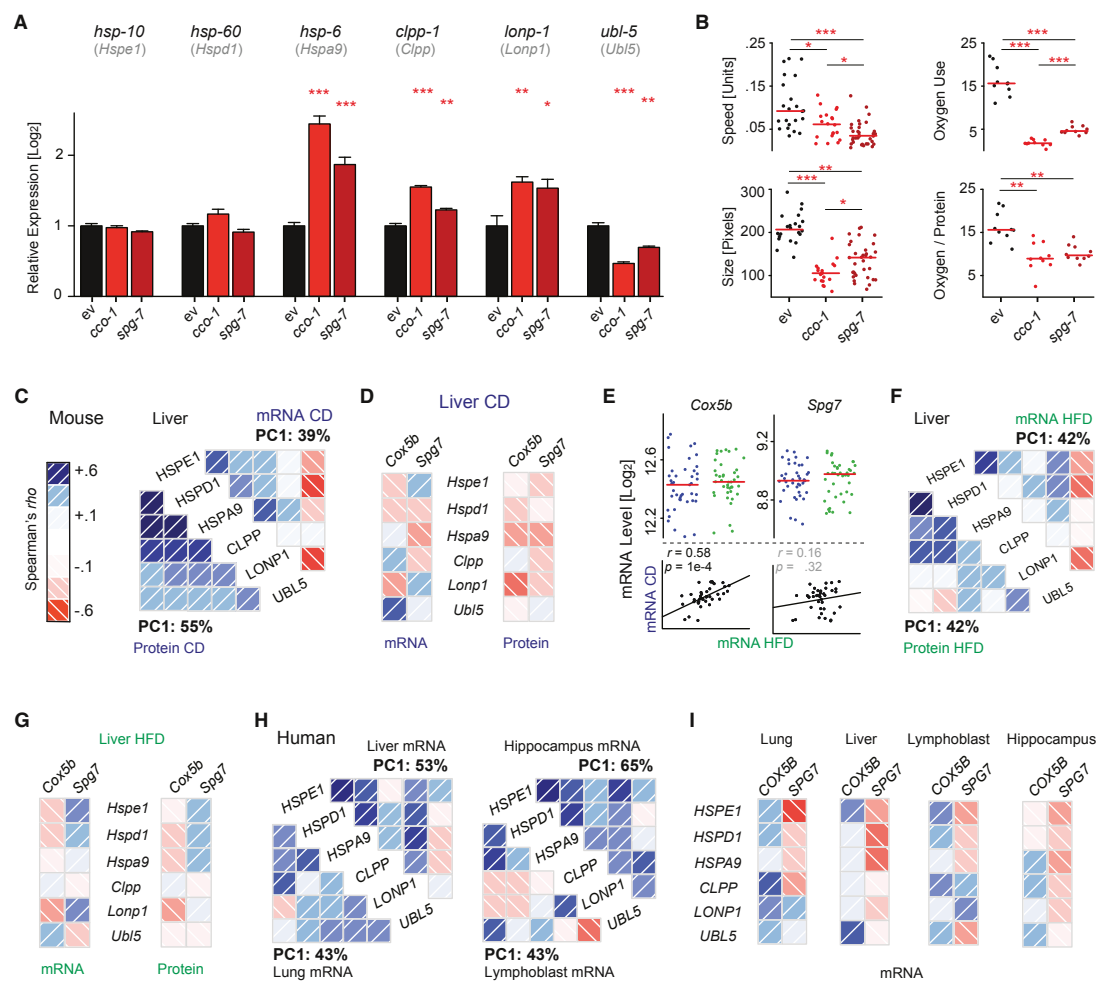
Figure 4:3 The mitochondrial unfolded protein response

(A) UPR[mt] induction in *C. elegans* triggered by interference with ETC (RNAi of *cco-1*) or mitochondrial proteostasis (RNAi for *spg-7*). These triggers result in upregulation of UPR[mt] effectors *hsp-6*, *clpp-1*, and *lonp-1* and a reduction in *ubl-5*. The orthologous mouse genes are indicated below the respective *C. elegans* gene symbol. Error bars represent mean +/- SEM. (B) UPR[mt] induction in *C. elegans* decreases movement, size, and oxygen consumption. (C) UPR[mt] genes and proteins form a network of coordinately expressed mRNAs and proteins in vivo in mice, which is stronger at the protein than at the mRNA level. (D) *Cox5b* and *Spg7* (orthologs of *C. elegans cco-1* and *spg-7*) are generally negatively associated with the levels of all UPR[mt] genes in CD cohorts, particularly at the protein level, in line with observations in the worm. (E) While the levels of *Cox5b* and *Spg7* are not affected by diet, expression is consistent by strain across the two diets only for *Cox5b*. (F) The UPR[mt] network in HFD livers is similar to that observed in CD, but somewhat weaker. *Ubl5* remains a striking negative correlate at the mRNA level. (G) In HFD, *Cox5b* remains a negative correlate of UPRmt transcripts and proteins, while *Spg7* does not. (H) The features of the UPR[mt] network are also conserved in 427 human liver biopsies (Schadt et al., 2008), 405 lung biopsies (Ding et al., 2004), 180 lymphoblast lines (Monks et al., 2004), and 43 hippocampi (Berchtold et al., 2008). (I) In humans, *SPG7* is a consistent negative correlate of the UPR[mt] transcripts.

transcriptional studies of human tissue biopsies, we observe similar transcriptional links, particularly including a strong network between all the UPR[mt] genes (Figure 4:3H). In humans, *SPG7* is a consistent negative correlate of this network, in contrast to *COX5B,* which generally has positive covariation with the UPR[mt] response (Figure 4:3I).

Thus, while many of the overall regulators of UPR^{mt} remain coregulated across species—worm, mouse and human—particular nuances of its activation pathways appear variable dependent on species, environment, tissue, and likely other factors.

4.1.4 Discussion

Due to major differences in transcript and protein regulation, it has become increasingly clear that systems proteomics is essential for the analysis of complex systems such as metabolism [134,151]. Traditionally this was attempted by semi-quantitative immunoassays such as ELISA or Western blotting, yet these techniques allow only a handful of proteins to be measured in parallel, and are moreover limited by the scarcity of quantitative immunoassays and the dubious quality of many antibodies [152]. Recent shotgun proteomics experiments on diverse populations have provided fundamental data on protein variance in populations of yeast [134,135], mammals [131], and humans [153]. However, the inability to measure target proteins has limited the application of this approach in the study of disease pathways. New developments in mass spectrometry have led to SRM, a targeted quantitative systems proteomics technique in which choice proteins can be quantified based on *a priori* information. This technique has been recently applied in a moderate-sized yeast population study [144], but until now has not been applied in multicellular species nor for the study of a choice pathway.

In this study, we quantified 192 metabolism genes at the transcript and protein level in livers from 77 cohorts of the BXD GRP under two different dietary conditions. Along with sequence variants, basic metabolomics, and phenotype data, this combined multilayered population dataset enabled us to accurately estimate abundance changes in gene products due to genotype, diet, and gene-by-environment interactions (GXE).

It is worth stressing that novel regulatory mechanisms can be found either through QTL analysis and their equivalent from GWAS, SNP analysis, or through network analyses, which are a complementary and powerful approach to dissect complex traits. The network approach is particularly viable when backed by high-depth multilayered datasets such as illustrated by our example on the UPR^{mt}. The UPR^{mt} is a reparative pathway activated by mitochondrial proteotoxic stress that has been primarily studied in the *C. elegans* and in cultured mammalian cells, but little is known about whether it occurs *in vivo* in mammals. We examined six genes that are known to be major regulators of the *C. elegans* UPR^{mt} and which are conserved in mammals. These six genes form a robust coexpression network in both diets at the transcriptional and proteomic levels, with the proteomic connections being stronger, befitting the role of the UPR^{mt} as a sensor and regulator of

protein stress. One observation that stood out in the analysis of the UPR^{mt}, was the striking "contradiction" between the *Ubl5* transcript and UBL5 protein correlations to the UPR^{mt} network. *Ubl5* is a transcriptional regulator known to induce the UPR^{mt}, yet in both worms and mice, its transcript levels decrease when the UPR^{mt} is activated. Conversely, the UBL5 protein is increased with UPR^{mt} activation in the BXDs, an observation also previously reported in *C. elegans* [56]. This discordance in protein/transcript regulation suggests the existence of posttranscriptional mechanisms or a negative feedback loop, which could not be detected at the transcript or protein level alone. While there remains a great deal of this pathway left to be explored, it is clear that accurate, systems-scale protein measurements are essential to effectively model complex protein response networks like the UPR^{mt}.

Today, there is an unprecedented capacity for accurate measurement quantification of nearly all aspects of biology. Surprisingly perhaps, proteins remain one of the most difficult aspects of biology to precisely measure at a systems scale, though it has been long clear that transcripts only serve as a weak proxy for protein levels [133]. Our data show that the integration of systems proteomics datasets with different layered systems measurements provides unprecedented insights into the mechanistic regulation of complex systems, such as exemplified by metabolism, that can eventually lead to the improved diagnosis and treatment of metabolic disease.

4.1.5 Materials and methods

Animals

40 strains of the BXD population—40 on CD, 37 on HFD—with ~10 male animals from each strain were separated into two cohorts of five for each diet. Food access was *ad libitum* for CD—Harlan 2018 6% kCal/fat, 74% carbohydrates, 20% protein—or for HFD—Harlan 06414 (60% kCal/fat, 20% carbohydrate, 20% protein). HFD cohorts received the diet from week 8 until sacrifice. Each cohort was communally housed until wk 23, after which animals were single caged until tissues collection at 29 wks after an overnight fast. Tissues were collected from 183 CD and 168 HFD animals, with at least 3 biological replicates for all cohorts.

Sample Preparation and Analysis

For liver analyses, three ~100 mg pieces were taken from cold storage for each individual, then weighed and sorted for mRNA, protein, and metabolite measurements. For microarray, mRNA from 3–5 individuals per cohort were prepared separately then pooled

equally after nanodrop quantification and run on the Affymetrix Mouse Gene 1.0 ST array platform. For proteomics, protein was prepared from one to three biological replicates per cohort. For metabolite measurements, all individuals in all cohorts were measured individually after polar extraction of samples.

SRM Assay Development and Protein Quantification

Generation of peptide library and development of SRM assays were performed as described [144]. Identical SRM assays for all 192 target proteins were run on all 77 cohorts. SRM traces were manually checked according to established criteria [139]. For relative quantification of each protein across the set of different cohorts, the raw intensity of transitions of the native and ($^{13}C_6$, $^{15}N_4$)-Arginine, ($^{13}C_6$, $^{15}N_2$)-Lysine peptides were considered. Technical reproducibility of SRM-based quantification was validated by measuring the individual samples with three independent mass-spectrometry injections.

General Informatic Analyses

Outliers were Windsorized prior to all analyses. SNP analysis was also performed using GeneNetwork, which contains the full sequence data of C57BL/6J and DBA/2J, as well as high density genotype information for all the BXD lines. Correlations are Pearson's *r* or Spearman's *rho*, depending on the absence or presence of outliers. Student's *t*-test was used for comparing two groups in normalized data (all protein and mRNA are normalized). Bonferroni's correction for multiple testing was performed, and cutoffs for both nominal significance ($p < 0.05$) and corrected significance ($p < 0.05/n\text{-tests}$) are displayed. Except for QTL plots, graphs and analyses were performed in R.

Data Repository

All BXD data can be found at http://www.GeneNetwork.org. To download the clinical phenotype data, change the type to ''Phenotypes'' and enter ''LISP2'' to find all associated results. Select all and export to recover the data, or analyze it online. Microarray data and protein measurements can be found on the same resource; change the type to ''Liver Proteome'' or ''Liver mRNA'' and navigate to the named EPFL data sets under CD or HFD (e.g., EPFL/LISP BXD CD Liver Affy Mouse Gene 1.0 ST [Apr13] RMA). To download these data, please click the ''INFO'' button at the right-hand side of the search page and download the raw data set in the upper right box of the screen.

C. elegans experiments

Wild-type Bristol N2 *C. elegans* provided by the *Caenorhabditis* Genetics Center (University of Minnesota) were cultured at 20°C and sustained on the OP50 *E. coli* strain.

Bacterial feeding RNAi experiments were carried out as described [111]. *cco-1* (F26E4.9) and *spg-7* (Y47G6A.10) clones were purchased from GeneService and sequenced.

For qPCR analysis, five biological replicates for each condition were prepared, consisting of ~600 worms per sample in M9 minimal liquid medium. Before mRNA preparation, samples were washed twice with 5 mL M9 to eliminate residual bacteria. Total RNA was prepared using TRIzol (Invitrogen) according to the manufacturer's instructions. RNA was treated with DNase, and 1 µg of RNA was used for reverse transcription (RT). 15X diluted cDNA was used for RT- quantitative PCR (RT-qPCR) reactions. The RT-qPCR reactions were performed using the LightCycler 480 System (Roche Applied Science) and a qPCR Supermix (QIAGEN) with the indicated primers. *act-1* was used as normalization control. Three technical replicates were used for each biological replicate.

The primers used for the *C. elegans* genes were as follows:

cco-1 (F26E4.9): fw: gctcgtcttgctggagatgatcgtt, rv: ggtcggcgtcgactcccttg.
spg-7 (Y47G6A.10): fw: aagtatgcaggacaaacgtgc, rv: tgaggtttgggatttcgcgt.
hsp-6 (C37H5.8): fw: aaccaccgtcaacaacgccg, rv: agcgatgatcttatctccagcgtcc.
hsp-60 (Y22D7AL.5): fw: ttctcgccagagccatcgcc, rv: tctcttcgggggtggtgaccttc.
hsp-10(Y22D7AL.10): fw: gggaaaagtccttgaagccac, rv: ctccgagaagatcagactcgc.
clpp-1 (ZK970.2): fw: tgcacagggaacctgctcgg, rv: ttgagagcttcgtgggcgct.
lonp-1 (C34B2.6): fw: cgatgatggccattgtgcag, rv: cgctttgaaacatcaatttcatcca.
ubl-5 (F46F11.4): fw: acgaatcaagtgcaatccatcag, rv: gctcgaaattgaatccctcgtg.
act-1 (T04C12.6): fw: gctggacgtgatcttactgattacc, rv: gtagcagagcttctccttgatgtc.

For *C. elegans* phenotyping, oxygen consumption was measured using the Seahorse XF96 equipment (Seahorse Bioscience Inc.) as described previously [154]. Typically, 100 worms per condition were recovered from plates with Nematode Growth Medium (NGM), then washed three times in 2 mL of M9 liquid medium to eliminate residual bacteria, and resuspended again in 500 µL of M9. Worms were transferred in 96-well standard Seahorse plates (#100777-004) (10 worms per well) and oxygen consumption was measured 6 times. Respiration rates were normalized to the number of worms in each individual well.

Movement was recorded for 45 seconds at day 2 of adulthood using a Nikon DS-L2 / DS-Fi1 camera and controller setup, attached to a computerized Nikon bright field microscope. Five plates of worms, with 20 worms per plate, were measured in each condition. The movement of worms during this time was calculated by following the worm centroids using

the same modified version of the freely-available for the Parallel Worm Tracker in MATLAB [155].

4.1.6 Author contributions

4.1.7 Acknowledgments

4.2 Joint mouse-human phenome-wide association to test gene function and disease risk

Phenome-wide association is a novel reverse genetic strategy to analyze genome-to-phenome relations in human clinical cohorts. Here we test this approach using a large murine population segregating for ~5 million sequence variants, and we compare our results to those extracted from a matched analysis of gene variants in a large human cohort. For the mouse cohort, we amassed a deep and broad open-access phenome

consisting of 4,230 metabolic, physiological, pharmacological, and behavioral traits, and more than 90 independent eQTL transcriptome, proteome, metagenome, and metabolome datasets—by far the largest coherent phenome for any experimental cohort (www.genenetwork.org). We tested downstream effects of subsets of variants and discovered several novel associations, including a missense mutation in fumarate hydratase that controls variation in the mitochondrial unfolded protein response in both mouse and *C. elegans*.

4.2.1 Introduction

Identifying sequence variants that control or modify sets of linked phenotypes is fundamental to understanding the molecular basis of both Mendelian and complex traits [156-159]. A variety of reverse genetic approaches to induce loss- and gain-of-function have been used to causally tie DNA variants to discrete phenotypes [160]. However, reverse genetics presents two challenges. The first is evaluating a potentially broad spectrum of phenotypes, biomarkers, and endophenotypes that are downstream of sequence variants at different stages of development, in different tissues and cells, and under different conditions. The second is evaluating the impact of these variants across different genetic backgrounds that influence trait penetrance. Phenome-wide association studies (PheWAS) address both challenges [161,162].

In order to establish the first murine resource for phenome-wide association we have used a large cohort of recombinant inbred strains—the BXD family—that were generated by crossing two fully inbred parental strains—C57BL/6J (B6) and DBA/2J (D2). This family consists of ~150 isogenic lines, and as we show here, this family segregates for over 5 million common variants and ~12,000 missense mutations. To accompany these genomic data we assembled a high coverage phenome with over 4,500 quantitative metabolic, physiological, pharmacological, toxicological, morphometric, and behavioral phenotypes, along with linked references to the primary literature. This BXD phenome also includes ~90 large open access expression quantitative trait locus QTL (eQTL) studies generated over the past decade as well as recent metagenomic, metabolomics, and proteomic components [90,163,164]. Roughly half of the eQTL data sets are experimental, developmental, or related to aging. Almost all phenome data types and sequence are accessible online as a companion to this paper.

The impact of ~12,000 potentially damaging sequence variants was evaluated by systematically scanning against the phenome at molecular, cellular, and behavioral levels. We discovered new associations, some of which were subsequently validated in a large

human clinical cohort [161,162]. For example, missense mutations in *Col6a5* were linked to variation in bone mineral density in both mouse and human. However, downstream effects of allelic variants with presumed deleterious effects on gene expression or protein structure are often small or undetectable. This may often be due to a lack of technical sensitivity and power or to molecular and developmental compensation.

4.2.2 Phenomes

Phenome data were generated using a large cohort of recombinant inbred strains—the BXD family—that was generated by crossing two fully inbred parents—C57BL/6J (B6) and DBA/2J (D2). Members of the BXD family collectively segregate for all sequence variants that distinguish the two parents—and in this cross these are by definition common variants. There are also interesting rare but still undefined alleles unique to each family member. The level of both genetic and phenotypic variation between parents and among the strains is high (Figure 4:4A). This BXD phenome includes ~4,500 quantitative metabolic, physiological, pharmacological, toxicological, morphometric, and behavioral phenotypes (Figure 4:4B). These traits are almost all quantitative and have been systematically grouped into 15 major phenotype categories. We have also generated and assembled a large molecular phenome that includes expression phenotypes from ~90 large open access expression quantitative trait locus QTL (eQTL) studies generated over the past decade (Figure 4:4B). On average 1.5×10^6 mRNA, 1.7×10^4 proteomic, and 6.8×10^3 metabolomic assays are available per strain (Figure 4:4B). Most phenotypes vary markedly across strains within the family. For example, effect of high-fat and low-fat diets on adult body weight varies substantially across genotypes (Figure 4:4C). Similarly mRNA and protein expression of, for example, *Bckdhb* and many other mRNA, proteins, and metabolites vary greatly (Figure 4:4D) [164]. The online availability of well-organized classic and molecular traits from the BXD family (see www.genenetwork.org) provides the foundation for multiscalar phenome scans of any putatively functional sequence variant.

The human phenome used in this study is a large electronic health record (EHR linked cohort, BioVU (https://victr.vanderbilt.edu/pub/biovu/). BioVU currently contains >190,000 DNA samples linked to de-identified medical records to provide a large, clinically-relevant human resource to study genotype-phenotype associations; 29,722 of these individuals have extant exome variant data, which was used for matched mouse-to-human PheWAS in this study.
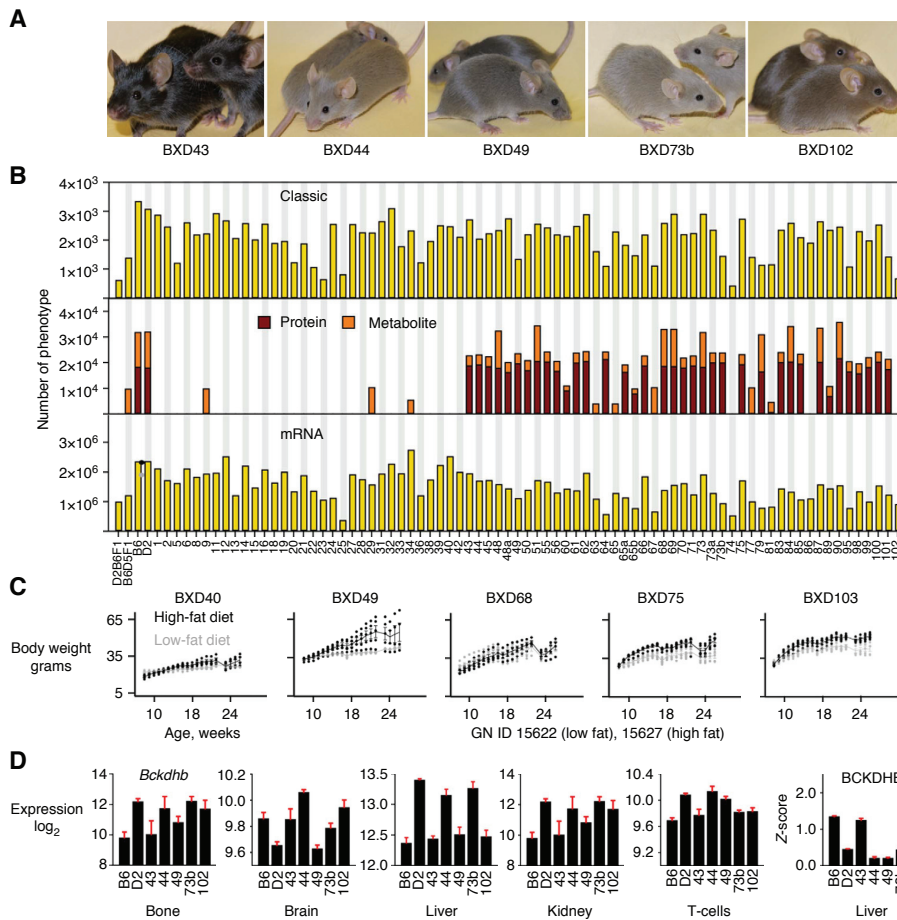
Figure 4:4 Overview of phenome data for the BXD cohort.

(A) Five pairs of isogenic BXD cohort strains—BXD43 to BXD102. There are now approximately 100 readily available BXD strains and another 50 that are almost fully inbred. Almost all current phenome data is restricted to the parents, F1 hybrids (B6D2F1, D2B6F1), and BXD1 through BXD102. (B) Phenome data categorized by type, including classic phenotypes (top), metabolic and proteomic trait data (middle), and independent mRNA expression assays (bottom, n = 86 unique eQTL data sets). (C) Body weight data for BXD strains on high fat (gray) and low fat (black) diets taken from Wu et al. [164]. (D) Expression of Bckdhb mRNA and its protein in six tissues for the five BXD strains. Protein data from Wu et al. [164].

4.2.3 Whole-genome sequencing and variants detection

To obtain accurate information on sequence variants across the BXD family (Figure 4:5A), we generated ~8.26 billion reads using six paired-end libraries with different insert sizes from the D2 parent using two sequencing platforms. A total of 4.5 billion reads (262 Gb nucleotides) were aligned to the genome of the other parent of the BXD family–B6–that serves as the mouse reference genome. The mouse genome consists of ~2.6 Gb, and we generated ~100-fold coverage (Figure 4:5B) and sequenced 99.96% of the reference genome excluding gaps and regions of low complexity.

The parents of the BXD cohort differ at 4.8 million single nucleotide polymorphisms (SNPs) (Figure 4:5C) at a high-confidence threshold, including 4,160,570 extracted from the SOLiD platform and 4,090,000 SNPs from Illumina. We resequenced a subset of 262 platform-specific SNPs. False positive rates (FPR) were 2.34% and 3.73% for SOLiD and Illumina platforms, respectively. Assuming that all 3,375,198 SNPs detected by both systems are valid, the false positive rates are 0.44% for SOLiD and 0.65% for Illumina.

We defined 35,068 coding SNPs (cSNPs), of which 23,089 are silent (synonymous) and 11,979 are missense (non-synonymous). Approximately 16% and 4% of non-synonymous SNPs have potentially deleterious effects on protein function as assessed using PolyPhen 2 [165] and SIFT [166] respectively. Approximately 2% (210 SNPs) were defined as deleterious by both algorithms (Figure 4:5D). We identified 58 nonsense SNPs in 53 genes, including 42 stop codon gains and 16 stop codon losses in D2. The functional consequence of 210 deleterious missense variants and 58 nonsense variants were further evaluated by comparative genomic analysis. In addition, 79 missense variants were confirmed by mass spectrometry-based proteomics.

Most SNPs (98%) occur within non-coding regions (ncSNPs). Variants at splice sites result in production of nonfunctional or abnormal proteins and are known to contribute to diseases [167]. We detected 70 SNPs that changed conserved bases at splice sites, including 29 acceptor sites (GT) and 40 donor sites (AG). In addition, 26 of the ncSNPs are predicted to alter processed miRNA sequence.

Insertions and deletions (indels) in coding sequences can be highly disruptive, especially when they introduce frame shift mutations. We found that most small indels (98.74%) are in introns or intergenic regions, but 542 small deletions and 641 small insertions are in coding exons. The small coding indels are enriched in trinucleotides, which account for 32% of small coding deletions and 38% of small coding insertions. Of the remaining coding indels, 45 are predicted to result in frame shift mutations through deletions (25) or insertions (20).

Sequences from SOLiD and Illumina platforms were combined to accurately detect copy number variants (CNVs). We detected 16,817 CNVs, consisting of 4,296 gains and 12,521 losses (Figure 4:5C) with an average length of 34.9 kb and 56.7 kb, respectively. Of copy number gains relative to the B6 genome, 79 cover 101 genes completely, while 300 cover one or more coding exons in 279 genes. Of the losses, 197 cover 259 genes completely, while 993 cover one or more coding exons in 276 genes.
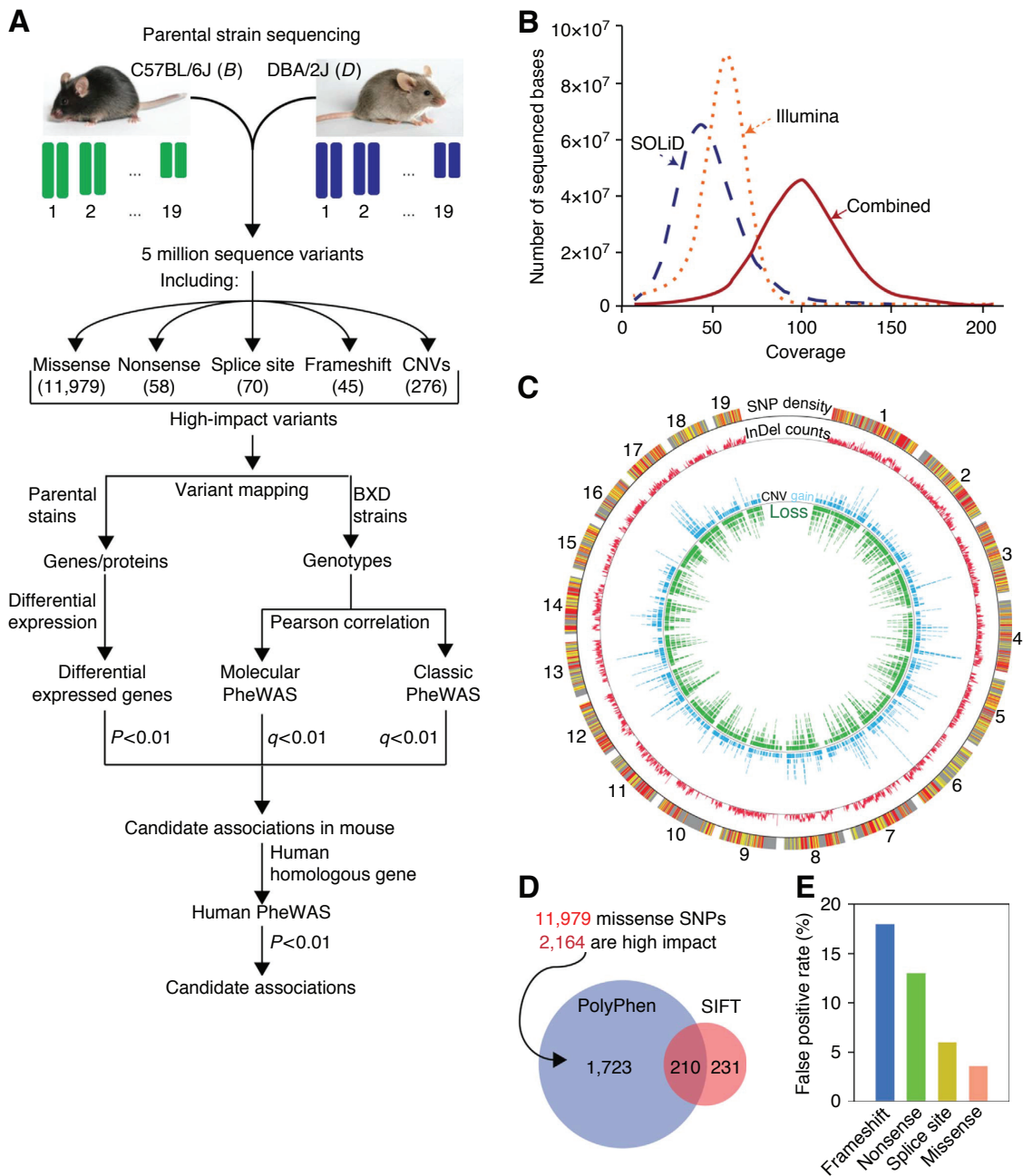
Figure 4:5 Overview of experimental phenome-wide association.

(A) Workflow for the PheWAS analysis. D2 genome was sequenced using Illumina and SOLiD platforms and aligned to the reference genome. Approximately 5 million sequence and structural variants were identified. A set of high-impact variants including 11,355 missense, 58 nonsense, 70 splice site, 45 frame shift, and 276 CNVs spanning at least one gene was used for classic and molecular PheWAS analyses. (B) Whole-genome read coverage. The distribution was generated using combined mapped reads from Illumina and SOLiD, and mapped reads from Illumina and SOLiD platforms individually. (C) Circos plot of sequence and structure variants segregating in the BXD cohort. The outmost circle represents SNP density per 100-kb window (black at the lowest density and orange at the highest density). The second circle represents indel density per 100-kb. The innermost circle represents CNVs. Blue and green ticks indicate D2 losses and gains, respectively. (D) Venn diagram of missense variants predicted to be deleterious by SIFT and PolyPhen2. (E) False positive rate of strong variants. A small subset of each type of variants was selected for validation by Sanger resequencing.

FPR of each type of variants is shown in Figure 4:5E. The functionally important variants (i.e. nonsense, missense, splice site, frameshift, and CNVs) were selected for subsequent Phenome-wide association study (PheWAS) analysis.

4.2.4 Phenome-wide association analysis in mouse

We used 3,805 genotypes that represent distinct haplotype blocks in the BXD family to perform PheWAS against 4,230 classic traits as well as 602,746 endophenotypic traits from 16 distinct tissues (Figure 4:4A). This analysis yielded ~14 million genotype-to-phenome correlations and ~2.0 billion genotype-to-endophenotype correlations. A total of 95 genotypes are significantly associated with 321 phenotypes, corresponding to 108 phenotypic groups, at a stringent q value threshold of <.01.

We interrogated the associations for 12,420 functionally important variants, including 11,979 missense, 58 nonsense, 70 splice site, and 45 frame shift mutations, and 276 CNVs, by mapping these variants to the nearest genotype markers within ±1 Mb. We found that 650 functionally important variants were associated with 97 classic phenotypes, including 634 missense variants that were associated with 62 phenotypes.

4.2.5 Examples of variant-phenome association

Among 321 classic phenotypic associations meeting a stringent q value threshold of < 0.01, a few variants, such as those in *Gpnmb, Comt* and *H2-B1,* have been associated previously with disease [168-171] using traditional forward genetics approaches, but the vast majority of variants have not been previously linked to any phenotype.

One PheWAS example is a missense variant (A296T; *rs32536342*) in the fumarate hydratase mitochondrial enzyme located on chromosome 1 at 175.60 Mb (*Fh1*; Figure 4:6A). *Fh1* catalyzes the hydration of fumarate to malate in the tricarboxylic acid (TCA) cycle and has been linked to renal cell cancer [172]. The missense variant in the lyase 1 domain is associated with a ~1.4-fold effect on expression of *Fh1* across many tissues, including midbrain, hypothalamus, striatum, and spleen (Figure 4:6B). This variant is strongly associated with *Fh1* mRNA expression, as well as the expression of other mitochondrial genes, including *Mrpl50*, *Sirt3* and *Dlst* (Figure 4:6C). Expression PheWAS shows that the *Fh1* locus modulates mRNA expression levels of 113 mitochondrial proteins, in addition to 8 genes linked to renal necrosis, and 7 genes involved in mTOR signaling, consistent with the known role of *FH1* in renal cancer. Interestingly, four mitochondrial genes, *Hspd1*, *Hspa9*, *ClpX*, and *Lonp1* that all encode components of the
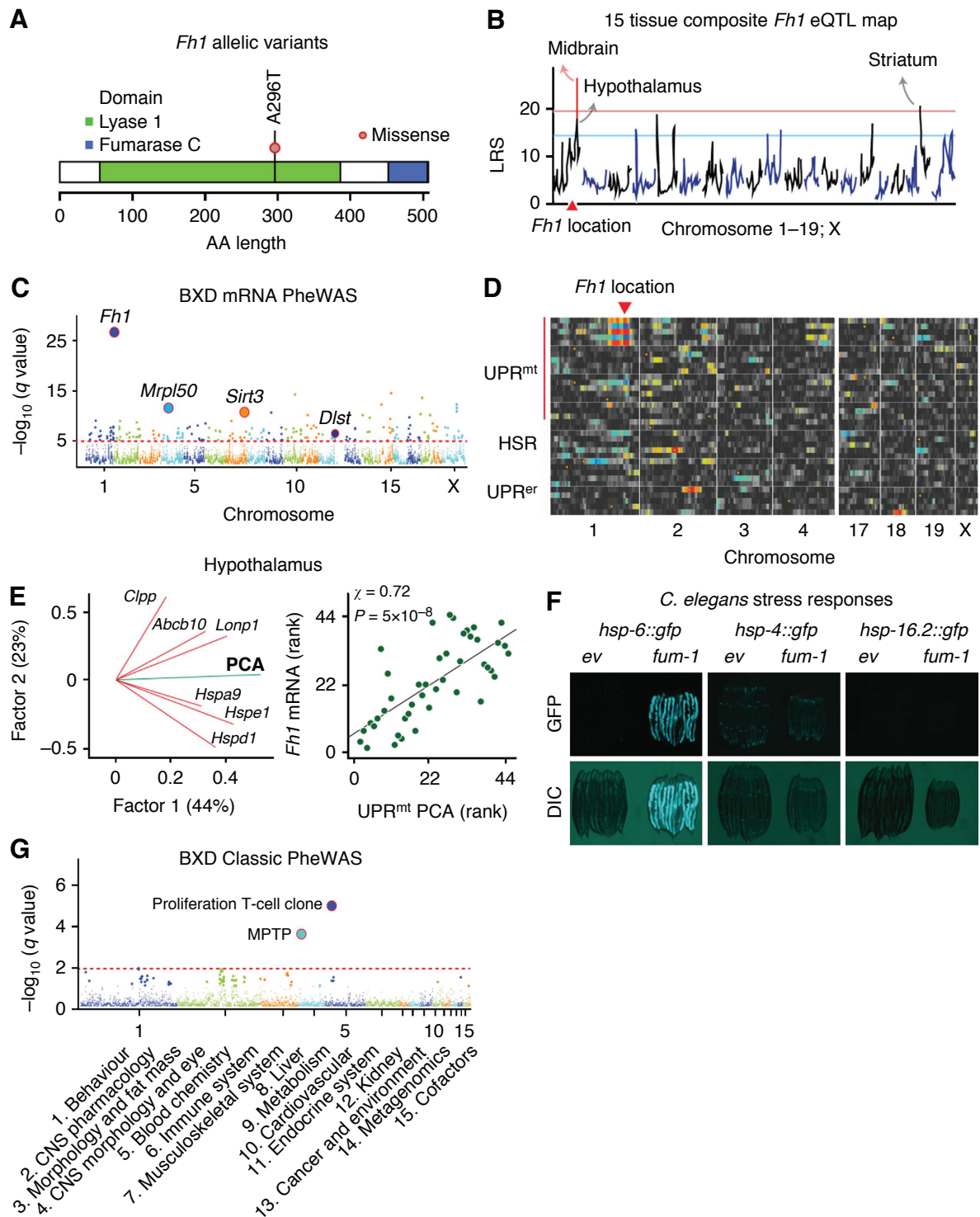
Figure 4:6 Association analysis for a missense variant in Fh1.

(A) Structure of the *Fh1* gene showing lyase 1 and fumarase c domains, the latter of which contains a missense mutation. (B) Combined eQTL mapping of Fh1 mRNA across 15 tissues. The eigenvalues associated with the first principal component map to Fh1 with a likelihood ratio statistic (LRS) of >20. The solid red line represents genome-wide significance. The yellow triangle indicates the genomic position of Fh1. (C) Manhattan plot of an expression phenome scan of molecular traits linked to the Fh1 locus in midbrain. The y-axis shows the –log10 q values of association, and the x-axis shows positions of 55,681 probe sets from Agilent SurePrint array. (D) QTL heat map of mRNAs involved in the unfolded protein response. The x-axis lists mouse chromosome numbers. Each horizontal line represents the QTL map for a

single transcript in midbrain. Transcripts are grouped into three major categories—genes involved in the canonical UPR^{mt}, cytoplasmic heat shock response (HSR) and unfolded protein response in the endoplasmic reticulum (UPR^{er}). The subset of UPR^{mt} genes at the top are strongly modulated by the Fh1 locus on Chr 1 (the intense colors to the upper left). In contrast, none of the UPR^{er} subsets are modulated by Fh1. (E) Principal component analysis (PCA) plot for six UPR^{mt} transcripts (left panel). The first two components explain ~67% of the variance in Fh1 expression in hypothalamus. There is significant correlation between UPR^{mt} expression and Fh1 (p = 5 × 10-8; Pearson product-moment correlation coefficient) (right panel). (F) Validation that fumarate hydratase selectively controls the UPR^{mt} in C. elegans. The left-most pair of images demonstrates effects of the *fum-1* RNAi knockdown on *hsp-6::gfp* signal—a marker of UPR^{mt} induction. The middle and right panels demonstrate that the fum-1 knockdown does not induce either the UPR^{er} (*hsp-4::gfp*), or the cytoplasmic heat shock response (*hsp-16.2::gfp*). (G) Manhattan plot of a phenome scan. The y-axis shows the –log10 q values of ~4,230 phenotypes, and the x-axis shows the 15 phenotypic categories.

mitochondrial unfolded protein response (UPR^{mt}) [41]—a still poorly characterized mitochondrial stress response pathway in mammals—show strong association with *Fh1* (Figure 4:6D). There is furthermore a significant correlation between *Fh1* transcript levels and principal component scores of a group of UPR^{mt} genes in mouse (Figure 4:6E). In contrast, no genes involved in the cytoplasmic heat shock response (HSR) or the ER unfolded protein response (UPR^{er}) are associated with *Fh1*, indicating a selective association between *Fh1* and UPR^{mt} in mammals (Figure 4:6D). To validate this association, we examined the phenotypic impact of the highly conserved *C. elegans Fh1* ortholog, *fum-1* (86% sequence similarity) on unfolded protein responses. RNAi against *fum-1* causes robust activation of the mitochondrial chaperone *hsp-6::gfp* reporter, indicative of the activation of the UPR^{mt} (Figure 4:6F). The response was organelle-specific, and *fum-1* RNAi does not induce either *hsp-4::gfp* or *hsp-16.2::gfp*, reporters for related to the UPR^{er} or HSR, respectively (Figure 4:6F). Thus, in the BXD family, a decrease of fumarate hydratase leads to a specific mitochondrial phenotype, characterized by an UPR^{mt}.

Fh1 is also associated with two candidate phenotypes: (1) T cell proliferation (GN ID 10237; *q* = 2.6x10^{-5}), linked previously to mitochondrial function [173], and (2) dopamine metabolism after treatment with the mitochondrial toxin 1-methyl-4-phenyl-1,2,3,6-tetrahydropyridine (MPTP, GN ID 15151; *q* =0.005). Both traits are linked to *Fh1* along with the control of mitochondrial components of a UPR^{mt} pathway (Figure 4:6G). No extant human genotype data are yet available for *FH*—the homolog of *Fh1*.

4.2.6 Discussion

Recent work has demonstrated that phenome scans are a powerful way to link from sequence variants to sets of phenotypes in clinical cohorts [161,162]. Here we have extended this approach to a murine cohort for which we have been generating cellular and molecular traits from many tissue and cell types and for which we can generate data on gene-by-environment interactions [90,164,174]. The variety and depth of phenotype data

that we have assembled over the last decade for the BXD cohort make this the largest coherent multiscalar data set for any segregating population. Of course, there are an almost unlimited numbers of ways to extend this BXD phenome—from much more extensive GXE studies to single cell omics, but at the current size, the phenome is certainly large enough to explore the utility of PheWAS in an experimental population. We demonstrate that phenome scans can be effective at linking sequence variants to a range of phenotypes and can be used to identify novel and unexpected genome-to-phenome relations, or to validate hypothesized associations from independent studies. Coupling mouse and human PheWAS cohorts also shows great promise, and provides an efficient method to validate and translate key genome-to-phenome relations.

The novel associations demonstrated in this study provide insight into the genetic basis of complex traits and variation in disease susceptibility. The missense variant in *Fh1* is a case in point. A variant in *Fh1* is linked to the UPR^{mt}, a protective stress pathway specific to mitochondria, and we confirmed that downregulation of *fum-1*, the *C. elegans* homolog of *Fh1*, activates the UPR^{mt}. Various disturbances have been shown to induce the UPR^{mt}, including treatment with paraquat, a pesticide that strongly induces reactive oxygen species [36], activation of mitochondrial biogenesis [46], overexpression of aggregation-prone mitochondrial proteins [33], and interference with electron transport chain protein expression and assembly [41,148]. Here, we show that a purely metabolic perturbation, such as induced by loss of function of the TCA cycle component, fumarate hydratase, can activate the UPR^{mt}. While we have detected a single missense variant in *Fh1*, the molecular cascade that links *Fh1* to other TCA cycle genes (e.g. *Dlst*, *Sdha*, *Sdhb*) and a UPR^{mt} proteostasis regulatory loop requires additional analysis.

4.2.7 Materials and methods

DNA sample for sequencing

DBA/2J foundation breeding stock at generation F223 was obtained from The Jackson Laboratory (www.jax.org). Genomic DNA was isolated from livers of filial generation F224 female littermates using a QIACube and DNeasy kits (Qiagen Inc., Valencia, CA). In order to obtain balanced coverage of the X chromosome, we choose the female mice.

All animal work was conducted according to an approved animal use protocol (UTHSC680) and in accordance with procedures approved by the Institutional Animal Care and Use Committee.

Libraries preparation

Six libraries were constructed. Three mate-paired libraries with insert sizes of 1 kb, 2 kb, and 3 kb were prepared for ligation-based sequencing (ABI SOLiD 2 and 3). Three paired-end libraries with insert sizes between 175 bp and 215 bp were prepared for sequencing by synthesis (Illumina GAII and HiSeq 2000). Standard protocols recommended by the manufacturers were used in all cases.

Sequencing

Three mate-paired libraries were sequenced using ABI systems according to the vendor's protocol. Three libraries were sequenced using reagent kit V4 and Illumina systems according to the manufacture's standard protocol. Read lengths for the SOLiD2 and SOLiD3 systems were 2×25 bp and 2×50 bp, respectively.

One library was sequenced using the sequencing reagent V4 on the Illumina HiSeq 2000 following the manufacture's standard cluster generation and sequencing protocol. Sequence reads with 101 bp on both ends were extracted from images files using the GA software (version 1.4).

Sequence alignment

The SOLiD reads was aligned to the B6 reference genome using two alignment tools: Corona Lite v4.0.2 (http://solidsoftwaretools.com/gf/) and the MAQ code v0.7.1[175]. Corona Lite parameters were set to allow up to two and six mismatches for 25 and 50 bp sequence fragments, respectively. The longer reads from Illumina were mapped to the reference genome using MAQ, allowing up to two mismatches in the first 24 bp of each read. All alignment files were converted into BAM format. Reads that aligned to only one location with no more than two mismatches in the first 24 bp were considered uniquely aligned.

SNP detection

ABI Bioscope software was used to align color-space reads and to detect SNPs against the B6 reference genome. Similarly, MAQ software was used to align reads to identify SNPs. A threshold of three or more supporting reads and a consensus quality score >30 (Illumina) and a confidence value >0.5 (SOLiD) was used to declare SNPs. Rare heterozygous calls, presumably generated by alignment errors, were discarded.

PheWAS analysis in mice

PheWAS were performed for a total of ~12,000 variants, including 11,979 missense, 58 nonsense, 68 splice site, 39 frame shift mutations, and 276 CNVs The closest marker for

each variant from a set of 3,804 genetic markers—each representing a unique haplotype block—was used to represent that variant in the PheWAS. We used 16 expression data sets representing different tissues of the BXD strains to explore the genetic basis of variation at mRNA levels. Similarly, we used 4,236 classic phenotypes from GeneNetwork.org (www.genenetwork.org) to study the association between variants and phenotypes. We calculated the p value of the Pearson correlation between each marker (variant) and 4,236 phenotypes and ~40,000 transcripts for the expression data. All p values of correlation were calculated as a two-tailed test, and the q values (false discovery rate; FDR) were calculated using QVALUE [176]. We used an FDR threshold of 0.01 for associations. The analyses were performed using in-house Python scripts, and the R statistical package.

C. elegans experiments

C. elegans were cultured at 20°C on nematode growth media agar plates seeded with bacteria. Strains were provided by the Caenorhabditis Genetics Center (University of Minnesota). The strains used were SJ4100 (zcIs13[hsp-6::GFP]), SJ4005 (zcIs4[*hsp-4*::GFP] and dvIs70 [hsp-16.2p::GFP + rol-6(su1006)]. RNAi constructs were isolated from the RNAi feeding library (GeneService) and experiments were carried out using standard feeding methods. The identity of each RNAi clone was verified by sequencing. RNAi treatment was started from embryonic stage. GFP was monitored in day 1 adults. Worms were immobilized with 6 mM solution of tetramisole hydrochloride (Sigma) in M9 and imaged using Nikon DS-L2 fluorescent microscope.

4.2.8 Author contributions

R.W.W., L. L., X.W. and A.K.P. designed all experiments. X.W. and A.P. led the sequencing analysis. D.C.C., Z.L. and W.L.T. performed sample preparation and generated sequencing data using ABI SOLiD. Z.C. and S.F.N. generated sequencing data using illumina GA2. M.K.M., E.G.W., K.M. provided bioinformatics support. E.G.W., V.J. and J.A. performed siRNA experiment. L.D.Q., Z.X., J.H. performed functional works on *Col6a5*. J.A.C. and K.S.P. performed functional analysis for noncoding SNP. A.O.R., A.V.T., I.B.Z. performed functional analysis for coding SNP. X.W. and J.P. generated proteomics data and bioinformatics analysis. J.C.D., J.A. and R.W.W preformed critical reading and contributed to the writing of the manuscript. X.W., A.K.P., M.K.M. and R.W.W. wrote the manuscript.

4.2.9 Acknowledgments

Chapter 5   Discussion and conclusion

Epigenetics in UPR^mt and longevity

My thesis focuses on one of the cellular PQC mechanisms, the UPR^mt, which maintains optimal proteostasis in the mitochondria. In work presented in this thesis, we describe two new regulators involved in mechanistic control of UPR^mt, histone demethylases *jmjd-3.1*/Jmjd3 and *jmjd-1.2*/Phf8 (chapter 2). Importantly, activation of the UPR^mt has been associated with increased longevity in *C. elegans* and mice [41,42]. It has been previously discovered that the UPR^mt can be activated and have positive effects on *C. elegans* lifespan only when mitochondrial stress is initiated during larval development stages, indicating the existence of epigenetic mechanisms that are persistent throughout life [42]. Since then, there was little insight into the molecular mechanism governing this epigenetic control, and our collaborative article was the first to point out the exact players, which are specific H3K27me3 demethylases [122]. We show that *jmjd-3.1* and *jmjd-1.2*, which remove the repressive H3K27me3 marks, are required for the UPR^mt and longevity triggered by the LOF of ETC components. At the same time, another repressive histone modification, H3K9m2 dimethylation, was identified to be important for the mitochondrial stress induced longevity [177]. This study identified that during mitochondrial stress, there is global chromatin silencing by dimethylation of H3K9 through the specific methyltransferase *met-2* and the nuclear cofactor *lin-65*. Both *met-2* and *lin-65* are also required for the ETC knockdown induced longevity. The authors show that while global chromatin is condensed after mitochondrial stress, the UPR^mt transcriptional regulator, specifically DVE-1, accumulates in those DNA areas, which are not labelled by H3K9me2 marks. Thus these two studies complement each other by showing that during mitochondrial stress, there is global transcriptional silencing by the accumulation of H3K9me2 chromatin marks, whereas transcription of specific UPR^mt players are activated by the removal of repressive H3K27me3 marks from their coding regions. We show by ChIP-qPCR, that the H3K27me3 enrichment on the *atfs-1* coding region is reduced upon

mitochondrial stress. Further experiments showing that the silencing mark is removed by specific demethylases, are still required to prove the exact molecular mechanism. In addition, global analysis, best by ChIP-seq matched with the RNA-seq data, should be performed to identify the precise genes targeted by the *jmjd-3.1* and *jmjd-1.2* demethylases. It will also be important to learn how these two enzymes work together. Our research suggests that *jmjd-3.1* also plays a role in another stress response, i.e. the UPR[er], consistent with a recent study [98], while *jmjd-1.2* appears to be more specific for mitochondrial stress. How these histone demethylases complement each other and whether they work sequentially, remains to be determined. In addition, the coexistence and interplay between histone modifications, such as H3K27me3 and H3K9me2, during mitochondrial stress has not yet been investigated and warrants further studies.

Metabolic control of UPR[mt]

Multiple genetic and pharmacological manipulations are known to induce UPR[mt]. Genetic screens have been performed to identify RNAi clones which activate UPR[mt] *hsp-6::gfp* reporter [30,73], and recent study shows that some bacterial species can also activate the response, most likely through microbial toxins and virulence factors that specifically antagonize mitochondria [37]. It has been generally accepted, that prototypical UPR[mt] activating conditions are associated with perturbations of either ETC or global mitochondrial protein synthesis [30,41]. We identify here that purely metabolic disturbances induced by the KD of some TCA cycle enzymes can also induce the UPR[mt], which has not yet been extensively described (chapter 3). How and why disturbance of the TCA cycle signals to induce the mitochondrial protein folding machinery, as well as what determines the specificity of the response activation depending on the downregulated enzyme, remains to be explored. Another novel finding is that a very important TCA enzyme, normally used as a marker of total mitochondrial activity, citrate synthase *cts-1* is associated with longevity. We show that *cts-1* downregulation only during development strongly increases lifespan of *C. elegans* in a UPR[mt] dependent fashion. Because of the specific temporal requirement, lifespan extension by *cts-1* KD has not been identified in whole genome RNAi screens for longevity regulators [123]. Until now, the most prominent example of lifespan extension after RNAi restricted to larval development described, was the KD of ETC components, such as the complex IV protein, *cco-1* [49]. As *cts-1* KD reduces the activity of the TCA cycle, which provides reducing equivalents, such as NADH and $FADH_2$, for oxidative phosphorylation, most likely the mechanisms determining increased longevity are similar between the perturbations of the TCA cycle and ETC;

however, further research is needed to prove this hypothesis. We identify that *cts-1* RNAi has opposing effects on lifespan depending on the timing of RNAi feeding: restriction of RNAi feeding during development increases lifespan, while RNAi only during adulthood decreases longevity. Exploring such negative effects of mitochondrial perturbation during adulthood can contribute to deeper understanding of mitohormesis, the concept that mild mitochondrial stress is beneficial for lifespan [178]. Alternatively, mechanisms defining the detrimental effects of *cts-1* KD during adulthood possibly go beyond only mitochondrial pathways and need further investigation. An aging theory which might help to explain the contradicting effects of *cts-1* RNAi timing on lifespan, is antagonistic pleiotropy, which describes the phenomenon of a protein/pathway being important in the beginning of life, e.g. for development or reproduction, and thus selected by evolution, but detrimental later in life [179]. One example is JNK signalling activation by KGB-1 in *C. elegans*, which is stress protective during development, but detrimental past development [180]. However, in the case of *cts-1*, the effect seems to be contrary, as KD experiments indicate that it negatively affects lifespan during development and is essential during adulthood. An example of 'reverse' antagonistic pleiotropy has been recently shown for mitochondrial antioxidant enzyme catalase [181]. Its overexpression in old mice is beneficial, while adverse in young mice. Whether this aging concept can be applied to *cts-1*, remains to be determined.

By gene expression analysis of 6 genetic mitochondrial dysfunction conditions associated with induction of the UPR^{mt}, namely RNAi of TCA components *fum-1, dlst-1, cts-1* and other mitochondrial proteins *spg-7, mrps-5, cco-1*, we identified an interesting set of genes that is commonly changed in all examined conditions. Our data confirm that genes involved in innate immunity and protection against pathogens are highly upregulated in response to mitochondrial perturbation, as recently described by two independent groups [37,38]. Another interesting group of genes that changes upon mitochondrial dysfunction are genes involved in lipid metabolism, which recently have appeared as intersecting with the UPR^{mt}. We find that the primary β-oxidation enzyme *acs-2* is induced in common in all conditions, and that expression of *asm-3*, involved in ceramide synthesis from sphingomyelin, is reduced in all examined conditions. Interestingly, a very recent study shows that upon *hsp-6* RNAi, which induces cytosolic heat shock response via the UPR^{mt}, termed mitochondrial to cytosolic stress response (MCSR), there is an increase of fat storage [129]. However, our data suggests that there is increased fatty acid oxidation. Possibly, the change of equilibrium between catabolism and anabolism of fatty acids depends on the exact conditions used to trigger mitochondrial stress. Our data also further

reinforce the role of ceramide in mitochondrial perturbation, which recently was discovered [37,129]. Overall, lipid metabolism seems to play an important role in mitochondrial stress, which definitely requires further studies. The other genes in the commonly changed list are also potent candidates for new directions of research about the UPR[mt]. What is more, a similar approach of systemic gene expression data analysis of multiple conditions, even from different unrelated studies, could help to identify strong novel candidate genes playing important roles in other specific processes.

UPR[mt] in mammalian systems

Despite the fact that the UPR[mt] was first discovered in mammalian cells [40], the research on the UPR[mt] in mammalian systems has been progressing more slowly compared to the analysis and understanding of the UPR[mt] in invertebrates. Since the identification of the main transcription factors CHOP and C/EBPβ and their mitochondrial effector genes [58], there has been little advance in the identification of other UPR[mt] players. Most recently, the transcription factor Atf5 has been suggested to regulate the UPR[mt] by a similar mechanism as *atfs-1* in *C. elegans*, i.e. by moving from mitochondria to nucleus to activate the transcriptional response at times of stress [182]. Here we suggest Jmjd3 and Phf8 as new epigenetic regulators of the UPR[mt] and longevity that are conserved from *C. elegans* to the mouse (chapter 2). This evidence comes from using the BXD GRP and gene expression data of cells with downregulated or inhibited enzymes. Further studies of these enzymes using LOF and GOF approaches in a system with stressed mitochondria should be performed to clearly define their mechanistic role in the mammalian UPR[mt]. In addition, the role of Jmjd3 and Phf8 in the UPR[mt] and physiology should be characterized in mammals. In particular, it would be interesting to explore, whether in mammals there are beneficial effects triggered by early life mitochondrial stress, which are dependent on H3K27me3 demethylases, similar to those observed in *C. elegans*. If this mechanism would be conserved, early developmental interference with mitochondrial stress pathways could have long-lasting implications. This may also shed light on certain diseases that are conditioned during early development and may open new strategies for therapeutic interventions aimed at resetting or erasing the epigenetic marks left earlier.

We explored the importance of the UPR[mt] in mammalian systems by exploiting new omics and sequencing data generated in the BXD mouse GRP (chapter 4). Proteome and transcriptome data on several UPR[mt] players clearly shows that the UPR[mt] signalling circuit is tightly correlated in mouse and humans, similar as in *C. elegans*. Furthermore, correlation analysis shows that altered expression of the mammalian orthologs *Spg7* and

Cox5b of the *C. elegans spg-7* and *cco-1* genes, respectively, induces the expression of a core set of UPR^{mt} genes and proteins in unstressed animals. This not only further underscores the evolutionary conservation of this ancient stress pathway, but as the mammalian data were collected in unstressed animals, it also shows its fine level of regulation. From another bioinformatics study, we found that fumarate dehydratase Fh1 regulates the UPR^{mt} in the BXD GRP. These data incited us to explore in more depth the relation between the UPR^{mt} and other TCA cycle proteins, as described in chapter 3. Further exploration of new associations between the UPR^{mt} and other genes/proteins could be performed using the same BXD resource, and could contribute to identification of novel potential candidates involved in UPR^{mt} signaling. The validity and power of such a strategy is underscored by the fact that the UPR^{mt} has been already linked with longevity phenotype in mammals using the same BXD GRP resource (chapter 2, [41]). Similarly, additional investigations of associations between variants in UPR^{mt} genes and variation in their expression levels, and panels of phenotypes, traits and diseases by genome wide association studies could benefit in generating hypotheses about physiological UPR^{mt} roles in humans.

Conclusion

Work in this thesis explores different aspects of the UPR^{mt}, such as its molecular signalling mechanisms, its interplay with metabolism and the TCA cycle, and the analysis of its presence in mammalian systems by bioinformatics tools. We identified a novel epigenetic mechanism, conserved across species, which plays an important role in UPR^{mt} signaling and associated lifespan extension. We show that perturbation of cellular metabolism by KD of specific TCA cycle enzymes can induce the UPR^{mt} and affect longevity in *C. elegans*. We also analysed gene expression changes and defined a common gene set that is induced by multiple conditions that activate the UPR^{mt}. Finally, we explored the conservation of the UPR^{mt} by analysis of expression data obtained from mouse GRP and humans. This work hence presents not only an advance in our fundamental knowledge about the conserved UPR^{mt} stress pathway, but the generated data can also contribute to our general understanding of the aging process and mitochondrial diseases.

List of abbreviations

ATP - adenosine triphosphate

BXD - a type of recombinant inbred mouse cross (C57BL/6J x DBA/2J)

CD – chow diet

ChIP-seq – chromatin immunoprecipitation sequencing

CNV – copy number variant

cSNP – coding single nucleotide polymorphism

CV – coefficient of variation

DEG – differentially expressed gene

eQTL – expression quantitative trait locus

ETC – electron transport chain

FCCP - carbonyl cyanide-p-trifluoromethoxyphenylhydrazone

GFP – green fluorescent protein

GO – gene onthology

GOF – gain of function

GRP – genetic reference population

GWA – genome-wide association

GXE – gene-by-environment interactions

HFD – high fat diet

HSP – heat shock protein

HSR – heat shock response

KD – knock-down

LOF – loss of function

MPTP - 1-methyl-4-phenyl-1,2,3,6- tetrahydropyridine

mtDNA – mitochondrial DNA

MTS – mitochondrial targeting sequence

ncDNP – non coding single nucleotide polymorphism

nDNA – nuclear DNA

NLS – nuclear localization sequence

OCR – oxygen consumption rate

OXPHOS – oxidative phosphorylation

PheWAS – phenome wide association study

PQC – protein quality control

pQTL – protein quantitative trait locus

qRT-PCR – quantitative real time polymerase chain reaction

QTL – quantitative trait locus

ROS – reactive oxygen species

SEM – standard error of the mean

SNP – single nucleotide polymorphism

SRM – selected reaction monitoring

TCA – tricarboxylic acid cycle

UPR – unfolded protein response

UPR^{er} – unfolded protein response in the endoplasmic reticulum

UPR^{mt} – mitochondrial unfolded protein response

WT – wild type

References

1. Badyaev A. V.: Stress-induced variation in evolution: from behavioural plasticity to genetic assimilation. *Proc Biol Sci* 2005, **272**:877-886.
2. Kourtis N., Tavernarakis N.: Cellular stress response pathways and ageing: intricate molecular relationships. *EMBO J* 2011, **30**:2520-2531.
3. Haigis M. C., Yankner B. A.: The aging stress response. *Mol Cell* 2010, **40**:333-344.
4. Kenyon C., Chang J., Gensch E., Rudner A., Tabtiang R.: A C. elegans mutant that lives twice as long as wild type. *Nature* 1993, **366**:461-464.
5. Holzenberger M., Dupont J., Ducos B., Leneuve P., Geloen A., Even P. C., Cervera P., Le Bouc Y.: IGF-1 receptor regulates lifespan and resistance to oxidative stress in mice. *Nature* 2003, **421**:182-187.
6. Kimura K. D., Tissenbaum H. A., Liu Y., Ruvkun G.: daf-2, an insulin receptor-like gene that regulates longevity and diapause in Caenorhabditis elegans. *Science* 1997, **277**:942-946.
7. Gems D., Partridge L.: Stress-response hormesis and aging: "that which does not kill us makes us stronger". *Cell Metab* 2008, **7**:200-203.
8. Mair W., Dillin A.: Aging and survival: the genetics of life span extension by dietary restriction. *Annu Rev Biochem* 2008, **77**:727-754.
9. Kikis E. A., Gidalevitz T., Morimoto R. I.: Protein homeostasis in models of aging and age-related conformational disease. *Adv Exp Med Biol* 2010, **694**:138-159.
10. Walter P., Ron D.: The unfolded protein response: from stress pathway to homeostatic regulation. *Science* 2011, **334**:1081-1086.
11. Vabulas R. M., Raychaudhuri S., Hayer-Hartl M., Hartl F. U.: Protein folding in the cytoplasm and the heat shock response. *Cold Spring Harb Perspect Biol* 2010, **2**:a004390.
12. Haynes C. M., Ron D.: The mitochondrial UPR - protecting organelle protein homeostasis. *J Cell Sci* 2010, **123**:3849-3855.
13. Dillin A., Gottschling D. E., Nystrom T.: The good and the bad of being connected: the integrons of aging. *Curr Opin Cell Biol* 2014, **26**:107-112.
14. Houtkooper R. H., Williams R. W., Auwerx J.: Metabolic networks of longevity. *Cell* 2010, **142**:9-14.
15. Andreux P. A., Houtkooper R. H., Auwerx J.: Pharmacological approaches to restore mitochondrial function. *Nat Rev Drug Discov* 2013, **12**:465-483.
16. Nunnari J., Suomalainen A.: Mitochondria: in sickness and in health. *Cell* 2012, **148**:1145-1159.
17. Jensen M. B., Jasper H.: Mitochondrial Proteostasis in the Control of Aging and Longevity. *Cell Metab* 2014, **20**:214-225.
18. Jovaisaite V., Mouchiroud L., Auwerx J.: The mitochondrial unfolded protein response, a conserved stress response pathway with implications in health and disease. *J Exp Biol* 2014, **217**:137-143.
19. Morimoto R. I.: The heat shock response: systems biology of proteotoxic stress in aging and disease. *Cold Spring Harb Symp Quant Biol* 2011, **76**:91-99.

20. Szegezdi E., Logue S. E., Gorman A. M., Samali A.: Mediators of endoplasmic reticulum stress-induced apoptosis. *EMBO Rep* 2006, **7**:880-885.
21. Gray M. W., Burger G., Lang B. F.: The origin and early evolution of mitochondria. *Genome Biol* 2001, **2**:REVIEWS1018.
22. Pagliarini D. J., Calvo S. E., Chang B., Sheth S. A., Vafai S. B., Ong S. E., Walford G. A., Sugiana C., Boneh A., Chen W. K., Hill D. E., Vidal M., Evans J. G., Thorburn D. R., Carr S. A., Mootha V. K.: A mitochondrial protein compendium elucidates complex I disease biology. *Cell* 2008, **134**:112-123.
23. Neupert W., Herrmann J. M.: Translocation of proteins into mitochondria. *Annu Rev Biochem* 2007, **76**:723-749.
24. Lane N.: Mitonuclear match: optimizing fitness and fertility over generations drives ageing within generations. *Bioessays* 2011, **33**:860-869.
25. Baker B. M., Haynes C. M.: Mitochondrial protein quality control during biogenesis and aging. *Trends Biochem Sci* 2011, **36**:254-261.
26. Tatsuta T., Langer T.: Quality control of mitochondria: protection against neurodegeneration and ageing. *EMBO J* 2008, **27**:306-314.
27. Rainbolt T. K., Atanassova N., Genereux J. C., Wiseman R. L.: Stress-regulated translational attenuation adapts mitochondrial protein import through Tim17A degradation. *Cell Metab* 2013, **18**:908-919.
28. Nargund A. M., Pellegrino M. W., Fiorese C. J., Baker B. M., Haynes C. M.: Mitochondrial import efficiency of ATFS-1 regulates mitochondrial UPR activation. *Science* 2012, **337**:587-590.
29. Schleit J., Johnson S. C., Bennett C. F., Simko M., Trongtham N., Castanza A., Hsieh E. J., Moller R. M., Wasko B. M., Delaney J. R., Sutphin G. L., Carr D., Murakami C. J., Tocchi A., Xian B., Chen W., Yu T., Goswami S., Higgins S., Holmberg M., Jeong K. S., Kim J. R., Klum S., Liao E., Lin M. S., Lo W., Miller H., Olsen B., Peng Z. J., Pollard T., Pradeep P., Pruett D., Rai D., Ros V., Singh M., Spector B. L., Vander Wende H., An E. H., Fletcher M., Jelic M., Rabinovitch P. S., MacCoss M. J., Han J. D., Kennedy B. K., Kaeberlein M.: Molecular mechanisms underlying genotype-dependent responses to dietary restriction. *Aging Cell* 2013, **12**:1050-1061.
30. Yoneda T., Benedetti C., Urano F., Clark S. G., Harding H. P., Ron D.: Compartment-specific perturbation of protein handling activates genes encoding mitochondrial chaperones. *J Cell Sci* 2004, **117**:4055-4066.
31. Wu Y., Williams Evan G., Dubuis S., Mottis A., Jovaisaite V., Houten Sander M., Argmann Carmen A., Faridi P., Wolski W., Kutalik Z., Zamboni N., Auwerx J., Aebersold R.: Multilayered Genetic and Omics Dissection of Mitochondrial Activity in a Mouse Reference Population. *Cell* 2014, **158**:1415-1430.
32. Burbulla L. F., Fitzgerald J. C., Stegen K., Westermeier J., Thost A. K., Kato H., Mokranjac D., Sauerwald J., Martins L. M., Woitalla D., Rapaport D., Riess O., Proikas-Cezanne T., Rasse T. M., Kruger R.: Mitochondrial proteolytic stress induced by loss of mortalin function is rescued by Parkin and PINK1. *Cell Death Dis* 2014, **5**:e1180.
33. Zhao Q., Wang J., Levichkin I. V., Stasinopoulos S., Ryan M. T., Hoogenraad N. J.: A mitochondrial specific stress response in mammalian cells. *EMBO J* 2002, **21**:4411-4419.
34. Papa L., Germain D.: SirT3 regulates the mitochondrial unfolded protein response. *Mol Cell Biol* 2014, **34**:699-710.
35. Pimenta de Castro I., Costa A. C., Lam D., Tufi R., Fedele V., Moisoi N., Dinsdale D., Deas E., Loh S. H., Martins L. M.: Genetic analysis of mitochondrial protein misfolding in Drosophila melanogaster. *Cell Death Differ* 2012, **19**:1308-1316.

36. Runkel E. D., Liu S., Baumeister R., Schulze E.: Surveillance-Activated Defenses Block the ROS-Induced Mitochondrial Unfolded Protein Response. *PLoS Genet* 2013, **9**:e1003346.
37. Liu Y., Samuel B. S., Breen P. C., Ruvkun G.: Caenorhabditis elegans pathways that surveil and defend mitochondria. *Nature* 2014, **508**:406-410.
38. Pellegrino M. W., Nargund A. M., Kirienko N. V., Gillis R., Fiorese C. J., Haynes C. M.: Mitochondrial UPR-regulated innate immunity provides resistance to pathogen infection. *Nature* 2014, **In press**.
39. Khan N. A., Auranen M., Paetau I., Pirinen E., Euro L., Forsstrom S., Pasila L., Velagapudi V., Carroll C. J., Auwerx J., Suomalainen A.: Effective treatment of mitochondrial myopathy by nicotinamide riboside, a vitamin B3. *EMBO Mol Med* 2014, **6**:721-731.
40. Martinus R. D., Garth G. P., Webster T. L., Cartwright P., Naylor D. J., Hoj P. B., Hoogenraad N. J.: Selective induction of mitochondrial chaperones in response to loss of the mitochondrial genome. *Eur J Biochem* 1996, **240**:98-103.
41. Houtkooper R. H., Mouchiroud L., Ryu D., Moullan N., Katsyuba E., Knott G., Williams R. W., Auwerx J.: Mitonuclear protein imbalance as a conserved longevity mechanism. *Nature* 2013, **497**:451-457.
42. Durieux J., Wolff S., Dillin A.: The cell-non-autonomous nature of electron transport chain-mediated longevity. *Cell* 2011, **144**:79-91.
43. Baker B. M., Nargund A. M., Sun T., Haynes C. M.: Protective coupling of mitochondrial function and protein synthesis via the eIF2alpha kinase GCN-2. *PLoS Genet* 2012, **8**:e1002760.
44. Owusu-Ansah E., Song W., Perrimon N.: Muscle mitohormesis promotes longevity via systemic repression of insulin signaling. *Cell* 2013, **155**:699-712.
45. Pulliam D. A., Deepa S. S., Liu Y., Hill S., Lin A. L., Bhattacharya A., Shi Y., Sloane L., Viscomi C., Zeviani M., Van Remmen H.: Complex IV-deficient Surf1-/- mice initiate mitochondrial stress responses. *Biochem J* 2014, **462**:359-371.
46. Mouchiroud L., Houtkooper R. H., Moullan N., Katsyuba E., Ryu D., Canto C., Mottis A., Jo Y. S., Viswanathan M., Schoonjans K., Guarente L., Auwerx J.: The NAD(+)/Sirtuin Pathway Modulates Longevity through Activation of Mitochondrial UPR and FOXO Signaling. *Cell* 2013, **154**:430-441.
47. Pirinen E., Canto C., Jo Y. S., Morato L., Zhang H., Menzies K. J., Williams E. G., Mouchiroud L., Moullan N., Hagberg C., Li W., Timmers S., Imhof R., Verbeek J., Pujol A., van Loon B., Viscomi C., Zeviani M., Schrauwen P., Sauve A. A., Schoonjans K., Auwerx J.: Pharmacological Inhibition of poly(ADP-ribose) polymerases improves fitness and mitochondrial function in skeletal muscle. *Cell Metab* 2014, **19**:1034-1041.
48. Rath E., Berger E., Messlik A., Nunes T., Liu B., Kim S. C., Hoogenraad N., Sans M., Sartor R. B., Haller D.: Induction of dsRNA-activated protein kinase links mitochondrial unfolded protein response to the pathogenesis of intestinal inflammation. *Gut* 2012, **61**:1269-1278.
49. Dillin A., Hsu A. L., Arantes-Oliveira N., Lehrer-Graiwer J., Hsin H., Fraser A. G., Kamath R. S., Ahringer J., Kenyon C.: Rates of behavior and aging specified by mitochondrial function during development. *Science* 2002, **298**:2398-2401.
50. Tsang W. Y., Lemire B. D.: Mitochondrial genome content is regulated during nematode development. *Biochem Biophys Res Commun* 2002, **291**:8-16.
51. Houtkooper R. H., Pirinen E., Auwerx J.: Sirtuins as regulators of metabolism and healthspan. *Nat Rev Mol Cell Biol* 2012, **13**:225-238.
52. Cerutti R., Pirinen E., Lamperti C., Marchet S., Sauve A. A., Li W., Leoni V., Schon E. A., Dantzer F., Auwerx J., Viscomi C., Zeviani M.: NAD(+)-dependent activation of

Sirt1 corrects the phenotype in a mouse model of mitochondrial disease. *Cell Metab* 2014, **19**:1042-1049.

53. Ryu D., Jo Y. S., Lo Sasso G., Stein S., Zhang H., Perino A., Lee J. U., Zeviani M., Romand R., Hottiger M. O., Schoonjans K., Auwerx J.: A SIRT7-Dependent Acetylation Switch of GABPbeta1 Controls Mitochondrial Function. *Cell Metab* 2014.

54. Haynes C. M., Petrova K., Benedetti C., Yang Y., Ron D.: ClpP mediates activation of a mitochondrial unfolded protein response in C. elegans. *Dev Cell* 2007, **13**:467-480.

55. Haynes C. M., Yang Y., Blais S. P., Neubert T. A., Ron D.: The matrix peptide exporter HAF-1 signals a mitochondrial UPR by activating the transcription factor ZC376.7 in C. elegans. *Mol Cell* 2010, **37**:529-540.

56. Benedetti C., Haynes C. M., Yang Y., Harding H. P., Ron D.: Ubiquitin-like protein 5 positively regulates chaperone gene expression in the mitochondrial unfolded protein response. *Genetics* 2006, **174**:229-239.

57. Horibe T., Hoogenraad N. J.: The chop gene contains an element for the positive regulation of the mitochondrial unfolded protein response. *PLoS One* 2007, **2**:e835.

58. Aldridge J. E., Horibe T., Hoogenraad N. J.: Discovery of genes activated by the mitochondrial unfolded protein response (mtUPR) and cognate promoter elements. *PLoS One* 2007, **2**:e874.

59. Jeyapaul J., Jaiswal A. K.: Nrf2 and c-Jun regulation of antioxidant response element (ARE)-mediated expression and induction of gamma-glutamylcysteine synthetase heavy subunit gene. *Biochem Pharmacol* 2000, **59**:1433-1439.

60. Rauthan M., Ranji P., Aguilera Pradenas N., Pitot C., Pilon M.: The mitochondrial unfolded protein response activator ATFS-1 protects cells from inhibition of the mevalonate pathway. *Proc Natl Acad Sci U S A* 2013, **110**:5981-5986.

61. Jin S. M., Youle R. J.: The accumulation of misfolded proteins in the mitochondrial matrix is sensed by PINK1 to induce PARK2/Parkin-mediated mitophagy of polarized mitochondria. *Autophagy* 2013, **9**:1750-1757.

62. Guo B., Huang X., Zhang P., Qi L., Liang Q., Zhang X., Huang J., Fang B., Hou W., Han J., Zhang H.: Genome-wide screen identifies signaling pathways that regulate autophagy during Caenorhabditis elegans development. *EMBO Rep* 2014, **15**:705-713.

63. Sentelle R. D., Senkal C. E., Jiang W., Ponnusamy S., Gencer S., Selvam S. P., Ramshesh V. K., Peterson Y. K., Lemasters J. J., Szulc Z. M., Bielawski J., Ogretmen B.: Ceramide targets autophagosomes to mitochondria and induces lethal mitophagy. *Nat Chem Biol* 2012, **8**:831-838.

64. Kroemer G., Marino G., Levine B.: Autophagy and the integrated stress response. *Mol Cell* 2010, **40**:280-293.

65. Thomas R. E., Andrews L. A., Burman J. L., Lin W. Y., Pallanck L. J.: PINK1-Parkin pathway activity is regulated by degradation of PINK1 in the mitochondrial matrix. *PLoS Genet* 2014, **10**:e1004279.

66. Wong A., Boutis P., Hekimi S.: Mutations in the clk-1 gene of Caenorhabditis elegans affect developmental and behavioral timing. *Genetics* 1995, **139**:1247-1259.

67. Munkacsy E., Rea S. L.: The paradox of mitochondrial dysfunction and extended longevity. *Exp Gerontol* 2014, **56**:221-233.

68. Pulliam D. A., Bhattacharya A., Van Remmen H.: Mitochondrial Dysfunction in Aging and Longevity: A Causal or Protective Role? *Antioxid Redox Signal* 2012.

69. Rea S. L., Ventura N., Johnson T. E.: Relationship between mitochondrial electron transport chain dysfunction, development, and life extension in Caenorhabditis elegans. *PLoS Biol* 2007, **5**:e259.

70. Ventura N., Rea S. L.: Caenorhabditis elegans mitochondrial mutants as an investigative tool to study human neurodegenerative diseases associated with mitochondrial dysfunction. *Biotechnol J* 2007, **2**:584-595.

71. Schieber M., Chandel N. S.: TOR signaling couples oxygen sensing to lifespan in C. elegans. *Cell Reports* 2014, **In press**.

72. Yokoyama K., Fukumoto K., Murakami T., Harada S., Hosono R., Wadhwa R., Mitsui Y., Ohkuma S.: Extended longevity of Caenorhabditis elegans by knocking in extra copies of hsp70F, a homolog of mot-2 (mortalin)/mthsp70/Grp75. *FEBS Lett* 2002, **516**:53-57.

73. Bennett C. F., Vander Wende H., Simko M., Klum S., Barfield S., Choi H., Pineda V. V., Kaeberlein M.: Activation of the mitochondrial unfolded protein response does not predict longevity in Caenorhabditis elegans. *Nat Commun* 2014, **5**:3483.

74. Kirkwood T. B.: Understanding the odd science of aging. *Cell* 2005, **120**:437-447.

75. Lopez-Otin C., Blasco M. A., Partridge L., Serrano M., Kroemer G.: The hallmarks of aging. *Cell* 2013, **153**:1194-1217.

76. Greer E. L., Maures T. J., Hauswirth A. G., Green E. M., Leeman D. S., Maro G. S., Han S., Banko M. R., Gozani O., Brunet A.: Members of the H3K4 trimethylation complex regulate lifespan in a germline-dependent manner in C. elegans. *Nature* 2010, **466**:383-387.

77. Han S., Brunet A.: Histone methylation makes its mark on longevity. *Trends Cell Biol* 2012, **22**:42-49.

78. Rando T. A., Chang H. Y.: Aging, rejuvenation, and epigenetic reprogramming: resetting the aging clock. *Cell* 2012, **148**:46-57.

79. Dillin A., Crawford D. K., Kenyon C.: Timing requirements for insulin/IGF-1 signaling in C. elegans. *Science* 2002, **298**:830-834.

80. Lee S. S., Lee R. Y., Fraser A. G., Kamath R. S., Ahringer J., Ruvkun G.: A systematic RNAi screen identifies a critical role for mitochondria in C. elegans longevity. *Nat Genet* 2003, **33**:40-48.

81. Copeland J. M., Cho J., Lo T., Jr., Hur J. H., Bahadorani S., Arabyan T., Rabie J., Soh J., Walker D. W.: Extension of Drosophila life span by RNAi of the mitochondrial respiratory chain. *Curr Biol* 2009, **19**:1591-1598.

82. Dell'agnello C., Leo S., Agostino A., Szabadkai G., Tiveron C., Zulian A., Prelle A., Roubertoux P., Rizzuto R., Zeviani M.: Increased longevity and refractoriness to Ca(2+)-dependent neurodegeneration in Surf1 knockout mice. *Hum Mol Genet* 2007, **16**:431-444.

83. Feng J., Bussiere F., Hekimi S.: Mitochondrial electron transport is a key determinant of life span in Caenorhabditis elegans. *Dev Cell* 2001, **1**:633-644.

84. Kirchman P. A., Kim S., Lai C. Y., Jazwinski S. M.: Interorganelle signaling is a determinant of longevity in Saccharomyces cerevisiae. *Genetics* 1999, **152**:179-190.

85. Liu X., Jiang N., Hughes B., Bigras E., Shoubridge E., Hekimi S.: Evolutionary conservation of the clk-1-dependent mechanism of longevity: loss of mclk1 increases cellular fitness and lifespan in mice. *Genes Dev* 2005, **19**:2424-2434.

86. Schon E. A., Przedborski S.: Mitochondria: the next (neurode)generation. *Neuron* 2011, **70**:1033-1053.

87. Baker M. J., Tatsuta T., Langer T.: Quality control of mitochondrial proteostasis. *Cold Spring Harb Perspect Biol* 2011, **3**.

88. Nargund A. M., Fiorese C. J., Pellegrino M. W., Deng P., Haynes C. M.: Mitochondrial and nuclear accumulation of the transcription factor ATFS-1 promotes OXPHOS recovery during the UPR(mt). *Molecular Cell* 2015, **58**:123-133.

89. Schroeder E. A., Raimundo N., Shadel G. S.: Epigenetic silencing mediates mitochondria stress-induced longevity. *Cell Metab* 2013, **17**:954-964.

90. Andreux P. A., Williams E. G., Koutnikova H., Houtkooper R. H., Champy M. F., Henry H., Schoonjans K., Williams R. W., Auwerx J.: Systems genetics of metabolism: the use of the BXD murine reference panel for multiscalar integration of traits. *Cell* 2012, **150**:1287-1299.

91. Kooistra S. M., Helin K.: Molecular mechanisms and potential functions of histone demethylases. *Nat Rev Mol Cell Biol* 2012, **13**:297-311.

92. Agger K., Cloos P. A. C., Christensen J., Pasini D., Rose S., Rappsilber J., Issaeva I., Canaani E., Salcini A. E., Helin K.: UTX and JMJD3 are histone H3K27 demethylases involved in HOX gene regulation and development. *Nature* 2007, **449**:731-734.

93. Kleine-Kohlbrecher D., Christensen J., Vandamme J., Abarrategui I., Bak M., Tommerup N., Shi X., Gozani O., Rappsilber J., Salcini A. E., Helin K.: A functional link between the histone demethylase PHF8 and the transcription factor ZNF711 in X-linked mental retardation. *Mol Cell* 2010, **38**:165-178.

94. Lakowski B., Hekimi S.: The genetics of caloric restriction in Caenorhabditis elegans. *Proceedings of the National Academy of Sciences of the United States of America* 1998, **95**:13091-13096.

95. Hsin H., Kenyon C.: Signals from the reproductive system regulate the lifespan of C. elegans. *Nature* 1999, **399**:362-366.

96. Baird N. A., Douglas P. M., Simic M. S., Grant A. R., Moresco J. J., Wolff S. C., Yates J. R., 3rd, Manning G., Dillin A.: HSF-1-mediated cytoskeletal integrity determines thermotolerance and life span. *Science* 2014, **346**:360-363.

97. Taylor R. C., Dillin A.: XBP-1 Is a Cell-Nonautonomous Regulator of Stress Resistance and Longevity. *Cell* 2013, **153**:1435-1447.

98. Labbadia J., Morimoto R. I.: Repression of the Heat Shock Response Is a Programmed Event at the Onset of Reproduction. *Molecular Cell* 2015, **59**:639-650.

99. Heinemann B., Nielsen J. M., Hudlebusch H. R., Lees M. J., Larsen D. V., Boesen T., Labelle M., Gerlach L.-O., Birk P., Helin K.: Inhibition of demethylases by GSK-J1/J4. *Nature* 2014, **514**:E1-E2.

100. Bender L. B., Cao R., Zhang Y., Strome S.: The MES-2/MES-3/MES-6 complex and regulation of histone H3 methylation in C. elegans. *Current biology: CB* 2004, **14**:1639-1643.

101. Huang da W., Sherman B. T., Lempicki R. A.: Systematic and integrative analysis of large gene lists using DAVID bioinformatics resources. *Nat Protoc* 2009, **4**:44-57.

102. Ntziachristos P., Tsirigos A., Welstead G. G., Trimarchi T., Bakogianni S., Xu L., Loizou E., Holmfeldt L., Strikoudis A., King B., Mullenders J., Becksfort J., Nedjic J., Paietta E., Tallman M. S., Rowe J. M., Tonon G., Satoh T., Kruidenier L., Prinjha R., Akira S., Van Vlierberghe P., Ferrando A. A., Jaenisch R., Mullighan C. G., Aifantis I.: Contrasting roles of histone 3 lysine 27 demethylases in acute lymphoblastic leukaemia. *Nature* 2014, **514**:513-517.

103. Fortschegger K., de Graaf P., Outchkourov N. S., van Schaik F. M. A., Timmers H. T. M., Shiekhattar R.: PHF8 targets histone methylation and RNA polymerase II to activate transcription. *Molecular and Cellular Biology* 2010, **30**:3286-3298.

104. Feng W., Yonezawa M., Ye J., Jenuwein T., Grummt I.: PHF8 activates transcription of rRNA genes through H3K4me3 binding and H3K9me1/2 demethylation. *Nat Struct Mol Biol* 2010, **17**:445-450.

105. Liu W., Tanasa B., Tyurina O. V., Zhou T. Y., Gassmann R., Liu W. T., Ohgi K. A., Benner C., Garcia-Bassets I., Aggarwal A. K., Desai A., Dorrestein P. C., Glass C. K., Rosenfeld M. G.: PHF8 mediates histone H4 lysine 20 demethylation events involved in cell cycle progression. *Nature* 2010, **466**:508-512.

106. Qi H. H., Sarkissian M., Hu G.-Q., Wang Z., Bhattacharjee A., Gordon D. B., Gonzales M., Lan F., Ongusaha P. P., Huarte M., Yaghi N. K., Lim H., Garcia B. A.,

Brizuela L., Zhao K., Roberts T. M., Shi Y.: Histone H4K20/H3K9 demethylase PHF8 regulates zebrafish brain and craniofacial development. *Nature* 2010, **466**:503-507.

107. Teperino R., Schoonjans K., Auwerx J.: Histone methyl transferases and demethylases; can they link metabolism and transcription? *Cell Metabolism* 2010, **12**:321-327.

108. Chin R. M., Fu X., Pai M. Y., Vergnes L., Hwang H., Deng G., Diep S., Lomenick B., Meli V. S., Monsalve G. C., Hu E., Whelan S. A., Wang J. X., Jung G., Solis G. M., Fazlollahi F., Kaweeteerawat C., Quach A., Nili M., Krall A. S., Godwin H. A., Chang H. R., Faull K. F., Guo F., Jiang M., Trauger S. A., Saghatelian A., Braas D., Christofk H. R., Clarke C. F., Teitell M. A., Petrascheck M., Reue K., Jung M. E., Frand A. R., Huang J.: The metabolite alpha-ketoglutarate extends lifespan by inhibiting ATP synthase and TOR. *Nature* 2014, **510**:397-401.

109. Chen L., Fu Y., Ren M., Xiao B., Rubin C. S.: A RasGRP, C. elegans RGEF-1b, couples external stimuli to behavior by activating LET-60 (Ras) in sensory neurons. *Neuron* 2011, **70**:51-65.

110. Warren C. E., Krizus A., Dennis J. W.: Complementary expression patterns of six nonessential Caenorhabditis elegans core 2/I N-acetylglucosaminyltransferase homologues. *Glycobiology* 2001, **11**:979-988.

111. Kamath R. S., Martinez-Campos M., Zipperlen P., Fraser A. G., Ahringer J.: Effectiveness of specific RNA-mediated interference through ingested double-stranded RNA in Caenorhabditis elegans. *Genome Biol* 2001, **2**:RESEARCH0002.

112. Langmead B., Trapnell C., Pop M., Salzberg S. L.: Ultrafast and memory-efficient alignment of short DNA sequences to the human genome. *Genome Biol* 2009, **10**:R25.

113. Love M. I., Huber W., Anders S.: Moderated estimation of fold change and dispersion for RNA-seq data with DESeq2. *Genome Biol* 2014, **15**:550.

114. Heberle H., Meirelles G. V., da Silva F. R., Telles G. P., Minghim R.: InteractiVenn: a web-based tool for the analysis of sets through Venn diagrams. *BMC Bioinformatics* 2015, **16**:169.

115. Edgar R., Domrachev M., Lash A. E.: Gene Expression Omnibus: NCBI gene expression and hybridization array data repository. *Nucleic Acids Res* 2002, **30**:207-210.

116. Mukhopadhyay A., Deplancke B., Walhout A. J., Tissenbaum H. A.: Chromatin immunoprecipitation (ChIP) coupled to detection by quantitative real-time PCR to study transcription factor binding to DNA in Caenorhabditis elegans. *Nat Protoc* 2008, **3**:698-709.

117. Goecks J., Nekrutenko A., Taylor J., Galaxy T.: Galaxy: a comprehensive approach for supporting accessible, reproducible, and transparent computational research in the life sciences. *Genome Biol* 2010, **11**:R86.

118. Thorvaldsdottir H., Robinson J. T., Mesirov J. P.: Integrative Genomics Viewer (IGV): high-performance genomics data visualization and exploration. *Brief Bioinform* 2013, **14**:178-192.

119. Akram M.: Citric acid cycle and role of its intermediates in metabolism. *Cell Biochem Biophys* 2014, **68**:475-478.

120. Raimundo N., Baysal B. E., Shadel G. S.: Revisiting the TCA cycle: signaling to tumor formation. *Trends Mol Med* 2011, **17**:641-649.

121. Haynes C. M., Fiorese C. J., Lin Y. F.: Evaluating and responding to mitochondrial dysfunction: the mitochondrial unfolded-protein response and beyond. *Trends Cell Biol* 2013.

122. Merkwirth C., Jovaisaite V., Durieux J., Matilainen O., Jordan S. D., Quiros P. M., Steffen K. K., Williams E. G., Mouchiroud L., Tronnes S. U., Murillo V., Wolff S. C.,

Shaw R. J., Auwerx J., Dillin A.: Two Conserved Histone Demethylases Regulate Mitochondrial Stress-Induced Longevity. *Cell* 2016, **165**:1209-1223.

123. Hamilton B., Dong Y., Shindo M., Liu W., Odell I., Ruvkun G., Lee S. S.: A systematic RNAi screen for longevity genes in C. elegans. *Genes Dev* 2005, **19**:1544-1555.

124. Curran S. P., Ruvkun G.: Lifespan regulation by evolutionarily conserved genes essential for viability. *PLoS Genet* 2007, **3**:e56.

125. Williams D. S., Cash A., Hamadani L., Diemer T.: Oxaloacetate supplementation increases lifespan in Caenorhabditis elegans through an AMPK/FOXO-dependent pathway. *Aging Cell* 2009, **8**:765-768.

126. Edwards C. B., Copes N., Brito A. G., Canfield J., Bradshaw P. C.: Malate and fumarate extend lifespan in Caenorhabditis elegans. *PLoS One* 2013, **8**:e58345.

127. Salminen A., Kauppinen A., Hiltunen M., Kaarniranta K.: Krebs cycle intermediates regulate DNA and histone methylation: epigenetic impact on the aging process. *Ageing Res Rev* 2014, **16**:45-65.

128. Pellegrino M. W., Nargund A. M., Kirienko N. V., Gillis R., Fiorese C. J., Haynes C. M.: Mitochondrial UPR-regulated innate immunity provides resistance to pathogen infection. *Nature* 2014, **516**:414-417.

129. Kim H. E., Grant A. R., Simic M. S., Kohnz R. A., Nomura D. K., Durieux J., Riera C. E., Sanchez M., Kapernick E., Wolff S., Dillin A.: Lipid biosynthesis coordinates a mitochondrial to cytosolic stress response. *Cell* 2016, **In press**.

130. Riobo N. A.: Cholesterol and its derivatives in Sonic Hedgehog signaling and cancer. *Curr Opin Pharmacol* 2012, **12**:736-741.

131. Ghazalpour A., Bennett B., Petyuk V. A., Orozco L., Hagopian R., Mungrue I. N., Farber C. R., Sinsheimer J., Kang H. M., Furlotte N., Park C. C., Wen P. Z., Brewer H., Weitz K., Camp D. G., 2nd, Pan C., Yordanova R., Neuhaus I., Tilford C., Siemers N., Gargalovic P., Eskin E., Kirchgessner T., Smith D. J., Smith R. D., Lusis A. J.: Comparative analysis of proteome and transcriptome variation in mouse. *PLoS Genet* 2011, **7**:e1001393.

132. Schwanhausser B., Busse D., Li N., Dittmar G., Schuchhardt J., Wolf J., Chen W., Selbach M.: Global quantification of mammalian gene expression control. *Nature* 2011, **473**:337-342.

133. Gygi S. P., Rochon Y., Franza B. R., Aebersold R.: Correlation between protein and mRNA abundance in yeast. *Mol Cell Biol* 1999, **19**:1720-1730.

134. Skelly D. A., Merrihew G. E., Riffle M., Connelly C. F., Kerr E. O., Johansson M., Jaschob D., Graczyk B., Shulman N. J., Wakefield J., Cooper S. J., Fields S., Noble W. S., Muller E. G., Davis T. N., Dunham M. J., Maccoss M. J., Akey J. M.: Integrative phenomics reveals insight into the structure of phenotypic diversity in budding yeast. *Genome Res* 2013, **23**:1496-1504.

135. Albert F. W., Treusch S., Shockley A. H., Bloom J. S., Kruglyak L.: Genetics of single-cell protein abundance variation in large yeast populations. *Nature* 2014.

136. Karpievitch Y. V., Dabney A. R., Smith R. D.: Normalization and missing value imputation for label-free LC-MS analysis. *BMC Bioinformatics* 2012, **13 Suppl 16**:S5.

137. Holdt L. M., von Delft A., Nicolaou A., Baumann S., Kostrzewa M., Thiery J., Teupser D.: Quantitative trait loci mapping of the mouse plasma proteome (pQTL). *Genetics* 2013, **193**:601-608.

138. Callister S. J., Barry R. C., Adkins J. N., Johnson E. T., Qian W. J., Webb-Robertson B. J., Smith R. D., Lipton M. S.: Normalization approaches for removing systematic biases associated with mass spectrometry and label-free proteomics. *J Proteome Res* 2006, **5**:277-286.

139. Lange V., Picotti P., Domon B., Aebersold R.: Selected reaction monitoring for quantitative proteomics: a tutorial. *Mol Syst Biol* 2008, **4**:222.

140. Picotti P., Clement-Ziza M., Lam H., Campbell D. S., Schmidt A., Deutsch E. W., Rost H., Sun Z., Rinner O., Reiter L., Shen Q., Michaelson J. J., Frei A., Alberti S., Kusebauch U., Wollscheid B., Moritz R. L., Beyer A., Aebersold R.: A complete mass-spectrometric map of the yeast proteome applied to quantitative trait analysis. *Nature* 2013, **494**:266-270.

141. Yvert G., Brem R. B., Whittle J., Akey J. M., Foss E., Smith E. N., Mackelprang R., Kruglyak L.: Trans-acting regulatory variation in Saccharomyces cerevisiae and the role of transcription factors. *Nat Genet* 2003, **35**:57-64.

142. De Luca M., Roshina N. V., Geiger-Thornsberry G. L., Lyman R. F., Pasyukova E. G., Mackay T. F.: Dopa decarboxylase (Ddc) affects variation in Drosophila longevity. *Nat Genet* 2003, **34**:429-433.

143. Deeb S. S., Fajas L., Nemoto M., Pihlajamaki J., Mykkanen L., Kuusisto J., Laakso M., Fujimoto W., Auwerx J.: A Pro12Ala substitution in PPARgamma2 associated with decreased receptor activity, lower body mass index and improved insulin sensitivity. *Nat Genet* 1998, **20**:284-287.

144. Picotti P., Rinner O., Stallmach R., Dautel F., Farrah T., Domon B., Wenschuh H., Aebersold R.: High-throughput generation of selected reaction-monitoring assays for proteins and proteomes. *Nat Methods* 2010, **7**:43-46.

145. Ihmels J., Friedlander G., Bergmann S., Sarig O., Ziv Y., Barkai N.: Revealing modular organization in the yeast transcriptional network. *Nat Genet* 2002, **31**:370-377.

146. Foster L. J., de Hoog C. L., Zhang Y., Zhang Y., Xie X., Mootha V. K., Mann M.: A mammalian organelle map by protein correlation profiling. *Cell* 2006, **125**:187-199.

147. Foss E. J., Radulovic D., Shaffer S. A., Ruderfer D. M., Bedalov A., Goodlett D. R., Kruglyak L.: Genetic basis of proteome variation in yeast. *Nat Genet* 2007, **39**:1369-1375.

148. Durieux J., Wolff S., Dillin A.: The cell-non-autonomous nature of electron transport chain-mediated longevity. *Cell* 2011, **144**:79-91.

149. Haynes C. M., Fiorese C. J., Lin Y. F.: Evaluating and responding to mitochondrial dysfunction: the mitochondrial unfolded-protein response and beyond. *Trends Cell Biol* 2013, **23**:311-318.

150. Wolff S., Weissman J. S., Dillin A.: Differential scales of protein quality control. *Cell* 2014, **157**:52-64.

151. Khan Z., Ford M. J., Cusanovich D. A., Mitrano A., Pritchard J. K., Gilad Y.: Primate transcript and protein expression levels evolve under compensatory selection pressures. *Science* 2013, **342**:1100-1104.

152. Marx V.: Finding the right antibody for the job. *Nature Methods* 2013, **10**:703-707.

153. Hwang H., Bowen B. P., Lefort N., Flynn C. R., De Filippis E. A., Roberts C., Smoke C. C., Meyer C., Hojlund K., Yi Z., Mandarino L. J.: Proteomics analysis of human skeletal muscle reveals novel abnormalities in obesity and type 2 diabetes. *Diabetes* 2010, **59**:33-42.

154. Yamamoto H., Williams E. G., Mouchiroud L., Canto C., Fan W., Downes M., Heligon C., Barish G. D., Desvergne B., Evans R. M., Schoonjans K., Auwerx J.: NCoR1 is a conserved physiological modulator of muscle mass and oxidative function. *Cell* 2011, **147**:827-839.

155. Ramot D., Johnson B. E., Berry T. L., Jr., Carnell L., Goodman M. B.: The Parallel Worm Tracker: a platform for measuring average speed and drug-induced paralysis in nematodes. *PLoS One* 2008, **3**:e2208.

156. Botstein D., Risch N.: Discovering genotypes underlying human phenotypes: past successes for mendelian disease, future approaches for complex disease. *Nature Genetics* 2003, **33 Suppl**:228-237.

157. Cooper G. M., Shendure J.: Needles in stacks of needles: finding disease-causal variants in a wealth of genomic data. *Nat Rev Genet* 2011, **12**:628-640.

158. Jelier R., Semple J. I., Garcia-Verdugo R., Lehner B.: Predicting phenotypic variation in yeast from individual genome sequences. *Nature Genetics* 2011, **43**:1270-1274.

159. Keane T. M., Goodstadt L., Danecek P., White M. A., Wong K., Yalcin B., Heger A., Agam A., Slater G., Goodson M., Furlotte N. A., Eskin E., Nellaker C., Whitley H., Cleak J., Janowitz D., Hernandez-Pliego P., Edwards A., Belgard T. G., Oliver P. L., McIntyre R. E., Bhomra A., Nicod J., Gan X., Yuan W., van der Weyden L., Steward C. A., Bala S., Stalker J., Mott R., Durbin R., Jackson I. J., Czechanski A., Guerra-Assuncao J. A., Donahue L. R., Reinholdt L. G., Payseur B. A., Ponting C. P., Birney E., Flint J., Adams D. J.: Mouse genomic variation and its effect on phenotypes and gene regulation. *Nature* 2011, **477**:289-294.

160. Nolan P. M., Peters J., Strivens M., Rogers D., Hagan J., Spurr N., Gray I. C., Vizor L., Brooker D., Whitehill E., Washbourne R., Hough T., Greenaway S., Hewitt M., Liu X., McCormack S., Pickford K., Selley R., Wells C., Tymowska-Lalanne Z., Roby P., Glenister P., Thornton C., Thaung C., Stevenson J. A., Arkell R., Mburu P., Hardisty R., Kiernan A., Erven A., Steel K. P., Voegeling S., Guenet J. L., Nickols C., Sadri R., Nasse M., Isaacs A., Davies K., Browne M., Fisher E. M., Martin J., Rastan S., Brown S. D., Hunter J.: A systematic, genome-wide, phenotype-driven mutagenesis programme for gene function studies in the mouse. *Nature Genetics* 2000, **25**:440-443.

161. Denny J. C., Bastarache L., Ritchie M. D., Carroll R. J., Zink R., Mosley J. D., Field J. R., Pulley J. M., Ramirez A. H., Bowton E., Basford M. A., Carrell D. S., Peissig P. L., Kho A. N., Pacheco J. A., Rasmussen L. V., Crosslin D. R., Crane P. K., Pathak J., Bielinski S. J., Pendergrass S. A., Xu H., Hindorff L. A., Li R., Manolio T. A., Chute C. G., Chisholm R. L., Larson E. B., Jarvik G. P., Brilliant M. H., McCarty C. A., Kullo I. J., Haines J. L., Crawford D. C., Masys D. R., Roden D. M.: Systematic comparison of phenome-wide association study of electronic medical record data and genome-wide association study data. *Nat Biotechnol* 2013, **31**:1102-1110.

162. Denny J. C., Ritchie M. D., Basford M. A., Pulley J. M., Bastarache L., Brown-Gentry K., Wang D., Masys D. R., Roden D. M., Crawford D. C.: PheWAS: demonstrating the feasibility of a phenome-wide scan to discover gene-disease associations. *Bioinformatics* 2010, **26**:1205-1210.

163. Chesler E. J., Lu L., Shou S., Qu Y., Gu J., Wang J., Hsu H. C., Mountz J. D., Baldwin N. E., Langston M. A., Threadgill D. W., Manly K. F., Williams R. W.: Complex trait analysis of gene expression uncovers polygenic and pleiotropic networks that modulate nervous system function. *Nat Genet* 2005, **37**:233-242.

164. Wu Y., Williams E. G., Dubuis S., Mottis A., Jovaisaite V., Houten S. M., Argmann C. A., Faridi P., Wolski W., Kutalik Z., Zamboni N., Auwerx J., Aebersold R.: Multilayered genetic and omics dissection of mitochondrial activity in a mouse reference population. *Cell* 2014, **158**:1415-1430.

165. Adzhubei I. A., Schmidt S., Peshkin L., Ramensky V. E., Gerasimova A., Bork P., Kondrashov A. S., Sunyaev S. R.: A method and server for predicting damaging missense mutations. *Nature Methods* 2010, **7**:248-249.

166. Ng P. C., Henikoff S.: SIFT: Predicting amino acid changes that affect protein function. *Nucleic Acids Res* 2003, **31**:3812-3814.

167. Aartsma-Rus A., Janson A. A. M., van Ommen G. J. B., van Deutekom J. C. T.: Antisense-induced exon skipping for duplications in Duchenne muscular dystrophy. *Bmc Medical Genetics* 2007, **8**.

168. Ema M., Ohe N., Suzuki M., Mimura J., Sogawa K., Ikawa S., Fujii-Kuriyama Y.: Dioxin binding activities of polymorphic forms of mouse and human arylhydrocarbon receptors. *Journal of Biological Chemistry* 1994, **269**:27337-27343.

169. Guidry P. A., Stroynowski I.: The murine family of gut-restricted class Ib MHC includes alternatively spliced isoforms of the proposed HLA-G homolog, "blastocyst MHC". *J Immunol* 2005, **175**:5248-5259.

170. Wang X., Mozhui K., Li Z., Mulligan M. K., Ingels F. J., Zhou X., T Hori R., Chen H., Cook N. M., Williams W. R., Lu L.: A promoter polymorphism in the Per3 gene is associated with alcohol and stress response. *Translational Psychiatry* 2012, **2**:81-85.

171. Williams E. G., Mouchiroud L., Frochaux M., Pandey A., Andreux P. A., Deplancke B., Auwerx J.: An evolutionarily conserved role for the aryl hydrocarbon receptor in the regulation of movement. *PLoS Genet* 2014, **10**:e1004673.

172. Tomlinson I. P., Alam N. A., Rowan A. J., Barclay E., Jaeger E. E., Kelsell D., Leigh I., Gorman P., Lamlum H., Rahman S., Roylance R. R., Olpin S., Bevan S., Barker K., Hearle N., Houlston R. S., Kiuru M., Lehtonen R., Karhu A., Vilkki S., Laiho P., Eklund C., Vierimaa O., Aittomaki K., Hietala M., Sistonen P., Paetau A., Salovaara R., Herva R., Launonen V., Aaltonen L. A., Multiple Leiomyoma C.: Germline mutations in FH predispose to dominantly inherited uterine fibroids, skin leiomyomata and papillary renal cell cancer. *Nat Genet* 2002, **30**:406-410.

173. Sena L. A., Li S., Jairaman A., Prakriya M., Ezponda T., Hildeman D. A., Wang C. R., Schumacker P. T., Licht J. D., Perlman H., Bryce P. J., Chandel N. S.: Mitochondria are required for antigen-specific T cell activation through reactive oxygen species signaling. *Immunity* 2013, **38**:225-236.

174. Ziebarth J. D., Cook M. N., Wang X., Williams R. W., Lu L., Cui Y.: Treatment- and population-dependent activity patterns of behavioral and expression QTLs. *Plos One* 2012, **7**:e31805.

175. Li H., Ruan J., Durbin R.: Mapping short DNA sequencing reads and calling variants using mapping quality scores. *Genome Res* 2008, **18**:1851-1858.

176. Storey J. D., Tibshirani R.: Statistical significance for genomewide studies. *Proc Natl Acad Sci U S A* 2003, **100**:9440-9445.

177. Tian Y., Garcia G., Bian Q., Steffen K. K., Joe L., Wolff S., Meyer B. J., Dillin A.: Mitochondrial Stress Induces Chromatin Reorganization to Promote Longevity and UPR(mt). *Cell* 2016, **165**:1197-1208.

178. Yun J., Finkel T.: Mitohormesis. *Cell Metab* 2014, **19**:757-766.

179. Maklakov A. A., Rowe L., Friberg U.: Why organisms age: Evolution of senescence under positive pleiotropy? *Bioessays* 2015, **37**:802-807.

180. Twumasi-Boateng K., Wang T. W., Tsai L., Lee K. H., Salehpour A., Bhat S., Tan M. W., Shapira M.: An age-dependent reversal in the protective capacities of JNK signaling shortens Caenorhabditis elegans lifespan. *Aging Cell* 2012, **11**:659-667.

181. Basisty N., Dai D. F., Gagnidze A., Gitari L., Fredrickson J., Maina Y., Beyer R. P., Emond M. J., Hsieh E. J., MacCoss M. J., Martin G. M., Rabinovitch P. S.: Mitochondrial-targeted catalase is good for the old mouse proteome, but not for the young: 'reverse' antagonistic pleiotropy? *Aging Cell* 2016, **15**:634-645.

182. Fiorese C. J., Schulz A. M., Lin Y. F., Rosin N., Pellegrino M. W., Haynes C. M.: The Transcription Factor ATF5 Mediates a Mammalian Mitochondrial UPR. *Curr Biol* 2016, **26**:2037-2043.

Curriculum Vitae

Virginija Jovaisaite

virginija.jovaisaite@gmail.com, +41799043703

Rue de la gare 11B, 1110 Morges

Education

Ph.D. in Biotechnology and Bioengineering, 2016
Ecole Polytechnique Fédérale de Lausanne (EPFL), Switzerland

M.Sc. in Cell Biology, 2011
Eidgenössische Technische Hochschule Zürich (ETHZ), Switzerland

B.Sc. in Biochemistry, 2009
Vilnius University, Lithuania

Research experience

Institute of Bioengineering, Laboratory of Integrative Systems Physiology, Ecole Polytechnique Fédérale de Lausanne (EPFL), Switzerland, 2012-2016
Ph.D. thesis with Prof. Johan Auwerx "Mitochondrial unfolded protein response, its molecular mechanism and physiological impact"

Department of Urology, Laboratory for Urologic Tissue Engineering and Stem Cell Therapy, University Hospital Zürich, Switzerland, 2010-2011
Master thesis with Dr. Daniel Eberli "Tracking of human Muscle Precursor Cells by MRI *in vivo*"

Institute of Cell Biology, ETH Zürich, Switzerland, 2010
Semester project with Prof. Romeo Ricci "Regulation of insulin secretion by PKD1 and Arfaptin1"

Institute of Molecular Systems Biology, ETH Zürich, Switzerland, 2009
Semester project with Prof. Ernst Hafen "Functional characterization of BunA-Madm growth regulating complex".

Institute of Biotechnology, Laboratory of protein-DNA interactions, Vilnius, Lithuania, 2006-2009
Bachelor thesis with Prof. Virginijus Siksnys "Crystallographic studies of restriction endonucleases, recognising CCGG nucleotide motif".

Department of Chemistry, Biophysical Chemistry group, University of Copenhagen, Denmark, 2008
Semester project with Prof. Leila Lo Leggio "Structural studies of the bZIP domain of HACA"

Publications

Merkwirth C*, Jovaisaite V*, Durieux J, Matilainen O, Jordan SD, Quiros PM, Steffen KK, Williams EG, Mouchiroud L, Uhlein SN, Murillo V, Wolff SC, Shaw RJ, Auwerx J*, Dillin A*. Two conserved histone demethylases regulate mitochondrial stress-induced longevity. *Cell* 2016, 165:1209-1223.
*equal contribution

Wang X, Pandey AK, Mulligan MK, Williams EG, Mozhui K, Li Z, Jovaisaite V, Quarles LD, Xiao Z, Huang J, Capra JA, Chen Z, Taylor WL, Bastarache L, Niu X, Pollard KS, Ciobanu DC, Reznik AO, Tishkov AV, Zhulin IB, Peng J, Nelson SF, Denny JC, Auwerx J, Lu L, Williams RW. Joint mouse–human phenome-wide association to test gene function and disease risk. *Nat Commun* 2016, 7:10464.

Cornaglia M, Mouchiroud L, Marette A, Narasimhan S, Lehnert T, Jovaisaite V, Auwerx J, Gijs MA. An automated microfluidic platform for C. elegans embryo arraying, phenotyping, and long-term live imaging. *Sci Rep* 2015, 5:10192.

Moullan N, Mouchiroud L, Wang X, Ryu D, Williams EG, Mottis A, Jovaisaite V, Frochaux MV, Quiros PM, Deplancke B, Houtkooper RH, Auwerx J. Tetracyclines disturb mitochondrial function across eukaryotic models: a call for caution in biomedical research. *Cell Rep* 2015, 10:1681-1691.

Jovaisaite V, Auwerx J. The mitochondrial unfolded protein response-synchronizing genomes. *Curr Opin Cell Biol* 2015, 33C:74-81

Azzabi F, Rottmar M, Jovaisaite V, Rudin M, Sulser T, Boss A, Eberli D. Viability, differentiation capacity and detectability of super-paramagnetic iron oxide labeled muscle precursor cells for magnetic-resonance imaging. *Tissue Eng Part C Methods* 2015, 21:182-191.

Wu Y, Williams EG, Dubuis S, Mottis A, Jovaisaite V, Houten SM, Argmann CA, Faridi P, Wolski W, Kutalik Z, Zamboni N, Auwerx J, Aebersold R. Multilayered genetic and omics dissection of mitochondrial activity in a mouse reference population. *Cell* 2014, 158:1415-1430.

Andreux PA, Mouchiroud L, Wang X, Jovaisaite V, Mottis A, Bichet S, Moullan N, Houtkooper RH, Auwerx J. A method to identify and validate mitochondrial modulators using mammalian cells and the worm C. elegans. *Sci Rep* 2014, 4:5285.

Mottis A, Jovaisaite V, Auwerx J. The mitochondrial unfolded protein response in mammalian physiology. *Mamm Genome* 2014, 25:424-433.

Jovaisaite V, Mouchiroud L, Auwerx J. The mitochondrial unfolded protein response, a conserved stress response pathway with implications in health and disease. *J Exp Biol* 2014, 217:137-143.

Gluderer S, Brunner E, Germann M, Jovaisaite V, Li C, Rentsch CA, Hafen E, Stocker H. Madm (Mlf1 adapter molecule) cooperates with Bunched A to promote growth in Drosophila. *J Biol* 2010, 9:9.

Conferences and courses

The 5th Lausanne Integrative Metabolism and Nutrition Alliance (LIMNA) Symposia, Lausanne, Switzerland, 2016, poster presentation.

Protein homeostasis in health & disease, CSHL, USA, 2016, poster presentation

Welcome Trust advanced course "Functional genomics and systems biology", Cambridge, UK, 2015